Pomeron in Holographic QCD

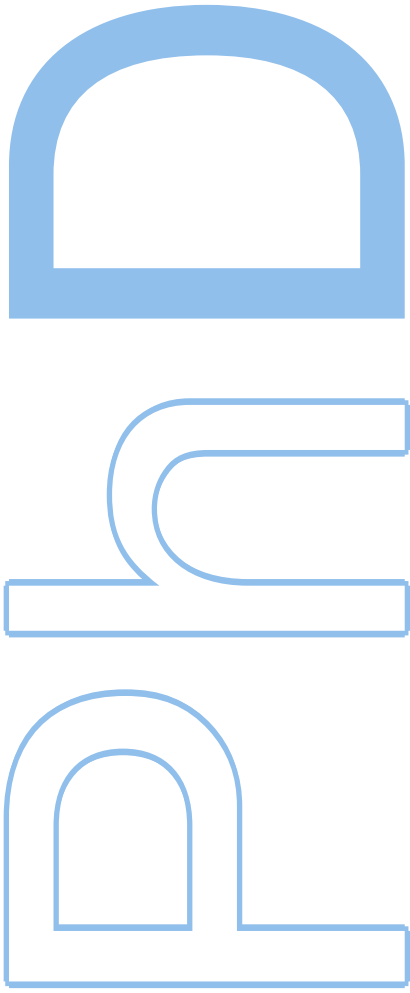

Robert Carcassés Quevedo
Program Doutoral em Física
Departamento de Física e Astronomia
2018

Orientador
Miguel Sousa da Costa, Faculdade de Ciências, Universidade do Porto

Coorientador
João Penedones, École Polytechnique Fédérale de Lausanne

Robert Carcassés Quevedo

Pomeron in Holographic QCD

Departamento de Física e Astronomia
Faculdade de Ciências da Universidade do Porto
June 2018

Robert Carcassés Quevedo

Pomeron in Holographic QCD

Tese submetida Faculdade de Ciências da
Universidade do Porto para obtenção do grau de Doutor
em Física

Departamento de Física e Astronomia
Faculdade de Ciências da Universidade do Porto
June 2018

To Rubén Quevedo Molina (1938-2016), with love.

Acknowledgements

First and foremost I would like to thank my supervisor Miguel Costa for giving me a chance of being part of the Porto node of the GATIS network. This was a game changing move in my life, both personal and professional. I would like also to thank João Penedones and Vasco Gonçalves for teaching me about CFT and bootstrap techniques, and for being there for discussing about anything related to physics. I am grateful as well to Alfonso Ballon Bayona and Marko Djuric for coaching me in my early studies about the Pomeron, and as well to Catarina, Niaz, Emilio and Lauren for being great roommates at the CFP. I would also thank Roberto Trinchero, for encouraging me to apply for this PhD and Artur Amorin for being a great partner in the late stage of this work.

Thank you Yuselis, Camila, Carolina, Marisol, Dulce, Rodi and Roberto for making my life beautiful and supporting me during all these years.

Publication list

This thesis is based in the following publications:

- Soft Pomeron in Holographic QCD,
  Phys. Rev. D 93, 035005 (2016), arXiv:1508.00008.
- Unity of pomerons from gauge/string duality,
  J. High Energ. Phys. (2017) 2017: 85, arXiv:1704.08280.
- Non-minimal coupling contribution to DIS at low x in Holographic QCD,
  arXiv:1804.07778. Accepted in Phys. Rev. D.

Contents

List of Tables

List of Figures

Abstract

The Pomeron is studied in the context of bottom-up AdS/QCD phenomenological models with explicitly broken conformal symmetry. It is realized as the graviton Regge trajectory, which is obtained by extending phenomenologically the free higher spin equation of motion in AdS. By considering a quadratic approximation for the curve $\Delta(J)$, where Δ is the dimension of the dual operator of spin J, around $J = 2$, it is found that Soft Pomeron phenomenology can be reached. Considering further possible corrections to this curve using an ansatz based in the α' expansion of string theory, it is shown that the idea of Donnachie and Landshoff of the Hard Pomeron can be realized holographically. In this case it is shown quantitatively how the model can explain the latest available joint data of Deep Inelastic Scattering, by finding the optimal values for the free parameters of the model. Moreover, considering further possible couplings between the higher spin fields and the spin 1 gauge field dual to the hadronic current, it is shown that the previous fit can be improved. Finally, aiming to look for the true holographic description of the Pomeron, a global fit for Deeply Virtual Compton Scattering total and differential cross-sections is found, showing that is possible to have a model that fits both datasets simultaneously.

1 Preliminaries

The construction of high energy particle colliders during the second half of the last century unveiled many new features about subatomic physics, pushing the bound of our knowledge about nature. In particular, two new different types of interaction were found, the weak and the strong interactions, which were later unified together with the electromagnetic one in a single theoretical framework, known nowadays as the Standard Model. The Standard Model condenses, in a consistent way, all the experimental evidence collected from these high energy colliders, in a Yang-Mills theory with a relative simple gauge group $SU(3) \times SU(2)_L \times U(1)$. The recent discovery of the Higgs boson [6], one of the last pieces to be found, reaffirms the validity of the Standard Model in the energy scales in which we are currently able to perform experiments.

There are however, some "loose ends", if one is allowed to say that. Being a QFT its predictability has been basically ruled by our ability to make perturbative computations through Feynman diagrams. But these perturbative computations require a small parameter to work, usually a coupling constant. It happens, for example, that in certain kinematical window of a typical high energy scattering process, one can find such small parameter, but beyond this the perturbative machinery fails and new approaches are needed. It is in this region where the Pomeron problem falls, an unsolved problem still nowadays which lies in the heart of the link between String Theory and QCD. The Pomeron has a long story which starts with the development of Regge theory.

Back in the days people were attempting to explain the available high energy scattering data available at the time by guessing the analytic structure of the S-matrix as a function of the Lorentz's invariants of the specific processes, like the Mandelstam variables s, t and u of a $2 \to 2$ process. It was figured out, for instance, that the

presence of poles in these variables had the meaning of bound states or resonances, and that branch points appears at threshold energies where a new set of virtual particles could be interchanged. Tullio Regge took the initiative of analyzing the analytic structure of the S-matrix in a new variable: the complex angular momentum, and he found that poles in this case indicate the interchange of an infinite set of particles. These infinite set of particles is what we call nowadays *Regge trajectories*, and it happened that the first modern high energy experiments, which started with the Stanford Linear Accelerator (SLAC) back in the 60's, could be easily explained using Regge's proposal. More precisely, the total cross-section σ_t of these experiments exhibited a power law dependence with the center of mass energy s, whose exponent could be derived from Regge theory as the "intercept" of an already observed at the time meson family of particles. Regge theory therefore provided a beautiful bridge between spectra of particles and resonances and its related scattering process. At this time the total cross-section seems to decay with the center of mass energy but with the subsequent development of the accelerator capabilities higher energies were reached and it became clear that this decay, specifically in elastic proton-proton scatterings, was no longer true after certain energy and a raise in the total cross-section was observed. It was clear at this point that another pole in the complex angular momentum plane of the scattering amplitude would be needed to explain this raising. This extra trajectory would have an intercept slightly bigger than 1 and, in opposition to the earlier case, there were not any clear candidates of families of particles or resonances compatible with this fact. Nevertheless it was basically assumed that the components of this mysterious trajectory would eventually be found, a mystery that has remained unsolved although we have learnt a lot about it, and still nowadays its existence provides a simple way to explain most of the high energy total cross-section data [7]. This trajectory was originally introduced by Gribov, who called it the pole of the vacuum, and many results were later developed by one of his students, Issak Pomeranchuk, and on his honor is known nowadays as the Pomeron. The intercept was known to be around 1.08.

Later experiments leaded to the establishment of QCD as the theory of strong interactions. Regge theory should be compatible with QCD, the dynamic of the last giving raise to the expected analytical structure in the complex angular momentum plane supported by the experiments. The most advanced computations starting from QCD to explain such structure is nowadays known as BFKL pomeron [8–10]. In this approach the Pomeron appears after the resummation of an infinite set of gluon ladder diagrams. There are still however some problems. Firstly the computation lead to a branch cut in the complex angular momentum plane instead of a discrete set of poles.

This breaks the connection with the spectrum of the theory. In recent approaches by introducing a momentum cut-off, a discrete set of poles instead was obtained such that can been confronted with HERA data [11]. Secondly, there are some technical issues in the computation. For example the next leading order NLO in the computation of the BFKL kernel was shown to be larger than the leading order LO itself, which obviously demand for the computation of the next to next to leading order NNLO, a remarkable task. Thirdly, it may be the case that the true nature of the Pomeron is non perturbative, meaning that some of its features may not be seen even if we manage to compute and sum all Feynman diagrams.

The gauge-gravity duality is a new tool to unveil QCD strongly coupled physics [12]. In particular, the Pomeron is conjectured to be the graviton Regge trajectory of the dual string theory [13]. This fact has been explored in diffractive processes dominated by Pomeron exchange, like low-x deep inelastic scattering (DIS) [14–16], deeply virtual Compton scattering [17], vector meson production [18] and double diffractive Higgs production [19].

In low-x DIS, for instance, one observes a rise of the intercept j_0 from 1.1 to ~ 1.4 as Q grows, where Q is the momentum scale of the photon probe. The conventional approach is to start from the perturbative BFKL hard pomeron [8–10], which still exhibits conformal symmetry. Introducing a cut-off, one explains the observed rise of the structures functions and even the running of the intercept, provided the cut $Q^2 > 4$ GeV^2 is imposed in the kinematics [11]. However, dual models that also start from a conformal limit and introduce a hard wall cut off in AdS space, give even better fits to data, without imposing any restriction in the kinematics [16]. This is a strong motivation in favor of treating pomeron physics using the gauge/gravity duality. The purpose of this thesis is to realize the idea of the holographic Pomeron beyond the hard wall approximation considering more realistic bottom-up approaches to holographic QCD. The ultimate goal would be to build the Regge theory of Holographic QCD.

This thesis is organized as follows. In the remaining of this chapter S-matrix fundamentals and Regge theory are reviewed. Then the AdS/CFT duality is introduced and we make a bird eye overview of the holographic QCD models existing. In particular the Soft Wall model is reviewed with more detail, particularly in the parts relevant for the present work. Then the Witten diagram expansion is reviewed. Later the dynamics of a spin 1 field in the bulk is carefully revisited, making emphasis in the logic to follow to derive the bulk-to-bulk and bulk-to-boundary propagators, showing how normalizable and non-normalizable modes enter in concrete computations and why.

Chapter 2, which is based on [20], introduces the basic machinery and discussion about how to generalize the higher spin equation of motion away from the conformal case. As result it is shown that the Soft Pomeron phenomenology can be reached. Chapter 3, which is based on [21], address the problem of explaining Deep Inelastic Scattering data, considering an extension of the kernel obtained in chapter 2. Chapter 4, which is based on [22], explores the possibility of having different couplings tensor structures between the spin 1 gauge field and the higher spin fields. Chapter 5 extends the results of chapter 3, showing that it is possible to use a single model for the Pomeron to explain both DIS and DVCS experimental data. Finally we conclude in chapter 6, making a short resume of the results obtained and discussing about possible future new lines of research.

1.1 High energy hadronic scattering and Regge theory

In this section we will review some concepts about the S-matrix program and will introduce Regge theory.

1.1.1 S-matrix properties

In quantum field theory the S-matrix is the unitary operator that connects asymptotic particle states. The matrix element for an in state $|m\rangle$ and an out state $\langle n|$ is

$$\langle n\,|S|\,m\rangle \qquad S = e^{i\alpha}U\left(\infty\right), \tag{1.1}$$

where U is the evolution operator $e^{-i\hat{H}t}$ and $e^{i\alpha}$ a phase factor [1].The S-matrix should respect the following principles in order to be meaningful:

- The superposition principle of quantum mechanics.
- The requirements of special relativity.
- The conservation of probability. This implies unitarity $S^{\dagger}S = 1$.
- The short range of the forces.

[1]Perturbatively $S = \sum_{n=0}^{\infty} \frac{(-i)^n}{n!} \int \cdots \int d^4x_1 \ldots d^4x_n \hat{T}\left(H_{int}\left(x_1\right) \ldots H_{int}\left(x_n\right)\right)$, where $H_{int}\left(x\right)$ is the interacting part of the Hamiltonian. This is known as Dyson series.

- Causality and existence of macroscopic time. This is usually replaced by the asumption that transition amplitudes are the values on the real axis of some analytic function, which mathematically is more precise and convenient.

The transition matrix $\mathcal{T}$ is defined such that

$$\langle n\,|S|\,m\rangle = \delta_{mn} + i\,(2\pi)^4\,\delta^4\,(p_m^\mu - p_n^\mu)\,\langle n\,|\mathcal{T}|\,m\rangle\,. \tag{1.2}$$

The scattering amplitude is $\mathcal{A} = \langle n\,|\mathcal{T}|\,m\rangle$. In scatterings of the type $1+2 \to 3+4$ the scattering amplitude depends on the Mandelstam variables s, t and u. Notice that only two of them are actually independent variables due to the relation $s+t+u = \sum_i m_i^2$, which have the kinematic information of the process, see appendix A. In general, for a 2 to n particle process the total cross section is

$$\sigma_t = \frac{1}{4|\boldsymbol{p}_1|\sqrt{s}} \sum_n (2\pi)^4\,\delta^4\,(p_n^\mu - p_{12}^\mu)\,|\langle n\,|\mathcal{T}|\,12\rangle|^2\,. \tag{1.3}$$

where $\boldsymbol{p}_1$ is the center-of-mass three momentum and $p_{12} \equiv p_1 + p_2$. For the transition matrix $\mathcal{T}$ unitarity of S-matrix implies

$$\langle l\,|\mathcal{T}|\,m\rangle - \left\langle l\,\middle|\mathcal{T}^\dagger\middle|\,m\right\rangle = \sum_n i\,(2\pi)^4\,\delta^4\,(p_n^\mu - p_m^\mu)\,\left\langle l\,\middle|\mathcal{T}^\dagger\middle|\,n\right\rangle\langle n\,|\mathcal{T}|\,m\rangle\,. \tag{1.4}$$

Setting $m = l = |12\rangle$ in the last expression and considering (1.3) one obtains

$$\sigma_t^{12} = \frac{1}{2|\boldsymbol{p}_1|\sqrt{s}}\mathrm{Im}\,\langle 12\,|\mathcal{T}|\,12\rangle\,. \tag{1.5}$$

Here $\langle 12\,|\mathcal{T}|\,12\rangle$ is the scattering amplitude for the process $1+2 \to 1+2$ in which the direction of motion of the particles are unchanged, that is the forward scattering amplitude $\theta_s = 0$, and σ_t^{12} the total cross section of a 2 vs 2 particle scattering. The last relation is known as the optical theorem, and it will be used while computing the structure function F_2 of Deep Inelastic Scattering (DIS) process throughout the body of this thesis. For a s-channel scattering with all masses equals $m_i = m$ the forward direction correspond to $t = 0$, thus

$$\sigma_t^{12} = \frac{1}{2|\boldsymbol{p}_1|\sqrt{s}}\mathrm{Im}\mathcal{A}\,(s, t=0)\,. \tag{1.6}$$

1.1.2 Analytic structure of the S-matrix

The underlying idea of the S-matrix program is to analytically extend the Mandelstam variables to the complex plane. The physical amplitude will be then the value on the

real axis of the correspondent analytic extension of the scattering amplitude. The poles of this complex variable function represent bound states and the branch points indicate thresholds energies. The sole fact of considering an analytic S-matrix has strong implications on the dynamic of the theory such as the Froissart bound for the total cross section and the Pomeranchuk theorem. For instance the Pomeranchuk theorem states that in the high energy limit the total cross section of a particle and the corresponding antiparticle on the same target are asymptotically the same. For example the total cross section of the process $\sigma^{tot}(\pi^+ p)$ will be asymptotically the same as the total cross section of $\sigma^{tot}(\pi^- p)$, an observed experimental fact. The derivation of the theorem is based on the analysis of the properties of the scattering amplitude on the s and u channels and on the optical theorem [23]. For an axiomatic QFT, Wightman axioms implies analyticity for some scattering amplitudes [24–26].

A hint about the existence of branch points on the real axis at the threshold energies comes from analyzing the formula (1.3): the sum over l is a sum over all possible intermediate states, as the energy grows, terms related to n particles virtual states will appear when the energy is bigger than the threshold energy for creating such states. This suggest a non analytic behavior of the total scattering cross section at the threshold energies $s = M_1^2 + \cdots + M_n^2$, as the inclusion of new terms will eventually involve a jump or discontinuity. As a consequence of the optical theorem (1.5), this behavior extends also to the imaginary part of the scattering amplitude. A rigorous proof about the interpretation of branch cuts as normal threshold was given by R. J. Eden in 1952 by analyzing Feynman diagrams for any renormalizable theory [27]. A detailed discussion can be found in chapter 4 of [28]. On the other hand, if instead a branch point there is a pole, then this non analyticity is due to the interchange of a single particle or resonance state.

The figure 1.1.2 shows the analytic structure of the scattering amplitude on the s plane for a $2 \to 2$ scattering of identical particles $m_i = m$. Although this is a simplistic case it serves to expose the main ideas about how to extract, and the meaning of, singularities in the scattering amplitude. Is is assumed also that there are not conservation laws except energy that forbids the creation of new particles. On the positive part of the real axis there is a pole at m^2, and branch points at $(km)^2$ with $k = 2, 3, \ldots$. The fact that the singularity at the unphysical value $s = m^2$ is a pole rather than a branch point can be shown using perturbation theory, unitarity and causality (section 4.5 of [28]). Branch cuts go from the branch point to infinity over the real axis by convention. For the positive real axis branch points represent the energies of normal thresholds on the s-channel.

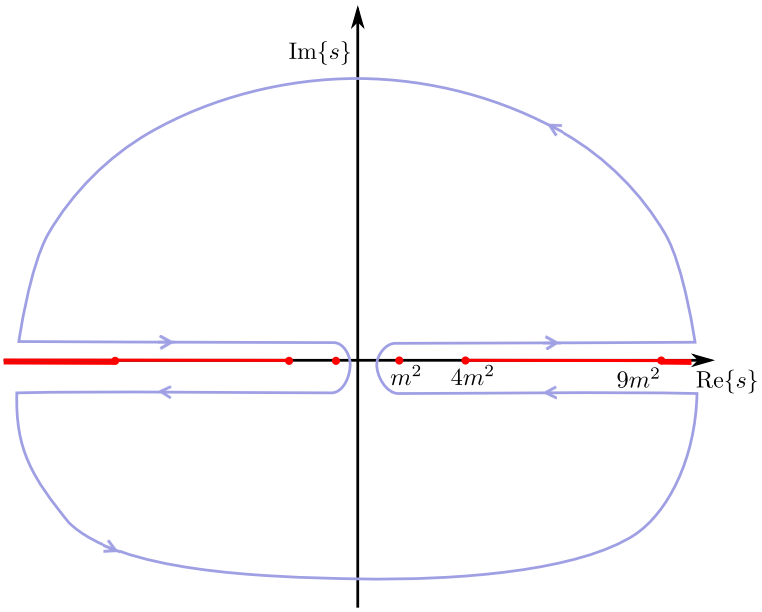

Figure 1.1: Analytic structure of the scattering amplitude $\mathcal{A}(s,t)$ for $m_i = m$, branch cuts are denoted by red lines, poles and branch points by red dots. The structure for $\mathrm{Re}\{s\} < 0$ comes from the analytic properties of the amplitude on the t-channel.

The analytic structure of $\mathcal{A}_{1+2\to3+4}(s,t,u)$ and $\mathcal{A}_{1+\bar{3}\to\bar{2}+4}(t,s,u)$ is the same because of crossing symmetry, thus considering that t has the role of s on the second amplitude one expects poles and branch points in the t plane in the same position where they appear in the s plane. For example for the case of the scattering of identical particles described by a real scalar field considering now a fixed value of $u = u_0$ then the analytic structure in the t plane can be mapped to the s plane: the pole at $t = m^2$ on the t plane is mapped to a pole at $s = 4m^2 - u_0 - m^2 = 3m^2 - u_0$ in the s plane and the branch points at $t = (km)^2$ with $k = 2, 3, \ldots$ in the t plane maps to branch points $s = 4m^2 - u_0 - (km)^2$ in the s plane. All these points fall into the negative real axis in the s plane.

1.1.3 Partial wave expansion

In many cases it is convenient to express the scattering amplitude as a function of the scattering angle and of one of the Mandelstam variables, for instance s and $\zeta = \cos\theta_s = \frac{u-t}{u+t}$ in the s-channel and similarly for other channels. In this way the unitarity condition for scattering amplitudes with a given angular momentum becomes diagonal. The expansion of the amplitude in the harmonic polynomials in d dimension is known

as the *partial wave expansion*

$$\mathcal{A}(s,t(s,\zeta)) = 16\pi \sum_{l=0}^{\infty} A_l(s)(2l+1) P_l(\zeta) \qquad s\text{-channel}, \tag{1.7}$$

where in 4 dimension $P_l(\zeta)$ are the Legendre polynomials of the first kind of order l. By inverting (1.7) the partial amplitudes can be obtained

$$A_l(s) = \frac{1}{32\pi} \int_{-1}^{1} d\zeta \mathcal{A}(s,t(s,\zeta)) P_l(\zeta). \tag{1.8}$$

The unitary condition imposes a constrain on the $A_l(s)$, which implies that in general they can be parametrized by an elasticy parameter $0 \leq \eta_s(s) \leq 1$

$$A_l(s) = \frac{\eta_s(s) e^{i\delta_l(s)} - 1}{2i\rho(s)} \qquad \delta_l(s), \rho_l(s) \epsilon \mathbb{R}, \tag{1.9}$$

which in turn implies a bound from above for the partial amplitudes $\mathrm{Im}A_l(s) \leq |A_l(s)| \leq \rho^{-1}(s)$.

The above partial wave expansion does not encode properly the expected analytic structure for the scattering amplitude: there should be poles and branch points for certain values of t as discussed before but this is not explicit in the expansion (1.7), since the polynomials $P_l(\zeta)$ never diverge as a function of t. In the complex ζ plane for a fixed physical value of s the singularities of the t channel should appear for values of $\mathrm{Re}\zeta > 1$ and similarly the u-channel poles and branch points should appear for $\mathrm{Re}\zeta < 1$. It is possible to derive an alternative expression for the partial wave amplitude in such that the expected analytic structure for the scattering amplitude is more explicit, and which also provides a basis for the analytic continuation of the partial wave expansion for complex values of l. The basic idea is to consider Legendre polynomials of the second kind $Q_l(\zeta)$, which have branch points at $\zeta = \pm 1$. Moreover, for the physical $l = 0, 1, 2, \ldots$ it is possible to choose the cuts of the amplitude to go from -1 to 1 over the real axis. The discontinuity of $Q_l(\zeta)$ across this cut is

$$Q_l(\zeta + i\epsilon) - Q_l(\zeta - i\epsilon) = P_l(\zeta) \qquad \epsilon \to 0^+. \tag{1.10}$$

This last formula can be used as a definition for $P_l(\zeta)$ and replacing it on (1.8) the partial amplitudes now are computed by integration over a closed contour on the ζ plane that encloses the cut going from -1 to 1 over the real axis and no other singularity. Deforming this contour and using Cauchy's theorem it is possible to show that [23]

$$32\pi^2 i A_l(s) = \int_1^{\infty} d\zeta' D_s(s,t(s,\zeta')) Q_l(\zeta') + \int_{-1}^{-\infty} d\zeta' D_u(s,u(s,\zeta')) Q_l(\zeta') \tag{1.11}$$

for l large enough, this is known as the *Froissart-Gribov formula*. Considering the asymptotic form of the $Q_l(\zeta)$ for large l from the previous formula it is possible to deduce the *Froissart bound* for the total cross section

$$\sigma^{tot}(s) \leq \frac{\pi}{m^2} \ln^2 \frac{s}{s_0} \tag{1.12}$$

The Froissart bound is an important constraint that suggest that single Pomeron exchange can not be what dominates scattering amplitudes at all energies, since it leads to amplitudes that grow as power law in s.

1.1.4 Regge theory

For large values of s with t fixed, the so-called Regge limit, Feynman diagrams from the t-channel dominate over the other channels. This comes from the fact that the propagators depend on $(p^2 - M^2)^{-1}$ where M is the mass of the interchanged particle, which at tree level has to be equal to s, t or u on the corresponding channel. Forward scattering ($\theta_s \to 0 \Leftrightarrow s \to \infty$, t fixed) peaks are then closely related with the interchange of particles in the t-channel and directly connected to the quantum numbers of those. An original idea from Mandelstam is to relate the asymptotic behavior in the s-channel with the partial wave expansion in the t-channel

$$\mathcal{A}(s,t) = 16\pi \sum_{l=0}^{\infty} A_l(t)(2l+1) P_l(\zeta) \qquad \zeta = \frac{u-s}{u+s} \qquad t\text{-channel.} \tag{1.13}$$

This representation is not suited for the analysis in the Regge limit as in this limit $\zeta \to \infty$ and $P_l(\zeta) \sim \zeta^l \sim s^l$ thus the series diverges. It is convenient then to extend analytically (1.13) from the values where it is well defined, $t \geq \sum_i m_i$ and $s, u < 0$, up to the values we need $s \geq \sum_i m_i$ and $t, u < 0$. In order to do so one has to replace the $A_l(t)$, which are defined for l integer and positive, with new functions $a(l,t)$ which are defined for any l and coincide with $A_l(t)$ for $l = 0, 1, 2, \ldots$. The reader should notice that this does not define $a(l,t)$ uniquely, as one can add any function $f(l,t)$ which is zero for $l = 0, 1, 2 \ldots$ and the new $a(l,t)$ still fits the previous definition. It is the asymptotic behavior of the scattering amplitude, together with the Carlson theorem[2] and the Froissart-Gribov formula (1.11), what makes the definition unique.

It is not possible to achieve this analytic extension in a relativistic theory with only one function $a(l,t)$, but with two $a^{\pm}(l,t)$

$$a^{+}(l,t)|_{l=n=2k} = a(n,t) \qquad a^{-}(l,t)|_{l=n=2k+1} = a(n,t) \qquad k \in \mathbb{N}. \tag{1.14}$$

[2] In a few words it states that two different analytic functions which do not grow very fast at infinity can not coincide at the integers.

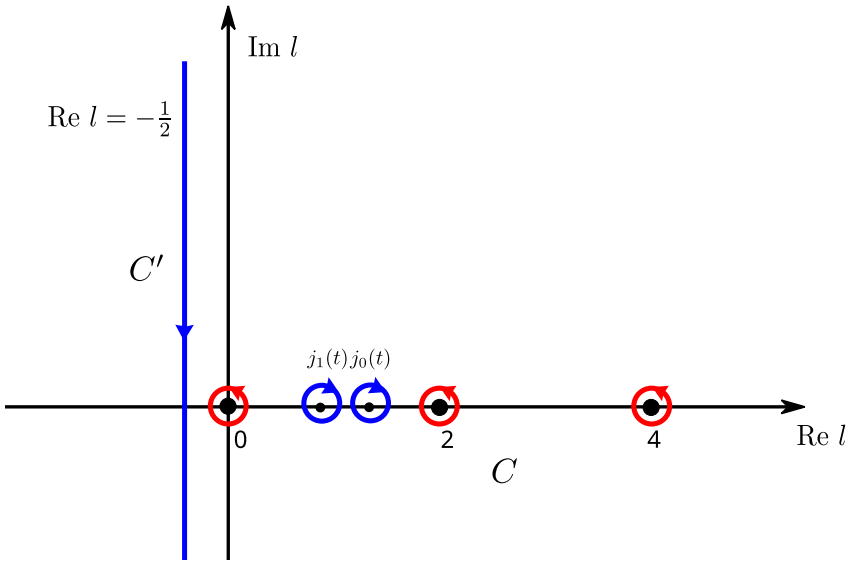

Figure 1.2: Illustration of the Sommerfeld-Watson transform for $\mathcal{A}^+$. The original contour C is the red one while the deformed one C' is the blue. Big points over the real axis represent the integer values over which the original sum runs, small points denote possible poles in $\mathcal{A}^+(l)$ existing for non integer values of $l = j_0, j_1, \ldots$. The position of these poles depends on t.

The amplitude is then $\mathcal{A}(s,t) = \mathcal{A}^+(s,t) + \mathcal{A}^-(s,t)$, where

$$\mathcal{A}^{\pm}(s,t) = 16\pi \sum_l a^{\pm}(l,t)(2l+1)\left(P_l(\zeta) \pm P_l(-\zeta)\right) \qquad l = \begin{cases} + & 0,2,\ldots \\ - & 1,3,\ldots \end{cases}. \tag{1.15}$$

In order to do an analytical extension the sum is written as an integral over the l complex plane around a contour C as illustrated in the figure 1.1.4

$$\mathcal{A}^{\pm}(s,t) = 8\pi i \int_C dl\,(2l+1)\,a^{\pm}(l,t)\,\frac{P_l(\zeta) + P_l(-\zeta)}{\sin(\pi l)}. \tag{1.16}$$

This is called Sommerfeld-Watson transformation. The $a(l,t)$ are analytic extensions of the $A_l(t)$ on (1.13) for complex values of l. In the Regge limit it is more useful to write the above transformation in a different way taking advantage of the asymptotic form of the Legendre polynomials. In this limit ($\zeta \to \infty$) they are well approximated by

$$P_l(\zeta) \simeq \frac{\Gamma\left(l+\frac{1}{2}\right)}{\sqrt{\pi}\Gamma(l+1)}(2\zeta)^l \simeq \frac{\Gamma\left(l+\frac{1}{2}\right)}{\sqrt{\pi}k_t^{2l}\Gamma(l+1)}s^l \qquad \zeta \simeq \frac{s}{2k_t^2}. \tag{1.17}$$

Using this one can write the asymptotic form of the Sommerfeld-Watson transform after deforming the original contour which only included non negative integer poles

up to a vertical line $\mathrm{Re}\{l\} = a$,

$$\mathcal{A}^{\pm}(s,t) = 8\pi i \int_{a-i\infty}^{a+i\infty} dl \mathcal{A}^{\pm}(l,t) \frac{s^l \pm (-s)^l}{\sin(\pi l)}, \tag{1.18}$$

$$\mathcal{A}^{\pm}(l,t) \equiv \frac{\Gamma\left(l+\frac{1}{2}\right)}{\sqrt{\pi} k_t^{2l} \Gamma(l+1)} (2l+1) a^{\pm}(l,t). \tag{1.19}$$

The form (1.18) is particular useful as it can be interpreted as some kind of inverse Mellin transform [3]. Indeed, for example for $\mathcal{A}^+$ taking the imaginary part of (1.18).

$$\mathrm{Im}\mathcal{A}^+(s,t) = \int_{l_0-i\infty}^{l_0+i\infty} \frac{dl}{2\pi i} s^l \mathcal{A}^+(l,t), \tag{1.20}$$

we realize that $\mathrm{Im}\mathcal{A}(s,t)$ is the inverse Mellin transform of $\mathcal{A}(l,t)$, therefore inverting this expression we can find

$$\mathcal{A}^+(l,t) = \int_0^{\infty} ds s^{-l-1} \mathrm{Im}\mathcal{A}^+(s,t). \tag{1.21}$$

Now we proceed to find the asymptotic form of the amplitude in the Regge limit. The contour C is deformed up to C', which is the vertical line $\mathrm{Re}l = -\frac{1}{2}$ plus a closing path which is a infinite semicircle that closes the contour by the right. The integral over C' can be computed by summing the residues of the integrand on the singularities enclosed by C'. The integrand have two sets of singularities: the poles at integer values of l which come from the $1/\sin(\pi l)$ factor, and the singularities of $\mathcal{A}^{\pm}(l,t)$ which, to keep the discussion simple, we will assume to be simple poles at $j_i(t)$. The integral over the semicircle goes to zero as $|l| \to \infty$ as long as the $\mathcal{A}^{\pm}(l,t)$ does not grow exponentially in l. In the Regge limit $s \to \infty$ the integral over the vertical line $\mathrm{Re}l = -\frac{1}{2}$, vanish as $s^{-1/2}$, so the integral over C' vanishes. Then the sum over the residues on integer values of l, which give the original amplitude, have to be minus the sum over the residues on $j_i(t)$

$$\mathcal{A}^{\pm}(s,t) \sim \sum_i \beta_i^{\pm}(t) \Gamma\left(-j_i^{\pm}(t)\right) \left(1 \pm e^{i\pi j_i^{\pm}(t)}\right) \left(\frac{s}{s_0}\right)^{j_i^{\pm}(t)}. \tag{1.22}$$

The last expression is known as the Regge form of the scattering amplitude, the factors $\xi_j^{\pm} = 1 \pm e^{i\pi j_i^{\pm}(t)}$ are known as signature factors. In the appendix A of [23] it is shown that for t values in the s-channel physical region, the amplitudes $\mathcal{A}^{\pm}(s,t)$ are real for real l as well as the position of the poles $j_i^{\pm}(t)$ and the values of the residues $\beta_i^{\pm}(t)$, thus the phase of the high energy behavior of a Regge pole contribution is given by the signature factors.

[3] Additional information can be found in section 12 of [29].

There is a beautiful interpretation of the Regge form of the scattering amplitude in terms of the interchange of particles in the t channel. The poles of (1.22) come from the gamma function and are at $j_i^{\pm}(t) = 0, 1, 2, \ldots$. At this points the signature factor ξ_j^+ vanish if $j_i^{\pm}(t)$ is odd so the positive signature amplitude has poles at those values of t such that $j_i^+(t) = \sigma^+ = 0, 2, 4, \ldots$ and similarly for the negative signature amplitude. This will allow to identify these poles after some work with the interchange of particles of spin $\sigma^{\pm}$ and mass squared t. Indeed, it is possible to write the poles in the l-plane as poles in the t-plane and writing the leading term of the amplitude close to the pole, it is possible to cast it into the Breit-Wigner form for a resonance of mass $m_R^2 = t$ and width $\Gamma_i = \frac{\text{Im } j_i^{\pm}(m_R)}{j_i^{\pm\prime}(m_R)}$. This is for Im $j_i^{\pm}(m_R) > 0$, if Im $j_i^{\pm}(m_R) = 0$ then the singularity is associated with a bound state rather than a resonance. It can be said then that poles in the $\mathcal{A}^{\pm}(s,t)$ are associated with resonances or bound states being exchange in the t-channel with mass $m_R^{\pm}$ given by:

$$\text{Re } j_i^+\left(m_R^{+2}\right) = \sigma^+ = 0, 2, 4, \ldots \tag{1.23}$$

$$\text{Re } j_i^-\left(m_R^{-2}\right) = \sigma^- = 1, 3, 5, \ldots \tag{1.24}$$

The aforementioned allow us to interpret the Regge form for the scattering amplitudes as the amplitudes produce by the interchange of a family of particles, those that are in the Regge trajectory, in the Regge limit. The interchange of an entire family of particles lying on the same Regge trajectory is usually expressed as the interchange of a single pseudo-particle called *Reggeon*, which represents the whole family interaction. It is possible to go one step forward and consider now the exchange of several Reggeons, this is known as *Reggeon calculus* and was originally developed by Gribov. Unfortunately this technique has not produced meaningful quantitative results, but has shown to be useful to the analysis of the analytic structure of the Regge amplitudes.

1.1.5 Deep Inelastic Scattering and low x

The high energy version of the Rutherford experiment is nowadays known as Deep Inelastic Scattering (DIS). This is the process where an electron, or another lepton, scatters off a proton with such high energy that the internal structure of the proton becomes manifest. This process provided the first convincing evidence of the existence of quarks, as well as to the idea that baryons were formed by three quarks and mesons by a quark and anti-quark. It is considered that modern high energy physics have born in the sixties with the advention of the Standford Linear Accelerator, where the first DIS experiments were done.

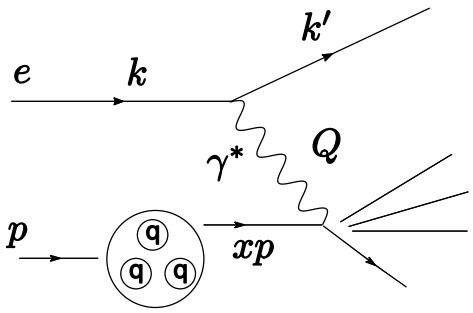

Figure 1.3: QCD picture of Deep Inelastic Scattering process.

The inleastic part in the name is because the scattering produces many other hadrons as final state. In QCD, effectively, the leading interaction between the electron and the proton comes from the emission of an *off-shell* photon with momentum $q = k - k'$ from the electron, or the corresponding lepton, which then struck off a quark from inside the proton which carries a certain fraction of the proton momentum, so the process become effectively a virtual Compton scattering. In the Regge limit this process is dominated by the subprocess in which the virtual photon decomposes into a quark-antiquark pair, a color dipole, which then interacts with the quark struck off the proton by the exchange of ladder-like diagrams of gluon propagators.

In the analysis of DIS is conventional to define the following variables[4]

$$Q^2 = -q^2 \qquad \nu = p \cdot q \qquad x = \frac{Q^2}{2\nu} \qquad y = \frac{p \cdot q}{p \cdot k}. \tag{1.25}$$

Then $Q^2 \geq 0$ and $0 \leq x \leq 1$. In the parton model x is the fraction of the proton momentum carried by the struck quark. The center-of-mass energy of the scattering $\gamma^* p$ is usually denoted by W, then W^2 is just the s Mandelstam variable for such scattering. In terms of the above defined variables

$$W^2 = Q^2 \left(\frac{1}{x} - 1 \right) + m^2, \tag{1.26}$$

with m the mass of the proton. Following QCD rules the cross-section of the process in the lowest order of perturbation theory can be written as a contraction of a leptonic and hadronic tensors[5]

$$\frac{d^2\sigma}{dxdy} = \frac{2\pi y \alpha}{Q^4} L^{\mu\nu} W_{\mu\nu}, \tag{1.27}$$

[4]Let's point out that in the next chapters we will use instead $Q^2 \equiv q^2$, a change of sign due to the fact that we will use, in opposition to the most used convention in particle physics, the metric signature usually used in General Relativity $(-,+,+,+)$ with $x^0 \equiv t$.

[5]In this section we will consider only neutral-current processes.

where α is the fine structure constant. For incoming leptons of charge $e = \pm 1$ and helicity $\lambda = \pm 1$

$$L_{\mu\nu} = 2\left(k_\mu k'_\nu + k_\nu k'_\mu - (k \cdot k' - m_l^2) - i\epsilon_{\mu\nu\alpha\beta}k^\alpha k'^\beta\right). \tag{1.28}$$

The hadronic tensor, which describe the interaction of the electroweak currents with the target nucleon can be found to be

$$W_{\mu\nu} = \frac{1}{4\pi}\int dx e^{iq\cdot x}\langle P|\left[J_\mu^\dagger(x), J_\nu(0)\right]|P\rangle. \tag{1.29}$$

Using now gauge, Lorentz and time reversal invariance plus parity conservation and considering unpolarized beams we can decompose the hadronic tensor as

$$W_{\mu\nu} = \left(-\eta_{\mu\nu} + \frac{q_\mu q_\nu}{q^2}\right)F_1(x,Q^2) + \frac{\hat{p}_\mu \hat{p}_\nu}{p\cdot q}F_2(x,Q^2), \qquad \hat{p}_\mu \equiv p_\mu - \frac{p\cdot q}{q^2}q_\mu. \tag{1.30}$$

The F_1 and F_2 are known as *structure functions*, and contain all the non trival information encoded in the hadronic tensor. The differential cross-section in terms of these functions is then

$$\frac{d^2\sigma}{dxdy} = \frac{4\pi\alpha^2}{xyQ^2}\left((1-y)F_2 + xy^2F_1 - \frac{m^2}{Q^2}x^2y^2F_2\right) \tag{1.31}$$

Electromagnetic current conservation implies $q_\mu W^{\mu\nu} = q_\nu W^{\mu\nu} = 0$, which implies that, at fixed W, F_2 should go linearly to zero with Q^2.

For both theoretical and phenomenological reasons it is convenient to think DIS as a $\gamma^* p$ scattering. Using the optical theorem the total cross-section of such process is related to the imaginary part of its amplitude, and the last is given by the expectation value of the time ordered product of the hadronic current $e^2T_{\mu\nu}$, known as the Compton tensor. Considering the scattering of a virtual photon has some subleties. For example for computing such total cross-section one in principle needs to define what is the flux factor of γ^*. The most used convention is that the flux is given by the energy that a real photon would need to create the final state, and is the one we will use. Also since the photon is not on its mass shell there are contributions coming from states with longitudinal polarizations. Is not hard to show that [30] the relation between the structure functions and the total cross-section of the virtual process with the above convetion is the following

$$\sigma_T = \frac{4\pi\alpha}{Q^2}2xF_1, \tag{1.32}$$

$$\sigma_T + \sigma_L = \frac{4\pi\alpha}{Q^2}F_2, \tag{1.33}$$

where σ_T and σ_L are the total cross-section of the virtual processes $\gamma^* p \to X$ with the virtual photon having transverse and longitudinal polarization respectively. We will be using extensively the last formula in chapters 3, 4 and 5, using the gauge/string duality to compute the correspondent total cross-sections and therefore computing F_2 and comparing with real data.

1.1.6 Pomeron in QCD

As we have already mentioned, after the consolidation of QCD as the theory of strong interactions many efforts were done aiming to find the analytical structure of the scattering amplitude that Regge theory suggested in order to explain experimental data. In this section we will overview the most prominent advaces in this sense, the BFKL approach, the BK improvements and the color glass condensate.

BFKL

The BFKL pomeron [8–10], also known as the hard or perturbative pomeron, is an effort to find the leading contributions from perturbative QCD in the low x regime. In this approach, the Pomeron is obtained in the leading $\ln s$ approximation by considering color singlet ladder diagrams, which can be shown to be the leading contributing diagrams. In this diagrams loop corrections are taken into account by replacing the gluon's propagators by effective ones, the effective gluons being exchange in this sense are called "reggeized" gluons. These "reggeized" gluons couple to the ladder rung through effective vertices. We will not describe the derivation of the effective propagators and vertices here, instead we will fast forward to the BFKL equation. The goal is to compute the amplitude for quark-quark elastic scattering via the exchange of a color singlet. The incoming quarks have momentum p_1, p_2 and helicity λ_1, λ_2, and the outgoing quarks have momentyum $p_1 - q$, $p_2 + q$ and helicity λ_1', λ_2'. The BFKL equation at $t = 0$ is[6]

$$\omega f = \delta^2 \left(\boldsymbol{k_1} - \boldsymbol{k_2} \right) + \mathcal{K}_0 \cdot f, \tag{1.34}$$

where

$$\mathcal{K}_0 \cdot f = \frac{\bar{\alpha}_s}{\pi} \int \frac{d^2 \boldsymbol{k'}}{\left(\boldsymbol{k_1} - \boldsymbol{k'} \right)^2} \left[f - \frac{{\boldsymbol{k_1}}^2}{{\boldsymbol{k'}}^2 + \left(\boldsymbol{k_1} - \boldsymbol{k'} \right)^2} f \right]. \tag{1.35}$$

[6]In this section we will denote the complex angular momentum variable as ω, in opposite of J which is used for the rest of the thesis. This is to stick to the same convention usually used in BFKL approaches.

The function $f = f(\omega, \boldsymbol{k_1}, \boldsymbol{k_2}, t = 0)$ is related to the amplitude through a Mellin transform as follows

$$\int_1^\infty d\left(\frac{s}{\boldsymbol{k^2}}\right)\left(\frac{s}{\boldsymbol{k^2}}\right)^{-\omega-1}\frac{\mathcal{A}^{(1)}(s,t)}{s} = 4i\alpha_s^2\delta_{\lambda_1'\lambda_1}\delta_{\lambda_2'\lambda_2}G_0\int\frac{d^2\boldsymbol{k_1}d^2\boldsymbol{k_2}}{\boldsymbol{k_2}^2\,(\boldsymbol{k_1}-\boldsymbol{q})}f(\omega,\boldsymbol{k_1},\boldsymbol{k_2},\boldsymbol{q}), \tag{1.36}$$

where $G_0 = \frac{2}{N^3}\mathrm{Tr}\left(\tau_a\tau_b\tau_c\right)^2$ is called the color factor[7]. The equation (1.34) is an integro-differential equation which can be solved using a spectral decomposition for the kernel operator $\mathcal{K}_0$ in a suitable basis that diagonalizes it

$$\mathcal{K}_0\cdot\phi_i(\boldsymbol{k}) = \lambda_i\phi_i(\boldsymbol{k}). \tag{1.37}$$

We will omit here the details of the computation, instead we will just write here the result

$$f(\omega,\boldsymbol{k_1},\boldsymbol{k_2},\boldsymbol{0}) = \sum_{n=0}^{\infty}\int_\infty^\infty d\nu\frac{k_1^2}{k_2^2}\frac{e^{in(\theta_1-\theta_2)}}{2\pi^2k_1k_2}\frac{1}{\omega-\bar{\alpha}_s\chi_n(\nu)}, \tag{1.38}$$

$$\chi_n(\nu) = 2\int_0^1 dz\frac{z^{(n-1)/2}\cos\left(\nu\ln z\right)-1}{1-z} = 2\left(-\gamma_E - \mathrm{Re}\left[\psi(\frac{n+1}{2})+i\nu\right]\right), \tag{1.39}$$

where $\gamma_E \approx 0.577$ is the Euler's constant and ψ is the digamma function. From the equation (1.38) we can see that since the variable ν is continuous we do not get isolated poles which can be associated with the intercept of the Pomeron. Instead we get a branch cut in the complex angular momentum plane, which a branch point at $\omega_0 = 4\bar{\alpha}_s\ln 2$ as can be shown by doing the appropriated asymptotic analysis. So we simply do not get the Regge picture directly from this [8].

Among the criticism that the BFKL approach receives is that, being a perturbative computation, it will fail to capture any of the possible non-perturbative effects related to the Pomeron. Also the previous computation was done under the assumption that the coupling $\bar{\alpha}_s$ does not run considerably within the energy scale of the process, which is essentially not true for a variety of interesting process like DIS. Moreover, the next to leading order (NLO) in the $\ln s$ contribution to the scattering amplitude turned out to be larger than the leading order, requiring the NNLO computation to be done with the hope that could counteract with the NLO to give a meaningful result.

BK

The Balitsky–Kovchegov equation (BK) corresponds, as BFKL, to a re-summation of the leading terms in $\ln s$. It is an integro-differential equation that, given the

[7] The τ_a are the gerators of $SU(3)$ in the fundamental representation.

[8] Some variations can indeed lead to the picture of the set of poles in the ω plane, see for example [11].

initial condition which is the dipole-hadron scattering amplitude, gives the evolution of scattering amplitude at any rapidity y. This initial condition however is essentially a non-perturbative object and has to be modeled. In the limit of large number of colors N_c it can be shown to be a sum of fan diagrams of BFKL ladders [31]. The equation was derived by Balitsky [32] by using the OPE in QCD to derive a hierarchy of coupled evolution equations[9] which in the limit of large N_c becomes a single one. Kovchegov derived a similar equation by considering instead the dipole mode in high energy scattering [33].

We will describe now the motivation and the ingredients of the equation following [34]. The starting assumption is that at high enough energy scattering particles move across its straight line classical path and quantum effects manifest only through a phase adquired along this path. This eikonal phase factor for a fast quark or gluon scattering off some target is just a Wilson line

$$U^{\eta}\left(x_{\perp}\right)=\mathcal{P}\exp\left(ig\int_{-\infty}^{\infty}dun_{\mu}A^{\mu}\left(un+x_{\perp}\right)\right), \tag{1.40}$$

where A^{μ} is the gluon field of the target, $x_{\perp}$ is the transverse position of the particle which does not change during the collision, n^{μ} is a unit vector in the direction of the velocity and η the rapidity of the particle. In Deep Inelastic Sattering, the virtual photon decomposes into a quark-antiquark pair, a color dipole, which move along straight lines very fast. Then the structure function of a hadron would be proportional to a matrix element of the color dipole operator

$$\hat{\mathcal{U}}^{\eta}\left(x_{\perp},y_{\perp}\right)=1-\frac{1}{N_c}\mathrm{tr}\left\{U^{\eta}\left(x_{\perp}\right)U^{\dagger\eta}\left(y_{\perp}\right)\right\}. \tag{1.41}$$

The BK equation is an evolution equation for the last operator with the rapidity η. To the leading logarithmic approximation (LLA), where $\alpha_s \ll 1$ and $\alpha_s \ln x \sim 1$ the equation reads

$$\frac{d}{d\eta}\hat{\mathcal{U}}\left(x,y\right)=\frac{\alpha_s N_c}{2\pi^2}\int d^2z\frac{(x-y)^2}{(x-z)^2(z-y)^2}\Big[\hat{\mathcal{U}}\left(x,z\right)+\hat{\mathcal{U}}\left(y,z\right)-\hat{\mathcal{U}}\left(x,y\right)-\hat{\mathcal{U}}\left(x,z\right)\hat{\mathcal{U}}\left(z,y\right)\Big] \tag{1.42}$$

The linear part of this equation is equivalent to the BFKL equation and describes parton emission. The non linear part, which comes from the last term in (1.42), encodes parton annihilation, and for large enough values of x this term balances the

[9] This hierarchy of equations is known also as JIMWLK = Jalilian-Marian, Iancu, McLerran, Weigert, Leonidov, Kovner.

emission terms giving rise to *saturation*, with the characteristic scale Q_s growing with x^{-1}.

Among the advantages of the BK approach with respect to BFKL is the fact that BK solutions ensure unitarity locally in the transverse configuration space. From the phenomenological point of view the solutions of the BK equation turned out to express geometric scaling phenomena observed in lepton-proton and lepton-nucleus data, see for instance [35].

To our knowledge there is little understanding up to the present day how the BK equation may rise in the context of holographic QCD, so we think this could be a good pursuit for future works, which perhaps could point how to solve the unitary problems of the holographic Pomeron.

Color glass condensate

The *color glass condensate* is an effective field theory that describes the behavior of the supposed to be relevant degrees of freedom in the Regge limit $x \to 0$ of high energy scatterings. Intuitively, the scattering between a probe particle and the hadron occur in such a high energy scale such that what the probe "sees" is a very dense set of hadronic constituents, a sort of compact conglomerate of quarks and gluons. In this framework, these degrees of freedom are the color sources ρ at large x and the gluon fields A^μ at small x. At large energies, due to time dilatation, the color sources are frozen in the time scale of the strong interactions and are assumed to be randomly distributed from event to event. Then the gluon fields are the only dynamical fields in this frozen background. The "glass" part comes from the fact of the stochastic nature of the sources ρ and the time scales separation, characteristic of glassy system. The "condensate" part comes from the fact that saturated gluon states have large occupation numbers of order $1/\alpha_s$.

Figure 1.4 shows qualitatively a QCD evolution phase diagram. As it is well known, the evolution of the structure functions with Q^2 is well explained by the DGLAP equation. For the evolution in small x, the BFKL approach would be valid up to the scale where saturation effects become important, which is depicted in the figure by a straight line. It is in the region above this line where the color glass condensate theory should be valid.

Color glass condensate and its derived models have been successfully used to explain semi-quantitatively the phenomenology of high energy hadron-hadron and lepton-

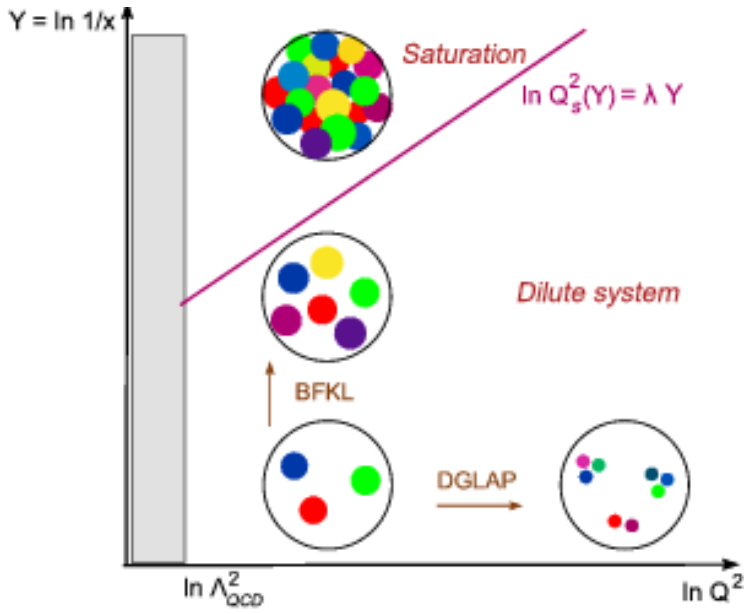

Figure 1.4: QCD evolution phase diagram, partons are represented by the small colored circles. Taken from [1].

hadron scatterings. The approach becomes better at the highest energies where the coupling is small and in consequence the occupation number is high. It is in this sense that it is believe that experiments at LHC can provide a good test of this theory. The connection between the color glass condensate and the traditional language of Regge theory of Pomerons is so far under development, therefore little is known about a possible interpretation of this idea in the context of the gauge/gravity duality.

We end this review of the Pomeron in the context of QCD by pointing out that an initial condition for the solution of the evolution equations is usually an input that has to be modeled, it can not be predicted. We will see later that in our Holographic QCD approach there is not such freedom: the $5d$ modes that enter in the computation of scattering amplitudes, which somehow are the equivalent of such initial conditions, are fixed first by matching spectral data, in the same way people used Regge theory in the S-matrix theory days.

1.2 AdS/CFT and Holographic QCD

The discovery of the AdS/CFT duality by J. Maldacena [12] gave a new different perspective about how to tackle computations of correlation functions in QFTs at their

strong coupling regime. The original results, and its many extensions, conjecture that there exist a duality between a (super) gravity theory or string theory in a AdS_{d+1}, and some CFT living on the boundary of this space. The duality between $SU(N)$ Yang-Mills and string theories were suggested long ago by t'Hooft and Polyakov, among others, by pointed out the resemblance of the perturbative expansion in Feynman diagrams in the gauge theory with the genus expansion in string theory, particularly in the large N limit. Early evidence towards these dualities included the map between the conformal group in d dimensions and the isometries of AdS_{d+1} space and the correspondency between the entropies of near extremal p-brane solutions and $p+1$ dimensional SYM among others. While there is still a lack of a formal proof, the subsequent discovery of integrability structures in the spectrum of both $\mathcal{N}=4$ SYM and semi classical TYPE IIB strings in $AdS_5 \times S_5$, the most studied and original duality, highly boosted our understanding about how the duality work, confirming always its validity. A large but pedagogical review of these results can be found in [36]. Among the non-supersymmetric examples we can find the conjectured duality between the $O(N)$ vector model and Vasiliev's higher spin gauge theories, first proposed by Klebanov and Polyakov [37] and first checked by Giombi and Yin [38] at the level of three point functions.

The statement of the duality can be enounced in the form

$$Z_{QFT}[J(x)]_{\partial\mathcal{M}} = Z_{gravity}[\phi(X)]_{\mathcal{M}}, \qquad \phi(X \to \partial\mathcal{M}) = J(x), \tag{1.43}$$

where $\mathcal{M}$ is a manifold which looks as AdS spacetime at its boundary $\partial\mathcal{M}$, $J(x)$ is the source of some operator $\mathcal{O}$ and $\phi(X)$ its associated dual field. The main motivation towards the study of these dualities, also known as gauge/gravity dualities, comes from the fact that usually they relate two different quantum theories at different regimes, mapping the strong/weak coupling behavior of one to the opposite regime in the other. Specifically, for $\mathcal{N}=4$ and type IIB strings in $AdS_5 \times S_5$, the relation between the gauge theory coupling constant and its string theory counterpart is the following

$$\frac{L^4}{l_s^4} = g_{YM}N = \lambda, \tag{1.44}$$

where λ is the t'Hooft coupling and L is the AdS radius. From this we can see that stringy corrections in the bulk will not be important as long as $l_s/L \ll 1$ which translate to λ large at the boundary. Thus computation of correlation functions in gauge theories at large coupling values, where perturbation theory requires many or infinite loop computations, can instead be mapped to a perturbative expansion in the dual theory, which would be weakly coupled. In spite of being around many years,

$SU(N)$ Yang-Mills theories still are mostly studied through the perturbation theory developed by Feynman and Schwinger, which works for those energy scales where its coupling is small. But many interesting problems lie beyond this scope, like the computation of mass spectrum of bound states, and in addition there may exist truly non-perturbative features which will not appear even at all loop computations. In this sense there exist a demand for new approaches and it is the hope of many that the gauge/gravity duality could solve or shed some light where conventional perturbation theory fails. The main obstacle however persist: the dual of $SU(N)$, or QCD, is not known yet, and there is not even a guarantee that it exist. Nevertheless the progress made in the understanding of dualities which involve similar theories, usually with some degree of supersymmetry, is encouraging. In the next subsection we will discuss the state of the art approaches to build the dual of certain sectors of QCD, making particular emphasis in the bottom-up approaches which are the one we choose to use in the studies carried on in this thesis. After we will describe the Witten's diagram expansion, which is what turns the duality into a computational machinery.

1.2.1 Overview of the holographic QCD models

As previously commented, much has been learnt about the AdS/CFT duality for the canonical case of $\mathcal{N} = 4$ SYM and strings in $AdS_5 \times S_5$, specially due to integrable structures discovered in certain sectors of both theories. While this duality has passed all kind of tests, the path to the dual of QCD, or alternatively large N Yang-Mills, remains elusive. The so called top-down approaches aim to solve the problem by proposing configurations where the Yang-Mill theory lives in the world volume of some branes. From the theoretical perspective this is the most interesting approach. The best known model obtained this way is the Sakai-Sugimoto model [39,40], which is an improved version of the Witten model, manage to explain some features of QCD at strong coupling like meson spectra, gluon condensate and the masses of some baryons. An updated review with the model improvements of last years can be found in [41].

In an effort to evade many theoretical problems to reach such goal and with the aim of not being strictly rigorous but to provide some guidance, many authors have adopted the bottom-up approach to the problem. Bottom-up approaches do not attempt to derive the bulk theory as an effective string field theory, rather it assumes the bulk theory exist and attempts to tame its shape according with the features known from QCD, both theoretical and experimental. Early attempts considered the introduction of a "hard wall" in the bulk, considering still an AdS metric, restricting where the

dual fields should live. This theory give a spectrum for the particles that goes linearly with the resonance index: $m_n \sim n$, which does not matches the pattern of known resonances masses, like for instance the mesons, which instead exhibit a behavior of the type $m_n^2 \sim n$. In a very interesting paper [42] Karch, Katz, Son and Stephanov have addressed this problem in a string theory inspired way by proposing the inclusion of a dilaton background field together with the metric, showing that choosing a suitable asymptotic behavior for both the warp factor $A(z)$ and the dilaton $\Phi(z)$, it can lead to linear spectrum in both the resonance number and spin. It should be stress that in this model neither the metric or the dilaton are considered to be dynamical fields, issue somehow addressed, among others, in the Improved Holographic QCD model [43, 44]. Since this is an important point which is widely used as guidance by many authors while constructing bottom-up approaches we review it in the next subsection.

1.2.2 The Soft Wall model

As already commented one of the most interesting challenges that AdS/CFT faces is about breaking conformal symmetry such that one obtains QCD in the boundary. It is expected that the warp factor $A(z)$ of the dual theory differ from AdS value $-\ln z$ as long as we move away from the holographic UV at $z = 0$, giving a non trivial renormalization group flow. From the string theory perspective it is also expected that in the supergravity approximation background fields, like the dilaton Φ, have non trivial profiles, in other words, they should be function of the warped spacetime radial coordinate. But computing these profiles from first principles in string theory is a formidable task. If QCD has a dual, it is natural then to ask what would be a suitable choice of such backgrounds such that we get the known experimental spectrum for hadronic resonances. We already saw that the simplest and crude way of breaking conformal symmetry, the hard wall model, leads to the wrong spectrum $m_n \sim n$ for the mesons. As a solution for the problem, the authors of the nowadays known as Soft Wall model [42], propose to consider instead a non trivial warp factor and dilaton profile such that they effectively create a "soft" wall, rather than an abrupt spacetime cut. More specifically, given the knowledge we have about the spectrum of mesons, which basically can be resumed in the fact that masses squared go linearly with the spin and the radial number n, what would be a suitable choice for $A(z)$ and $\Phi(z)$ such that the experimental spectrum is realized? It turns out that the answer is very simple and impose non trivial asymptotic behavior for both $A(z)$ and $\Phi(z)$ in the IR.

By considering backgrounds of the type[10]

$$S = \int d^5X\sqrt{g}e^{-\Phi}\mathcal{L}, \qquad ds^2 = e^{2A(z)}\left(dz^2 + \eta_{\mu\nu}dx^\mu dx^\nu\right), \tag{1.45}$$

with $\mathcal{L}$ the lagrangian density of the dual fields they arrive to the conclusion that at large z, or equivalently at the IR, the functions $\Phi(z)$ and $A(z)$ should satisfy $\Phi - A \sim z^2$ in order to guarantee a linear spectrum of the ρ mesons in the radial quantum number. In addition, if one analyzes how to impose linear Regge trajectories in the spin by considering now higher spin mesons then one finds that $A(z)$ should not grow as z^2 in the IR. On the other hand conformal invariance in the UV impose $\Phi - A \sim \ln z$. The simplest solutions to these constrains is $A(z) = -\ln z$ and $\Phi(z) = z^2$, however it should be expected a more complicated solution for a real dual effective field theory in the bulk for QCD gauge invariant operators, since this proposal give a trivial renormalization group flow, given that the metric is always AdS.

In the heart of the Soft Wall model, as we as in many of the papers that seek for holographic dynamical solutions, like Improved Holographic QCD [43,44], lies the fact that the following potential for a Schrodinger problem

$$U_2(z) = \frac{b^2-1}{4z^2} + \frac{9z^2}{4R^4}, \tag{1.46}$$

gives a linear spectrum

$$t_n = \frac{6}{R^2}n + \frac{3(b+2)}{2R^2}, \qquad n = 0, 1, 2, ... \tag{1.47}$$

$$\phi_n(z) = \left(\frac{3}{2}\right)^{\frac{b}{4}} \sqrt{\frac{3\Gamma(n+1)}{R\Gamma\left(\frac{b}{2}+n+1\right)}} \left(\frac{z}{R}\right)^{\frac{b+1}{2}} e^{-\frac{3z^2}{4R^2}} L_n^{\frac{b}{2}}\left(\frac{3z^2}{2R^2}\right) \tag{1.48}$$

If we assume that our experimental data have a linear spectrum, clearly from the distance between eigenvalues (masses) one would like to explain one can read $R = 6/\Delta$ with $\Delta \equiv t_{n+1} - t_n$. With this and with the value of the ground state one can then read the constant b. Here we changed slightly the notation with respect to [42] following closer [43,44], which is the model that is used mostly in this thesis. In particular we will see that the potential (1.46) is the one of the spin 2 glueballs for $b = 4$ and $R = 1$. In the next subsection we will review the derivation of the results commented in this section.

[10] Along this thesis we will use latin indices $a, b, \ldots$ to indicate 5d indices and greek indices $\mu, \nu, \ldots$ for the boundary 4d indices.

ρ mesons

As usual, the starting point is the assumption that there exists a local effective action in the bulk that is dual to the QCD gauge invariant operators that create the mesons. The proposed action to describe axial and vector fields is

$$\int d^5X\sqrt{g}e^{-\Phi(z)}\left(-|DX|^2+3|X|^2-\frac{1}{4g_5}\left(F_L^2+F_R^2\right)\right). \tag{1.49}$$

The overall factor $e^{-\Phi(z)}$ is consistent with the coupling of open strings. To get the spectrum of the ρ mesons it is sufficient to consider only the quadratic part of the action for the vector-like field $V = A_L + A_R$, from which this we get the respective equation of motion and find the normalizable modes v_n. As result the solutions only exist for discrete values of the four momentum $q^2 = m_n^2$

$$\partial_z\left(e^{-B}\partial_z v_n\right)+m_n^2e^{-B}v_n=0, \qquad B(z)\equiv\Phi(z)-A(z), \tag{1.50}$$

by doing the definition $v_n = e^{B/2}\psi_n$ this equation can be casted in a Schrodinger form

$$-\psi_n''+V(z)\psi_n=m_n^2\psi_n, \qquad V(z)=\frac{1}{4}\left(B'\right)^2-\frac{1}{2}B''. \tag{1.51}$$

In particular for the choice $B = \Phi - A = z^2 + \ln z$ the potential is of the form (1.46) described before, giving the desired linear spectrum with the radial quantum number n.

Higher spin mesons

To describe higher spin mesons we need to introduce higher spin fields in the bulk. These fields will be dual to the higher spin current operators that produce the higher spin mesons when acting on the vacuum. In the UV, these fields are conserved currents of defined twist 2, so the associated higher spin fields in the bulk would have equations of motion fixed by gauge and coordinate invariance, this is the well known Fronsdal equation of motion and action [45][11]. At the IR the higher spin field should become massive, consistent with the lost of current conservation, presumably through some sort of Higgs mechanism. Let us consider only massless higher spin fields in the bulk. The gauge field of spin S is represented by a totally symmetric tensor $\phi_{a_1,\ldots,a_S}$. Masslessness demands its equation of motion to be invariant under the following gauge transformation

$$\delta\phi_{a_1,\ldots,a_S}=\nabla_{(a_1}\xi_{a_2\ldots a_S)}, \tag{1.52}$$

[11] See [46] for a review of recent progress in higher spin gauge theories.

where ∇ is the general covariant derivative, $\xi_{a_2\dots a_S}$ is a gauge tensor, and the indices are symmetrized. The quadratic part of the action has the form

$$\int d^5X\sqrt{g}e^{-\Phi}\left(\nabla_a\phi_{a_1\dots a_S}\nabla^a\phi^{a_1\dots a_S}+M^2(z)\phi_{a_1\dots a_S}\phi^{a_1\dots a_S}+\dots\right), \tag{1.53}$$

where the dots represents extra terms required for gauge invariance. The mass-like $M(z)$ coefficient would be zero in flat space. For pure AdS instead, this term is constant and equal to S^2-S-4.

AdS/CFT requires us to evaluate the action (1.53) on-shell. The action is by construction gauge invariant, which means that we can evaluate it in any of the infinite solutions, but connected through gauge transformations (1.52), of the classical equation of motion and we will get exactly the same result. In particular, we can choose a suitable solution for our problem, by imposing additional restrictions to the solutions found. These additional constrains, should be such that the full space of solutions can be obtained by gauging the restricted solution found, otherwise they would be invalid. The first condition to impose is to make any of the tensor components with a z index to vanish, $\phi_{za_2\dots a_S}=0$, which is known as the axial gauge. Let us notice that it is equivalent to find the equation of motion from the action and later impose the axial gauge or to directly impose the axial gauge in the action and later derive the equation of motion, so we will look what happens in the action instead. In this gauge the part of the action that involves the transverse and traceless part of the field over the boundary indices decouples. These terms come from those written in the action (1.53) and not from the omitted ones. The axial gauge condition $\phi_{za_2\dots a_S}=0$ does not fix the gauge completely: transformations with gauge functions of the form

$$\xi_{\mu_1\dots\mu_S}(x,z)=e^{2(S-1)A(z)}\tilde{\xi}_{\mu_1\dots\mu_S}(x) \qquad\qquad \xi_{za_2\dots a_S}=0, \tag{1.54}$$

with $\tilde{\xi}_{\mu_1\dots\mu_S}(x)$ an arbitrary function of the boundary coordinates x, allow us to move between different solutions within the axial gauge. By demanding now the partially gauge fixed action obtained from (1.53) by setting $\phi_{za_2\dots a_S}=0$, to be invariant under this residual gauge transformation (1.54) we find that this is implemented by defining $\tilde{\phi}\equiv e^{-2A(S-1)}\phi$. The action for $\tilde{\phi}$ obtained through this process is then

$$\int d^5Xe^{5A-\Phi}\left(e^{4(S-1)A}e^{-2A(S+1)}\partial_a\tilde{\phi}_{\mu_1\dots\mu_S}\partial_a\tilde{\phi}_{\mu_1\dots\mu_S}\right). \tag{1.55}$$

At this point is simple to derive the equation of motion for $\tilde{\phi}$

$$\partial_z\left(e^{(2S-1)A-\Phi}\partial_z+m_n^2e^{(2S-1)A-\Phi}\right)\tilde{\phi}_n=0. \tag{1.56}$$

Putting this equation in a Schrodinger form one can realize that, in order to have dm_n^2/dn independent of S one needs to keep all the z^2 asymptotic in Φ and none in A. For the choice $A = -\ln z$ and $\Phi = z^2$ we get a Schrodinger potential of the type (1.46) whose mass spectrum is

$$m_{n,S}^2 = 4(n + S), \tag{1.57}$$

linear both in n and S.

For the purposes of this work we will need to propose what would be the equation of motion for the bulk higher spin fields that are dual to higher spin gluon operator in the boundary with twist 2. We will compute and re-sum all the tree level exchange of such fields in the bulk to get the hadronic tensor, resembling the well known OPE expansion of the hadronic current operators in QCD. From the bulk perspective the construction is roughly the same we described in this section. We will start with the gauge invariant equation of motion in AdS but we will see that in order to match experimental data we will need to break explicitly the gauge invariance, as expected since their dual operators are not conserved except in the UV, by adding some terms suggested by string theory. The details of this process will be explained in chapter 3. Breaking conformal invariance in the bulk means that eventually we will have more degrees of freedom, unless we simply demand as well that the gauge fixing conditions still to be valid for some reason. This and other questions about how to conceptually put all things in a proper framework will remain for future works, instead we will just try to check what are the essential key ingredients that a holographic formulation for the Pomeron needs in order to explain all the scattering processes dominated by Pomeron exchange.

1.2.3 Improved Holographic QCD

Among the plenty of bottom-up approaches existing currently in the literature we will use along this thesis the one known as Improved Holographic QCD model [43, 44]. While the model is build from the bottom-up, many of its features have been incorporated aiming to make contact with string theory, that is why sometimes it is called instead an "hybrid" approach. This is a Einstein-dilaton gravity model, with a potential for the dilaton in 5 dimensions. Asymptotic AdS geometry is imposed and the Yang-Mills perturbative expansion is simulated by an appropriated choice for the dilaton potential. In particular the model gives a good phenomenological description of the spectrum of glueballs known from lattice QCD computations, a critical feature

we need in our construction of the holographic Pomeron. The underlying guidance for the choice of the right potentials that lead to a "good" spectrum is the Soft Wall model described in the previous section. Beyond this the model has been used to compute other QCD quantities at finite temperature like transport coefficients, bulk viscosity, drag force and jet quenching parameters, providing a good phenomenological description as well.

We will review the model in chapter 2, particularly the parts more relevant to our construction of the holographic Pomeron, instead here we will just point out a few important facts about it, mostly taken from [43].

- The β function of the gauge theory is related to the superpotential of the Einstein-dilaton gravity system.
- Confinement is defined through the holographic computation of the rectangular Wilson loop. All confining backgrounds in this sense are shown to have a singularity in the metric at some value of the radial coordinate z.
- Superpotentials that lead to confining geometries as defined in the previous point are classified.
- For regular dilaton potentials the 't Hooft coupling λ always blows up at the IR singularity.
- All confining potentials give mass spectrum for the glueballs 0^{++} and 2^{++} with a mass gap.
- Of all possible confining asymptotic there is a unique choice that lead to linear Regge trajectories for all glueballs in the radial quantum number.

We end here way our review of the state of the art of holographic QCD models. In the next section we will review an important tool we will need in order to compute scattering amplitudes, the Witten diagrams expansion.

1.2.4 Witten diagrams expansion

In this section we revisit the Witten diagram expansion deriving its rules. As stated before, gauge/gravity dualities claim an equality between the partition function of a gravity theory in $\mathcal{M}$, and gauge theory in $\partial\mathcal{M}$ where $\mathcal{M}$ is an asymptotically AdS

space. Moreover in the regime that we will be interested the partition function on the gravity side can be computed semi-classically

$$Z_{gravity} \sim e^{iS_{o.s.}[\phi(X)]}, \tag{1.58}$$

that is, the partition function will be dominated by the saddle point configuration $\frac{\delta S}{\delta \phi} = 0$, where $S_{o.s.}[\phi(X)]$ is just the *on-shell* action. Witten's expansion is just a systematic way of computing $\exp(S_{o.s.}[\phi(X)])$. To fix ideas we will review perhaps what is the simplest non trivial case, which is a scalar field in the bulk with a cubic interaction term. Consider the action

$$S = \int_{\mathcal{M}} d^{d+1}X\sqrt{-g}\left((\partial\phi)^2 + m^2\phi^2 + \lambda\phi^3\right), \tag{1.59}$$

whose equation of motion $\frac{\delta S}{\delta \phi} = 0$ is

$$\left(\Box - m^2\right)\phi = \lambda\phi^2. \tag{1.60}$$

Now we need to solve this equation using the Dirichlet boundary condition $\phi(X)|_{\partial\mathcal{M}} = J(x)$ and plugin its result into (1.59) to get the *on-shell* action and with this the desired partition function which is a functional of $J(x)$. To solve this problem we define first a couple of objects. The first is the bulk-to-bulk propagator[12] which is just the Green function of the equation of motion operator with $\lambda = 0$. It satisfies

$$\left(\Box_X - m^2\right)G(X,\bar{X}) = \frac{1}{\sqrt{-g}}\delta^{d+1}(X,\bar{X}), \tag{1.61}$$

with $\int d^{d+1}X\delta^{d+1}(X,\bar{X}) = 1$. The second object is the bulk-to-boundary propagator, and is defined such that the solution of the equation of motion with $\lambda = 0$ is obtained as a convolution of this propagator with the value of the field at $\partial\mathcal{M}$

$$\phi^{(0)}(X) = \int d^d\bar{x}K(X,\bar{x})J(\bar{x}). \tag{1.62}$$

The superscript (0) is to emphasize that this definition is for the free $\lambda = 0$ equation of motion. We can find $K(X,\bar{x})$ from $G(X,\bar{X})$ as follows. Start with the divergence theorem

$$\int_{\mathcal{M}} d^{d+1}\bar{X}\sqrt{-\bar{g}}\bar{\nabla}^a T_a(\bar{X}) = \int_{\partial\mathcal{M}} d^d\bar{x}\sqrt{-\bar{\gamma}}n^a T_a(\bar{x}) \tag{1.63}$$

and choose $T_a(X)$ as

$$T_a(\bar{X}) = \phi(\bar{X})\left(\bar{\nabla}_a - m^2\right)G(X,\bar{X}) - G(X,\bar{X})\left(\bar{\nabla}_a - m^2\right)\phi(\bar{X}) \tag{1.64}$$

[12]To simplify the discussion we will consider an Euclidean signature for the metric in this section. In a Lorentzian signature the bulk-to-boundary and bulk-to-bulk propagators will be modified by a factor of $-i$.

then it is easy to see by plugin the last equation into (1.63) that

$$\phi(X) = \int_{\partial\mathcal{M}} d^d\bar{x}\sqrt{\bar{\gamma}}n^a\nabla_a G(X,\bar{X})\phi(\bar{X}). \tag{1.65}$$

Recalling that the boundary $\partial\mathcal{M}$ is defined as the hyperplane $z = 0$ in the Poincaré patch and $\phi(\bar{X})|_{\partial\mathcal{M}} = J(\bar{x})$, from the last we can read:

$$K(X,\bar{x}) = \lim_{\bar{z}\to 0}\sqrt{\bar{\gamma}}n^a\nabla_a G(X,\bar{x},\bar{z}). \tag{1.66}$$

A couple of comments are in order. Let us notice that in general taking the limit $\bar{z} \to 0$ lead to infinities, thus we need to consider the addition of counter-terms in the action such that this limit become instead finite. Notice also that in a general background, with fields like the dilaton $\Phi(X)$ or the tachyon $\tau(X)$ turned on, the presence of terms that multiply the entire action is common, and therefore the definition of the bulk-to-boundary propagator may change accordingly. Fortunately we will see in section 1.2.5, at least for the cases considered in this thesis, these terms contribute mostly to the divergent part of the integral and therefore its influence will disappears after renormalizing. The solution is found as a perturbative expansion in powers of λ: let's assume that

$$\phi(X) = \phi^{(0)} + \phi^{(1)}\lambda + \phi^{(2)}\lambda^2 + \dots. \tag{1.67}$$

Plugin (1.67) into (1.60) and demanding the equality of the coefficients of both left and right hand side polynomials in λ we get

$$\begin{aligned}
&(\Box - m^2)\,\phi^{(0)} = 0 \qquad &&\Rightarrow \quad \phi^{(0)}(X) = \textstyle\int d^dx_1 K(X,x_1)J(x_1),\\
&(\Box - m^2)\,\phi^{(1)} = (\phi^{(0)})^2 \quad &&\Rightarrow \quad \phi^{(1)}(X) = \textstyle\int d^{d+1}Y_1 d^dx_1 d^dx_2\sqrt{-g(Y_1)}K(Y_1,x_1)J(x_1)\times\\
& &&\qquad\qquad\qquad\qquad \times G(X,Y_1)K(Y_1,x_2)J(x_2),\\
& &&\quad \dots
\end{aligned} \tag{1.68}$$

In this expansion when we solve for $\phi^{(1)}$ we are just convoluting the inhomogeneity $(\phi^{(0)})^2$ with the Green function of the homogeneous equation of $\phi^{(1)}$, which is just $G(X,\bar{X})$, and so on for each one of the $\phi^{(n)}$. As one can easily realize to see the amount of integrals in this perturbative expansion grows quickly so, as in the case of Feynman diagrams, it is useful to write the expansion in a diagrammatic way

$$\phi(X) = \phi^{(0)}(X) + \lambda\phi^{(1)}(X) + \lambda^2\phi^{(2)}(X) + \dots$$

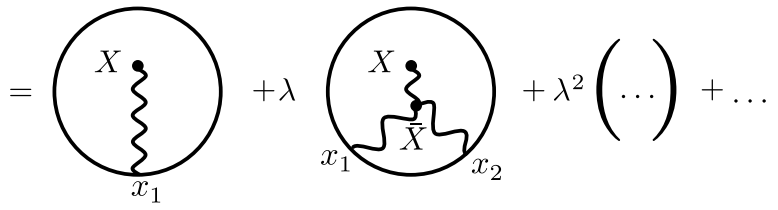

The wavy lines indicate the insertion of a bulk-to-bulk propagator if its two endpoints are in the bulk or a bulk-to-boundary propagator if one of its endpoints is at the boundary. Notice that at this level there are integrals over the boundary variables x_1, x_2, etc.. The diagrammatic rules for computing correlation functions come from evaluating the *on-shell* action using this expansion. Let's recall first that n-point correlation functions are obtained by taking functional derivatives of the generating functional and setting the sources to zero. Therefore the terms from the *on-shell* action that will survive have to have the right amount of $J(x)$, in this case n, and also taking the functional derivative will remove the integrals over the boundary variables x_1, etc., leaving only the bulk-to-boundary propagators where there were boundary insertions in the final expression. The entire process of the holographic computation of correlation functions in position space can be resumed in the following set of rules:

- The circle represents the AdS boundary and its interior the AdS bulk
- Operator insertions in correlation functions correspond to points over the circle.
- Lines departing from the boundary correspond to bulk-to-boundary propagators.
- Lines connecting two bulk points correspond to bulk-to-bulk propagators.
- An interaction point at bulk position X requires the insertion of an integral $\int dX\sqrt{g(X)}$. In the presence of background fields the vertex is modified, for example $\int dX\sqrt{g(X)}e^{-2\Phi}$, etc..

Similar to what happens with Feynman diagrams it is easier to use an equivalent set of rules but in momentum space while computing scattering amplitudes. Basically one has to add a z integral and the respective z dependence of each one of the parts of the diagrams to the equivalent Feynman rules in momentum space. As usual, disconnected diagrams do not contribute to the scattering amplitude, whereas connected ones give the desired result. In addition, we will need to use normalizable modes for real external

particles and non-normalizable ones for virtual external particles, as it will be derived in section 1.2.5.

Finally a few words about what happens when there is no explicit small parameter to make the perturbative expansion in the bulk, like the coupling λ of the previous example. This is usually the case for background fields, like for example the metric g_{ab} or the dilaton Φ. The strategy to follow to evaluate the *on-shell* action is the same as in the case described above. The equation of motion for such field is splitted in the usual way into its linear and non linear parts. The linear part, which is usually found by considering small perturbations, is used to find the propagators. The non linear part will give the interaction vertices. Type and amount of vertices depend of the order considered in perturbation theory. Witten diagrams with such fields are then computed using the same rules previously stated.

In the next section we will review the spin 1 gauge field in the bulk: its equation of motion as well as both bulk-to-boundary and bulk-to-bulk propagators. Its different modes will be used throughout the body of this work as the duals of the electromagnetic hadronic current operator $J_\mu(x)$ in the boundary. The matrix element $\langle P|T(J_\mu(p)J_\nu(0))|P\rangle$, know as the Compton tensor, is directly related to the DIS F_2 structure function as well as to the differential and total cross-sections of Deeply Virtual Compton Scattering (DVCS) and vector meson production processes. One of the main goals of this thesis is to use the gauge/string duality to evaluate such matrix element in existing holographic models and check whether is possible to confront the results with experimental data.

1.2.5 Spin 1 gauge field in the bulk

In this section we will review the dynamics of a spin 1 gauge field in the bulk and we will find its propagators and other useful quantities which we will use in chapters 3, 4 and 5. The exposition attempts to be as pedagogical as possible so expert readers can skip it.

The free action for the $U(1)$ gauge field in the bulk dual to the current operator in the boundary is

$$S[A_a(X)] = -\frac{1}{4}\int d^5X\sqrt{-g}e^{-\Phi}\left(F^{ab}F_{ab} + \beta R_{abcd}F^{ab}F^{cd}\right). \tag{1.69}$$

Here we consider the general case with a β-type term turned on, which we will consider

in chapter 4. The equation of motion can be easily derived from this

$$\nabla_a \left[e^{-\Phi} \left(F^{ab} + \beta R^{ab}{}_{cd} F^{cd} \right) \right] = 0 \tag{1.70}$$

Now let us notice that neither the inclusion of the dilaton term or the fact that the space is no longer AdS have spoiled gauge invariance. Indeed, (1.69) and (1.70) remain invariant under the gauge transformation $A_b \to A_b + \partial_b \lambda$. This is crucial since gauge invariance is related to current conservation in the boundary, so we want to preserve it. In this work we work in the commonly used axial gauge: we choose the representative $A(X)$ of the class of gauge equivalent physical configurations the solution that satisfies $A_z = 0$. It is not hard to check that the equation of motion in the previous gauge is still invariant under gauge transformation with a gauge parameter $\lambda(x)$ that does not depends on z, so the gauge is not completely fixed. Using this residual gauge symmetry allow us to impose as well $\partial_\mu A^\mu = 0$. . One can check then that this is a proper representative: all the possible equivalent physical configurations are accessible through a gauge transformation from it, and also that the gauge is completely fixed.

As we already saw in the previous section, going beyond free theory in general will produce some complicate terms in the right hand side of (1.70) depending on the interaction terms considered. To apply the AdS/QCD recipe we still need nevertheless to solve the equation with the right boundary condition at $z = 0$ and use it to evaluate the *on-shell* action, which will become the generating functional of the dual theory. In this case the solution is found iteratively and there are two key ingredients which are the bulk-to-bulk and bulk-to-boundary propagators, which we proceed to discuss.

The bulk-to-bulk propagator is just the Green function of the equation of motion (1.70) which is defined such that if

$$\nabla^b \left(e^{-\Phi} \nabla_{[b} A_{a]} + \beta R_{abcd} \nabla^{[c} A^{d]} \right) = J_a, \tag{1.71}$$

then the solution is

$$A_a(X) = \int d^5 \bar{X} \sqrt{-g(\bar{X})} G_{ab}(\bar{X}, X) J^b(\bar{X}), \tag{1.72}$$

up to terms which are solution of the homogeneous equation. Notice that in order to obtain solutions within the first gauge condition $A_z(X) = 0$ we will need $G_{az}(X, \bar{X}) = G_{za}(X, \bar{X}) = 0$ from this definition. Also gauge invariance will demand $J_b(X)$ to be a conserved current, just like in common electrodynamics, and therefore we have the freedom to shift $G_{ab} \to G_{ab} + \nabla_{Xa} \nabla_{\bar{X}b} \Lambda(X, \bar{X})$ and still have a Green function, since integrating the last term by part will produce a term proportional to the divergence of $J_b(\bar{X})$. We will use later this freedom to chose Λ such that the second gauge condition

$\nabla_a A^a = 0 \Leftrightarrow \partial_\mu A^\mu = 0$ is fulfilled. Applying the equation of motion to both sides of (1.72) we deduce then that the Green function should satisfy:

$$\left[\Box + e^{\Phi - A}\partial_z\left(e^{A-\Phi}\partial_z\right) + \beta\Delta_\beta\right] G_{ab}(X,\bar{X}) = e^{2A(\bar{z})+\Phi(\bar{z})}\frac{g_{ab}}{\sqrt{-g}}\delta^5(X,\bar{X}), \tag{1.73}$$

$$\Delta_\beta = -2e^{-2A}\left[\left(-\dot{A}\ddot{A} - \dot{\Phi}\ddot{A} + \dddot{A}\right)\partial_z + \ddot{A}\partial_z^2 + \dot{A}^2\Box\right] \tag{1.74}$$

where $\Box \equiv \partial_\mu\partial^\mu$[13]. To solve this, we consider first the solution of the homogeneous equation associated to (1.73). Let us first solve the following auxiliary problem

$$\left[-m^2 + e^{\Phi - A}\partial_z\left(e^{A-\Phi}\partial_z\right) + \beta\tilde{\Delta}_\beta\right] f(z) = 0, \tag{1.75}$$

where $\tilde{\Delta}_\beta$ is the Fourier transform of Δ_β. This is exactly the same thing we get by plugin the ansatz $A_\mu(X) = \epsilon_\mu f(z)e^{ik\cdot x}$ with $k^2 = m^2$ in the free theory equation (1.70) and then fixing the gauge. This equation can alternatively be written in the self-adjoint form

$$\left[\partial_z\left(p(z)\partial_z\right) + \left(q(z) + m^2 w(z)\right)\right] f(z) = 0, \tag{1.76}$$

$$p(z) = e^{-A(z)-\Phi(z)}\left(2\beta A''(z) - e^{2A(z)}\right), \qquad w(z) = e^{A(z)-\Phi(z)}, \qquad q(z) = 0.$$

We would impose regularity of the solution $f'(z) = 0$ at $z \to \infty$ and also $f(z) = 0$ when $z = 0$. These conditions, together with the equation (1.75), define a Sturm-Liouville problem. For the type of functions A and Φ we consider in this thesis[14], there are only solutions for certain values of m. In other words the spectrum of allowed values for m in (1.75) is discrete, m_n with $n = 0, 1, \ldots$ [15] . The associated solutions will be denoted by $f_n(z)$ and will be called *normalizable modes*. That f_n's are normalizable is guaranteed by the fact they are solutions of the Sturm-Liouville problem (1.76). Using the completeness relation of this problem $\sum_n e^{A(\bar{z})-\Phi(\bar{z})} f_n(z) f_n(\bar{z}) = \delta(z - \bar{z})$ we can easily solve (1.73)

$$G_{ab}(X,\bar{X}) = \begin{cases} e^{\Phi(\bar{z})-A(\bar{z})}\sum_n \int \frac{d^4k}{(2\pi)^4}\frac{f_n(z)f_n(\bar{z})e^{ik\cdot(x-\bar{x})}}{-k^2+m_n^2}\left(\eta_{\mu\nu} - \frac{k_\mu k_\nu}{k^2}\right) & a \wedge b \neq z \\ 0 & a \vee b = z. \end{cases} . \tag{1.77}$$

Here we have used the gauge freedom to choose a solution that satisfies the gauge conditions declared at the beginning. Bulk-to-boundary propagators can be derived

[13]Notice that in (1.73) there is some freedom to chose the right hand side functions evaluated on X or in $\bar{X}$: both choices give solutions.

[14]Recall that for the pure AdS case $A = -\ln z$ and $\Phi = 0$ the spectrum is continuous.

[15]It can be checked that by computing the 2-point function of the dual operator with the prescribed holographic recipe that the m_n are the masses of the associated resonances.

from bulk-to-bulk propagators by generalizing Green's third identity. Let's review first the case where there is no dilaton. The bulk-to-boundary propagator is defined such that the solution of the free equation of motion is obtained by convoluting it with the boundary value of the field

$$A_c(X) = \int d^d\bar{x}\mathcal{K}_c^{\ b}(X,\bar{x})\tilde{A}_b^{(0)}(\bar{x}). \tag{1.78}$$

Here $\tilde{A}_b^{(0)}(\bar{x})$ is the boundary value of the field, which is interpreted as the source of the dual operator. Starting with the divergence theorem

$$\int_{\mathcal{M}} d^{d+1}\bar{X}\sqrt{-\bar{g}}\bar{\nabla}^a T_a(\bar{X}) = \int_{\partial\mathcal{M}} d^d\bar{x}\sqrt{-\bar{\gamma}}n^a T_a(\bar{x}), \tag{1.79}$$

we will choose

$$T_a(\bar{X}) = A^c(\bar{X})\bar{\nabla}_a\left(G_{cb}(X,\bar{X})\right) - G_{cb}(X,\bar{X})\bar{\nabla}_a A^c(\bar{X}), \tag{1.80}$$

where we should keep in mind that the second index b of G_{cb} is related to the point X, so only one Christoffel symbol appears in the covariant derivative in (1.80). With this choice, in the gauge considered in this work, the left hand side of (1.79) becomes just $A_c(X)$ and by looking at the right hand side of the same formula and recalling the definition (1.78) we find

$$\mathcal{K}_{ab}(X,\bar{x}) = \lim_{\bar{z}\to 0}\sqrt{-\bar{\gamma}}e^{-\bar{A}}\partial_{\bar{z}}\left(e^{\bar{A}}G_{ab}(X,\bar{X})\right) \tag{1.81}$$

Now let's consider the case where the dilaton is non trivial. In that case we need to look for a field redefinition such that its equation of motion could be written on the form $(\Delta_1 - m^2(X))\tilde{A}(X) = 0$ where Δ_1 is the vector laplacian for some function $m^2(X)$. It turns out that this is the case for $\tilde{A}(X) = e^{-\frac{\Phi}{2}}A(X)$. Replacing $A^c \to \tilde{A}^c$ and $G_{cb} \to \tilde{G}_{cb}$ in (1.80) and repeating the previously described steps we find a slightly modified formula:

$$\mathcal{K}_{ab}(X,\bar{x}) = \lim_{\bar{z}\to 0}\sqrt{-\bar{\gamma}}e^{-\bar{A}-\frac{\bar{\Phi}}{2}}\partial_{\bar{z}}\left(e^{\bar{A}-\frac{\bar{\Phi}}{2}}G_{ab}(X,\bar{X})\right) \tag{1.82}$$

The important observation here is that this new formula has the same z dependence as the case where there was no dilaton: only divergent terms might be affected. The renormalized part will be

$$\Pi_{\mu\nu}(X,\bar{x}) = \int \frac{d^4k}{(2\pi)^4}\psi(z)e^{ik\cdot(x-\bar{x})}\left(\eta_{\mu\nu} - \frac{k_\mu k_\nu}{k^2}\right), \tag{1.83}$$

$$\Pi_{az}(X,\bar{x}) = \Pi_{za}(X,\bar{x}) = 0,$$

$$\psi(z,k) = C\sum_n \frac{g_n f_n(z)}{-k^2+m_n^2}, \tag{1.84}$$

where C is a constant that can be fixed by properly normalizing to match the two point function of the associated operator. The g_n constants are related to the n-th hadron decay constant and the renormalization procedure fixes them [47]. The functions $\psi(z,k)$ are the *non-normalizable modes*. In this thesis we will not compute the non-normalizable modes using (1.84), instead we will use the fact that they obey the same differential equation as the normalizable modes but with a different boundary condition $\psi(z=0) \sim z^0 = C$[16]. With the last expression inserted in the Witten diagrams we are able to compute correlation functions of the correspondent dual operators. We will use the non-normalizable modes whenever we have *off-shell* photons. To compute amplitudes with real particles as final states we will need to go further and apply the LSZ reduction formula. This is the standard procedure to go from vacuum expectation values of time ordered operators to scattering amplitudes in a QFT. For example for an outgoing vector meson of polarization $n_1^\mu(\lambda)$ and four momentum k_1, the sum over n disappears, we replace $k^2 \to k_1^2 = m_1^2$ everywhere else, the factor $e^{ik\cdot x}$ is absorbed in an overall Dirac delta which express momentum conservation, and the bulk-to-boundary propagator becomes

$$\mathcal{K}_a(X;k_1,n_1) = \begin{cases} Cn_{1\mu}(\lambda)f_{m_1}(z), & a=\mu \\ 0, & a=z \end{cases}. \tag{1.86}$$

From the last we see that *using normalizable modes in Witten diagrams will lead directly to the computation of scattering amplitudes*. Using this we can compute the $F_{ab}(X)$ *on-shell*, in the sense of evaluated in the bulk equation of motion solution, referenced as $F_{ab}^{1,3}(X)$ in chapters 3, 4 and 5, which will appear later in the computation

[16] It is interesting to see how normalizable and non-normalizable modes relate for the well known hard wall model case. Considering $k \gg \Lambda$, the different modes are,

$$\psi(z,k) = CkzK_1(kz) \qquad \text{non-normalizable mode,}$$

$$f_n(z) = \frac{\sqrt{2}\Lambda z J_1(\zeta_{0,n}\Lambda z)}{\pi^{\frac{3}{2}} J_1(\zeta_{0,n})} \qquad \text{normalizable mode,}$$

where $\zeta_{0,n}$ is the n-th zero of J_ν. These two functions are related through the mathematical identity

$$k^\nu K_\nu(kx) = \int_0^\infty dm \frac{m^{\nu+1}J_\nu(mx)}{k^2+m^2}. \tag{1.85}$$

For $\nu = 1$ this formula is the same as (1.84) with the difference that here we have an integral since the spectrum is continuous in the $k \gg \Lambda$ approximation. Additional information can be found in [47].

of many Witten diagrams

$$F_{ab}(X;k,n) = \begin{cases} 2ik_{[\mu}n_{\nu]}f_{k^2}(z) & a=\mu, b=\nu \\ n_\mu \partial_z f_{k^2}(z) & a=z, b=\mu \end{cases} \tag{1.87}$$

where k and n are the respective momentum and polarization vectors of the particle and the overall constant have been ignored. Notice that the last expression is valid for both computation of correlation functions and scattering amplitudes, we just need to replace f_{k^2} by the non-normalizable or normalizable mode respectively.

With this we end the review of the Witten diagram construction, its meaning and techniques. In the next section we will see what are the ingredients we need to consider in the bulk to obtain a holographic description for the Pomeron.

1.3 The BPST Pomeron

A breakthrough in the application of holographic techniques to explain Pomeron physics is the work of Brower, Polchinski, Strassler and Tan [13], sometimes known as BPST Pomeron. As noticed in that work, there is a remarkable similarity between the kernel of the Pomeron obtained through BFKL methods of a conformal field theory and the kernel of flat space string theory Regge amplitude Fourier transformed to position space for $t = 0$: both have a diffusive form, this is a power of s times a diffusion kernel where the role of the time is $\tau = \ln s$, and the diffusion variable is $\ln p_\perp$ in the conformal side while in the string theory side it is $x_\perp$.

This suggest that the gauge/string duality may be a valuable tool to understand Pomeron physics. In this work the authors also argued that the Pomeron of the gauge theory should correspond to the graviton Regge trajectory in the string theory side, providing a framework for unifying the different types of Pomeron. The different Pomerons would emerge for different values of the 't Hooft coupling.

In the next subsection the main ideas of this work will be reviewed.

1.3.1 A systematic derivation: main ideas

In the section of the same name in [13] the amplitude for a $2 \to 2$ scattering of general string states in the Regge limit is derived first in flat space and later guessed in a

warped spacetime. The amplitude have some improvements due to the renormalization group of the 2d sigma model in which the Polyakov action becomes when the background is no longer flat. The derivation is done in the closed bosonic string, and is somehow formal in curved space, since the vertex operators are approximated by their Gaussian versions. Straight to the point, the main ideas that lead to this final result are the following:

- The four tachyon amplitude on the sphere leads to the well know Virasoro-Shapiro amplitude, which in the large s limit exhibit a Regge form, in other words, it is the same as the one given by a Reggeon interchange. Since the 4 tachyon amplitude has more information than required to explain Regge physics, one can go back and check what is the minimum amount of information that has to be kept in the amplitude integrand such that Regge behavior is obtained after integration. The answer is very simple: in the large s limit the amplitude is dominated by the integration region near $w = t/(s+t) \to 0$ in the worldsheet complex plane w.

- Since what is required to obtain a Regge amplitude is the behavior near $w \to 0$, in terms of vertex operators this means that the amplitude is dominated by the OPE of the vertex operator at $w, \bar{w}$ and the one inserted at the complex plane origin. The form of the OPE can be easily worked out in flat space, and an interesting point is that not only the leading order of the OPE is required but also the next to leading one, otherwise, the Regge form of the amplitude is not obtained.

- From the knowledge that Regge physics is encoded in the $w \to 0$ region of the worldsheet and the details about it, one can go and generalize the 4 tachyon result to any set of scattering string states that have a large momentum difference between them. This is done by writing the amplitude in a general way with the worldsheet evolution operator $w^{L_0-2}\bar{w}^{\tilde{L}_0-2}$ inserted between the two sets of vertex operators and later inserting a complete set of string states between and keeping only the leading terms in the Regge limit, now defined as $w \to 0$. The result of this is that the relevant states are those in the graviton Regge trajectory: states of the form $(\alpha_{-1}^n \tilde{\alpha}_{-1}^m)\,|0\rangle$ with $n, m = 1, 2, ...$

- From the above it can be defined two interesting objects in string theory: the Pomeron vertex operator and the Pomeron propagator. In terms of them the amplitude has a remarkable simple expression and seems to be the most efficient way to do high energy scattering in string theory.

- The result can be formally extended to strings propagating in a curved background. Pomeron kernel acquire now corrections in α' as usually happens with operators in string theory in curved space.

In the next subsections these points will be reviewed.

1.3.2 Regge behavior of string states scattering amplitudes

Flat space: standard derivation

The analysis of the well known formula for the scattering of 4 tachyons at tree level in string theory (on the sphere) is the starting point for the later general statement about Regge behavior of high energy scattering of any kind of string states, including branes. Inserting the four vertex operators in the Riemann sphere, which is just the complex plane plus a point at infinity, fixing the position of 3 of them thanks to the Möbius symmetry at 0, 1 and ∞, and evaluating the expectation values in what it is in flat space a two dimensional free CFT one gets[17]:

$$\begin{aligned} \mathcal{A}(s,t) &= \left\langle e^{ip_1\cdot X(w,\bar{w})} e^{ip_2\cdot X(0)} e^{ip_3\cdot X(1)} e^{ip_4\cdot X(\infty)} \right\rangle \\ &= \int_{\mathcal{C}} d^2w \, |w|^{-4-\frac{\alpha'}{2}t} \, |1-w|^{-4-\frac{\alpha'}{2}s} , \end{aligned} \tag{1.88}$$

where the Mandelstam variables are defined as $s = -(p_1+p_3)^2$ and $t = -(p_1+p_2)^2$. Here the normalization constant in the front which includes a momentum conservation delta function has been omitted for the sake of clarity. The integrand has a saddle point at $w_s = t/(s+t)$, which is explicitly computed in the appendix B.1. For s large $w_s \to 0$ and the integrand can be conveniently manipulated to get the desired behavior

$$\begin{aligned} |1-w|^{-4-\frac{\alpha'}{2}s} &= \left(1 - \frac{\left(4+\frac{\alpha'}{2}s\right)(1-w)}{2}\right)\left(1 - \frac{\left(4+\frac{\alpha'}{2}s\right)(1-\bar{w})}{2}\right) \\ &= e^{\left(2+\frac{\alpha'}{4}s\right)(w+\bar{w})}, \end{aligned}$$

up to subleading terms of order w^2. The amplitude (1.88) become

$$\mathcal{A}(s,t) = \int_{\mathcal{C}} d^2w e^{\left(2+\frac{\alpha'}{4}s\right)(w+\bar{w})} \, |w|^{-4-\frac{\alpha'}{2}t} . \tag{1.89}$$

[17] Vertex operators are assumed normal ordered and with the ghost factors already set as constants if one works in the BRST quantization version.

This integral is explicitly computed in appendix B.2, giving

$$\mathcal{A}(s,t) = 2\pi \frac{\Gamma\left(1-\frac{\alpha'}{4}t\right)}{\Gamma\left(2+\frac{\alpha'}{4}t\right)} \left(\frac{\alpha'}{4} s e^{i\pi/2}\right)^{2+\frac{\alpha'}{2}t}, \tag{1.90}$$

which shows that the approximations made were the right ones to keep Regge physics.

Flat space: OPE derivation

Once it is realized that Regge physics is encoded in the region near $w \to 0$, due to the result of the previous computation, then it can be expected that this result can be obtained as well from the OPE, since in this region the vertex operators of particles 1 and 2 are very close. In flat space the OPE of these vertex operator is relatively easy to compute since the worldsheet CFT is free, thus it can be obtained by doing basically a bunch of Wick contractions

$$e^{ip_1\cdot X(w,\bar{w})} e^{ip_2\cdot X(0)} = |w|^{-4-\frac{\alpha'}{2}t}\, e^{ik\cdot X(0)+p_1\cdot\left(w\partial+\bar{w}\bar{\partial}\right)X(0)} + \ldots, \tag{1.91}$$

where $p_i^2 = 4/\alpha'$, $k = p_1 + p_2$ and $t = -k^2$. The details of this computation are done in the appendix B.3, the only important point to remark here is that in order to get the desired integrand one have to keep the next to leading order in the OPE, which is the part containing the w and $\bar{w}$ in the argument of the last exponential in (1.91). Indeed, now evaluating the expectation value of the remaining three operators

$$\left\langle e^{ik\cdot X(0)+p_1\cdot\left(w\partial+\bar{w}\bar{\partial}\right)X(0)} e^{ip_3\cdot X(1)} e^{ip_4\cdot X(\infty)} \right\rangle = e^{\left(2+\frac{\alpha' s}{4}\right)(w+\bar{w})}, \tag{1.92}$$

which, together with the factor $|w|^{-4-\frac{\alpha'}{2}t}$ gives exactly the integrand of (1.89), now derived using the OPE. The details are in the appendix B.4.

This suggest a step forward in the isolation of the Pomeron physics by interchanging the integral in the amplitude and the OPE to get an operator for the action of the Pomeron in vertex operators expectation values

$$\begin{aligned}\int d^2w e^{ip_1\cdot X(w,\bar{w})} e^{ip_2\cdot X(0)} &\sim \int d^2w\, |w|^{-4-\frac{\alpha'}{2}t}\, e^{ik\cdot X(0)+p_1\cdot\left(w\partial+\bar{w}\bar{\partial}\right)X(0)} \quad = \\ &= \frac{e^{ik\cdot X(0)}}{\Gamma\left(2+\frac{\alpha'}{4}t\right)} \int_0^\infty dx \int_{-\infty}^\infty d\sigma_1 d\sigma_2 x^{1+\frac{\alpha'}{4}t} e^{-xw\bar{w}+p_1\cdot\left(w\partial+\bar{w}\bar{\partial}\right)X(0)}\end{aligned}$$

This integral is essentially the same already computed (1.89) thus the details are omitted this time. The result is

$$2\pi \frac{\Gamma\left(-1-\frac{\alpha'}{4}t\right)}{\Gamma\left(2+\frac{\alpha'}{4}t\right)} e^{ik\cdot X(0)} \left(p_1\cdot\partial X(0)\, p_1\cdot\bar{\partial}X(0)\, e^{i\pi}\right)^{1+\frac{\alpha'}{4}t}. \tag{1.93}$$

The insertion of this matrix element into the expectation value gives immediately the Regge behavior of the amplitude. This is the Pomeron vertex operator.

curved space: generalization

The goal now is to repeat previous steps in a space with a metric

$$ds^2 = e^{2A(z)}\eta_{ab}dX^a dX^b + g_{\perp pq}dY^p dY^q. \tag{1.94}$$

In general string solutions in such background, which are the ones presumably relevant for QCD, are not known but still some progress can be made. In the Gaussian limit string wave functions $e^{ip\cdot x}\psi(y)$ give the associated vertex operators $e^{ip\cdot X}\psi(Y)$, with X and Y denoting worldsheet fields. The computation proceed in the same line as for the flat space derivation. To get terms of order up to $(\ln s)/\sqrt{\lambda} \sim |\ln w|/\sqrt{\lambda}$ in the OPE expansion of the vertex operators it is required to go beyond the Gaussian approximation, which is implemented by retaining terms of order $1/\sqrt{\lambda}$ in the worldsheet dimension operator L_0. Effectively this is a renormalization group improvement from the $2d$ worldsheet CFT. As final result an approximated expression for the amplitude of string states in curved spacetime is obtained, which essentially suggest to promote the Mandelstam variable t to an operator Δ_2

$$\mathcal{A}(s,t) \sim \int d^6y\sqrt{G_\perp}\psi_3(y)\,\psi_4(y)\,e^{2A(y)}\Pi(\alpha'\Delta_2)\,(\bar{\alpha}'s)^{2+\frac{\alpha'}{2}\Delta_2}\,e^{2A(y')}\psi_1(y)\,\psi_2(y)\,, \tag{1.95}$$

where

$$\Pi(\alpha' t) = 2\pi\frac{\Gamma\left(-1-\frac{\alpha' t}{4}\right)}{\Gamma\left(2+\frac{\alpha' t}{4}\right)}e^{-i\pi-i\pi\frac{\alpha' t}{4}}. \tag{1.96}$$

We end the review of BPST [13] by adding a few more comments. Firstly a similar analysis is done in the light-cone gauge for the worldsheet fields by computing semi-classically the Euclidean Polyakov path integral of the interacting string states, obtaining essentially the same result. Secondly it is customary to define the scattering amplitude as the convolution of external state wave functions with some kernel, the so called kernel of the Pomeron, a distribution which is the Green function of some diffusion-like (in the radial coordinate) operator. Its form is determined by the background used and it contains effectively the information about the exchange of an infinite set of string states: the graviton Regge trajectory. Thirdly the authors extend their analysis considering the effect of confinement while still considering UV-conformal theories. As a toy model they analyze how the Pomeron appears in the hard wall model and they arrive to the conclusion that for large positive t bound

states appear whereas for large negative t these disappears under a branch cut. While the hard wall model may capture key universal features of the Pomeron for large values of $|t|$, the kernel behavior near $t = 0$, which is the most interesting part for DIS for instance, is heavily model dependent. One of the goal of this thesis is the study of the holographic kernel of the Pomeron specifically in this region. We will use as QCD holographic model the Improved Holographic QCD model [43,44], a bottom up model that effectively captures some strong coupling regime features of QCD and is inspired by string theory .

2

Soft Pomeron in Holographic QCD

This chapter is based in [20]. We study the graviton Regge trajectory in Holographic QCD as a model for high energy scattering processes dominated by soft pomeron exchange. This is done by considering spin J fields from the closed string sector that are dual to glueball states of even spin and parity. In particular, we construct a model that governs the analytic continuation of the spin J field equation to the region of real $J < 2$, which includes the scattering domain of negative Maldelstam variable t. The model leads to approximately linear Regge trajectories and is compatible with the measured values of 1.08 for the intercept and of 0.25 GeV^{-2} for the slope of the soft pomeron. The intercept of the secondary pomeron trajectory is in the same region of the subleading trajectories, made of mesons, proposed by Donnachie and Landshoff, and should therefore be taken into account.

2.1 Introduction

The Pomeron plays a crucial role in QCD Regge kinematics, for processes dominated by exchange of the vacuum quantum numbers. This includes elastic scattering of soft states at high energies and low momentum transfer. The corresponding amplitude exhibits a universal behavior explained within Regge theory [7],

$$\mathcal{A}(s,t) \approx \beta(t)\, s^{\alpha(t)}\,, \qquad \alpha(t) = 1.08 + 0.25\, t\,, \tag{2.1}$$

in GeV units and for some function $\beta(t)$ that depends on the scattered states. A precise computation of the values of the intercept ($\alpha_0 = 1.08$) and slope ($\alpha' = 0.25$ GeV^{-2}) is beyond our current understanding of QCD, since long-range strong interaction effects

are important.

In the present chapter we build a soft-pomeron phenomenology in Holographic QCD. More concretely, we show the Regge theory for spin J exchanges in the dual geometry leads to the behavior (2.1) for the amplitude between soft probes.

2.2 Holographic QCD model

We will consider the Holographic QCD model proposed in the works [43, 44] based on gravity plus a dilaton field. We shall be working in the string frame because the Regge trajectory we are interested in is made of fundamental closed string states. As usual, the scalar field $\Phi = \Phi(z)$ and the dual geometry has metric

$$ds^2 = g_{ab}dx^a dx^b = e^{2A(z)}\left(dz^2 + \eta_{\alpha\beta}dx^\alpha dx^\beta\right) , \tag{2.2}$$

where $\eta_{\alpha\beta}$ is the Minkowski boundary metric. In the string frame the corresponding action is

$$S = \frac{1}{2\kappa^2}\int d^5x\sqrt{-g}\, e^{-2\Phi}\left[R + 4\left(\partial\Phi\right)^2 + V\right] , \tag{2.3}$$

with

$$V = e^{-\frac{4}{3}\Phi}\left[\frac{64}{27}W^2 - \frac{4}{3}\left(\frac{dW}{d\Phi}\right)^2\right] . \tag{2.4}$$

The field Φ is the dilaton without the zero mode that is absorbed in the gravitational coupling κ. The field equations arising from (2.3) take the form

$$\begin{aligned} R_{ab} + 2\nabla_a\nabla_b\Phi - \frac{1}{4}\frac{dV}{d\Phi}g_{ab} =& 0 , \\ 2\nabla^2\Phi - 4(\nabla\Phi)^2 + V + \frac{3}{4}\frac{dV}{d\Phi} =& 0 . \end{aligned} \tag{2.5}$$

The superpotential $W(\Phi)$ is fixed phenomenologically by demanding that the model reproduces basic QCD data, such as beta function, heavy quark/anti-quark linear potential and glueball spectrum. In this work we take the Background I of [43, 44] where

$$W = \frac{9}{4L}\left(1 + \frac{2}{3}b_0\lambda\right)^{\frac{2}{3}}\left[1 + \frac{(2b_0^2 + 3b_1)\log(1+\lambda^2)}{18a}\right]^{\frac{4a}{3}} , \tag{2.6}$$

$\lambda = e^\Phi$ and the length scale L fixes the units.

The 't Hooft coupling of the dual Yang-Mills theory $\bar{\lambda}$ is fixed by λ up to a multiplicative constant, i.e. $\bar{\lambda} = c_0\lambda$. For the model considered in this work the constants in

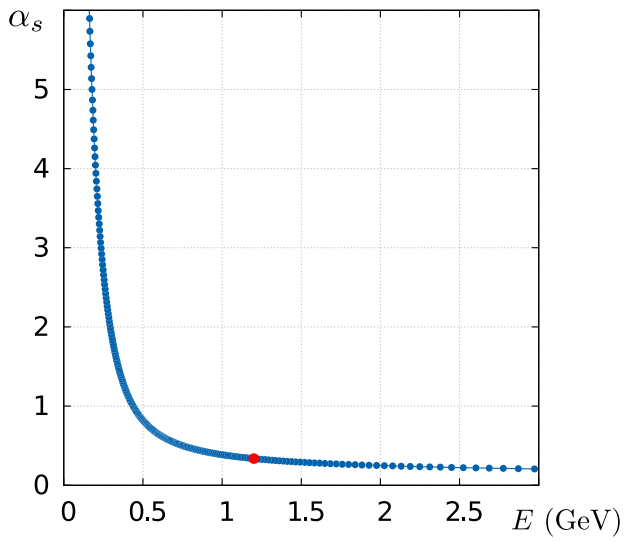

Figure 2.1: Running coupling α_s vs. energy scale. The red point is $\alpha_s(1.2\,\text{GeV}) = 0.34$.

(2.6) are given by

$$b_0 = 4.2\,, \quad \frac{b_1}{b_0^2} = \frac{51}{121}\,, \quad a = \frac{3}{16}\,. \tag{2.7}$$

The model has an additional integration constant that can be related to Λ_{QCD}, via the identification of the energy scale and warp factor, $\log E = A(z) - \frac{2}{3}\Phi(z)$. As shown in [43, 44], the UV behavior of the superpotential (2.6) leads to a beta-function

$$\beta = \frac{d\lambda}{d\log E} = -b_0\lambda^2 - b_1\lambda^3 + \dots\,. \tag{2.8}$$

This is consistent with the two-loop perturbative beta function in large-N Yang-Mills

$$\bar{\beta} = -\bar{b}_0\bar{\lambda}^2 - \bar{b}_1\bar{\lambda}^3\,, \quad \bar{b}_0 = \frac{2}{3}\frac{11}{(4\pi)^2}\,, \quad \frac{\bar{b}_1}{\bar{b}_0^2} = \frac{51}{121}\,. \tag{2.9}$$

if we take $c_0 = b_0/\bar{b}_0$. This fixes the second parameter in (2.7). The others parameters are fixed by the IR constraints coming from confinement, asymptotic linear glueball spectrum and lattice QCD.

Given that all of the parameters are already fixed at this point, one may ask how the field theory coupling runs with energy. Setting $N_c = 3$ the QCD running coupling can be identified with $\alpha_s = \bar{\lambda}/(12\pi)$. Figure 2.1 shows how α_s runs with the energy scale in the model, giving 0.34 for the value for $E = 1.2\,\text{GeV}$, which is very close to the experimental value 0.35.

We can recover the conformal limit by considering the parameters $b_0 = b_1 = 0$. Then we can set $\Phi = 0$, the superpotential becomes the cosmological constant $-12/L^2$, and the metric becomes that of AdS space, i.e. $A(z) = \ln(L/z)$.

2.3 Pomeron in Holographic QCD

2.3.1 Graviton

Since we are interested in the graviton Regge trajectory let us start by considering perturbations to the background in the string frame. We shall write the metric and dilaton, respectively, as

$$g_{ab} + h_{ab}\,, \qquad \Phi + \varphi\,. \tag{2.10}$$

It is then a mechanical computation to obtain from (2.5) the linearised equations of motion for the perturbations h_{ab} and φ,

$$\begin{aligned} &\nabla^2 h_{ab} - 2\nabla_{(a}\nabla^c h_{b)c} + \nabla_a\nabla_b h + 2R_{acbd}h^{cd} \\ &+4\nabla^c\nabla_{(a}\Phi\, h_{b)c} + 2\nabla^c\Phi\left(2\nabla_{(a}h_{b)c} - \nabla_c h_{ab}\right) \\ &-4\nabla_a\nabla_b\,\varphi + \frac{1}{2}\,g_{ab}V''(\Phi)\,\varphi = 0\,, \end{aligned} \tag{2.11}$$

$$\begin{aligned} &\nabla^2\varphi + \frac{1}{2}V'(\Phi)\,\varphi + \frac{3}{8}V''(\Phi)\,\varphi \\ &-4\nabla\varphi\cdot\nabla\Phi - \frac{1}{2}\nabla^a\Phi\left(2\nabla^b h_{ab} - \nabla_a h\right) \\ &-h^{ab}\nabla_a\nabla_b\Phi + 2h^{ab}\nabla_a\Phi\nabla_b\Phi = 0\,, \end{aligned} \tag{2.12}$$

where the covariant derivatives and Riemann tensor refer to the background and $h = h^a_a$. Field perturbations will be classified according to the $SO(1,3)$ global symmetry of the background. Thus we shall decompose the metric perturbations h_{ab} as

$$\begin{aligned} &h_{\alpha\beta} = h^{TT}_{\alpha\beta} + \partial_{(\alpha}h^T_{\beta)} + \left(4\partial_\alpha\partial_\beta - \,\eta_{\alpha\beta}\partial^2\right)\bar{h} + \eta_{\alpha\beta}h\,, \\ &h_{zz}\,, \qquad h_{z\alpha} = v^T_\alpha + \partial_\alpha s\,. \end{aligned} \tag{2.13}$$

As usual transverse and traceless (TT) tensor fluctuations, transverse (T) vector fluctuations and scalar fluctuations decouple. Moreover, since we are interested only in the TT metric fluctuations, we do not need to worry about mixing of perturbations. It is then simple to see that (2.11) gives for the TT metric fluctuations

$$\left(\nabla^2 - 2e^{-2A(z)}\dot{\Phi}\nabla_z + 2\dot{A}^2e^{-2A(z)}\right)h^{TT}_{\alpha\beta} = 0\,. \tag{2.14}$$

The term with the dilaton arises from the usual coupling $-2\partial^c\Phi\nabla_c h_{ab}$ for metric fluctuations in the string frame; the other term comes from the coupling to the Riemann tensor $R_{acbd}h^{cd}$, with $R_{\alpha\mu\beta\nu} = \dot{A}^2e^{2A}\left(\eta_{\alpha\nu}\eta_{\mu\beta} - \eta_{\alpha\beta}\eta_{\mu\nu}\right)$ and $R_{\alpha z\beta z} = -\ddot{A}e^{2A}\eta_{\alpha\beta}$. In the case of pure AdS space, $A(z) = \ln(L/z)$, so (2.14) simplifies to

$$\left(\nabla^2 - m^2\right)h^{TT}_{\alpha\beta} = 0\,, \tag{2.15}$$

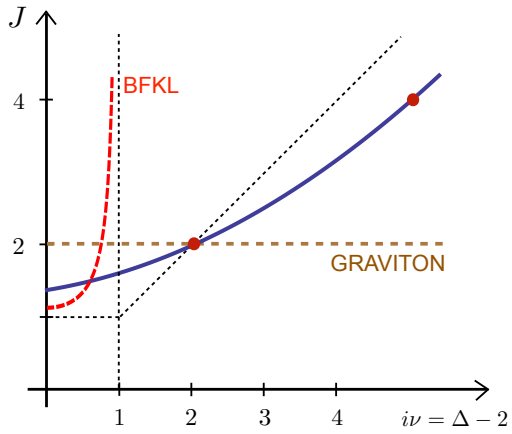

Figure 2.2: Expected form of the $\Delta = \Delta(J)$ curve (in blue).

with $(Lm)^2 = -2$, as expected for the AdS graviton.

2.3.2 Dual spin J field

We shall consider the exchange of twist 2 operators of Lorentz spin J formed from the gluon field [1]

$$\mathcal{O}_J \sim \mathrm{tr}\left[F_{\beta\alpha_1} D_{\alpha_2} \cdots D_{\alpha_{J-1}} F^{\beta}_{\ \alpha_J}\right], \tag{2.16}$$

where D is the QCD covariant derivative. The dimension of the operator $\mathcal{O}_J$ can be written as $\Delta = 2 + J + \gamma_J$, where γ_J is the anomalous dimension. In free theory the operator has critical dimension $\Delta = 2 + J$. Knowledge of the curve $\Delta = \Delta(J)$ is important when summing over spin J exchanges, since this sum is done by analytic continuation in the J-plane, and then by considering the region of real $J < 2$. Figure 2.2 summarizes a few important facts about the curve $\Delta = \Delta(J)$. Let us define the variable ν by $\Delta = 2 + i\nu$, and consider the inverse function $J = J(\nu)$. The figure shows the perturbative BFKL result for $J(\nu)$, which is an even function of ν and has poles at $i\nu = 1$. Beyond perturbation theory, the curve must pass through the energy-momentum tensor protected point at $J = 2$ and $\Delta = 4$. We shall use a quadratic approximation to this curve that passes through this protected point,

$$J(\nu) \approx J_0 - \mathcal{D}\nu^2\,, \qquad 4\mathcal{D} = 2 - J_0\,. \tag{2.17}$$

[1] In the singlet sector there is also the twist 2 quark operator $\mathcal{O}_J \sim \bar{\psi}\Gamma_{\alpha_1} D_{\alpha_2} \cdots D_{\alpha_J}\psi$, however we are considering processes dominated by exchange of the gluon field because it gives the dominant trajectory.

The use of a quadratic form for the function $J(\nu)$ is known as the diffusion limit and it is used both in BFKL physics and in dual models that consider the AdS graviton Regge trajectory (see for instance [17]).

Consider now the spin J field dual to the twist 2 operators (2.16). For pure AdS this field obeys the equation

$$\left(\nabla^2 - m^2\right) h_{a_1\cdots a_J} = 0\,, \quad (Lm)^2 = \Delta(\Delta-4) - J\,, \tag{2.18}$$

where L is the AdS length scale. Note that this field is symmetric, traceless and transverse ($\nabla^b h_{ba_2\cdots a_J} = 0$).

To consider the spin J field in a general background of the form (2.2), we need again to do a decomposition in $SO(1,3)$ irreps. The propagating degrees are described by components $h_{\alpha_1\cdots\alpha_J}$, since the other components $h_{z\cdots z\alpha_i\cdots\alpha_J}$ ($i \geq 2$) are fixed by the transversality condition. Thus we need to define the equation of motion for $h_{\alpha_1\cdots\alpha_J}$. Of course we do not know its form for the dual of QCD, but follow a phenomenological approach. We shall require that such equation is compatible with the spin 2 case (2.14), since in that case it must reduce to that of the graviton, whose dual operator has protected dimension. Moreover, we require the coupling to the dilaton to be that of closed strings in the graviton Regge trajectory arising from the term $-2\partial^c\Phi\nabla_c h_{a_1\cdots a_J}$. Finally, we require the equation to reduce to (2.18) in the conformal limit (constant dilaton). This leads to the following proposal

$$\left(\nabla^2 - 2\,e^{-2A}\dot{\Phi}\nabla_z - \frac{\Delta(\Delta-4)}{L^2} + J\dot{A}^2 e^{-2A}\right) h_{\alpha_1\ldots\alpha_J} = 0\,, \tag{2.19}$$

where here L is a length scale parameter. It is trivial to verify that setting $J=2$ (and $\Delta=4$) this equation reduces to the the graviton equation (2.14). Similarly, setting $A(z) = \ln(L/z)$ and $\Phi = 0$ we recover the spin J AdS equation (2.18). The dilaton term arises from considering tree level closed strings, which is justified since we work at large N. We expect that there will be more terms in this equation arising from other curvature couplings and derivatives of the dilaton field. Assuming the equation is analytic in J, these terms should be proportional to $J-2$, so that they are absent for $J=2$. Notice that there can be such terms still at the level of two derivatives, that is terms proportional to

$$e^{-2A}\left(\dot{A}^2 - \ddot{A}\right), \qquad e^{-2A}\dot{\Phi}^2\,, \qquad e^{-2A}\ddot{\Phi}\,, \tag{2.20}$$

which also vanish in the conformal limit. Terms with higher derivatives will appear in a α'/L^2 expansion. As already stated, we shall follow a phenomenological approach and

use the simple form (2.19) to describe the fluctuations of the spin J field in holographic QCD.

We will be interested in the continuation of (2.19) to the unphysical region of $J < 2$. It is here that we will use the diffusion limit (2.17), writing in (2.19)

$$\frac{\Delta(\Delta-4)}{L^2} \approx \frac{2}{l_s^2}(J-2)\,, \tag{2.21}$$

with l_s a length scale set by the QCD string. Notice that we are fixing l_s to a constant determined by IR physics, but in fact it should depend on energy scale, since the curve $\Delta = \Delta(J)$ in Figure 2.2 should vary with energy scale, keeping its general shape. However, for the soft-pomeron this should not matter [2]. We leave l_s as a phenomenological parameter to be fixed by data.

In the Regge limit we are actually interested in the $+\cdots+$ component of (2.19). To find the solution write

$$h_{+\cdots+}(z,x) = e^{iq\cdot x} e^{\frac{2J-3}{2}A(z)+\Phi(z)}\psi(z)\,, \tag{2.22}$$

where $q\cdot x = \eta_{\alpha\beta}q^\alpha x^\beta$ and we set $q_- = 0$ in the Regge limit. Then, a computation shows that (2.19) reduces to the Schrödinger problem

$$\left(-\frac{d^2}{dz^2} + U(z)\right)\psi(z) = t\,\psi(z)\,, \tag{2.23}$$

$$U(z) = \frac{15}{4}\dot{A}^2 - 5\dot{A}\dot{\Phi} + \dot{\Phi}^2 + \frac{\Delta(\Delta-4)}{L^2}e^{2A(z)}\,, \tag{2.24}$$

with $t = -q^2$. The energy spectrum for each J quantises $t = t_n(J)$, therefore yielding the glueball masses.

2.3.3 t-channel spin J exchange

Next consider the elastic scattering of QCD hadronic states of masses m_1 and m_2. We write the incoming momenta k_1, k_2 and the outgoing momenta k_3, k_4 in light-cone coordinates $(+,-,\perp)$ as

$$\begin{aligned} k_1 &= \left(\sqrt{s}, \frac{m_1^2}{\sqrt{s}}, 0\right), \quad k_3 = -\left(\sqrt{s}, \frac{m_1^2+q_\perp^2}{\sqrt{s}}, q_\perp\right), \\ k_2 &= \left(\frac{m_2^2}{\sqrt{s}}, \sqrt{s}, 0\right), \quad k_4 = -\left(\frac{m_2^2+q_\perp^2}{\sqrt{s}}, \sqrt{s}, -q_\perp\right), \end{aligned} \tag{2.25}$$

[2] For instance, the approximation (2.21) misses the dimensions of the operators with $J > 2$ in the free theory limit.

where we considered the Regge limit $s \gg t = -q_\perp^2$.

Each hadron is described by a normalizable mode $\Upsilon_i(z,x) = e^{ik_i\cdot x_i}\upsilon_i(z)$ where $\upsilon_3 = \upsilon_1^*$ and $\upsilon_4 = \upsilon_2^*$. The hadrons we consider are made of open strings. Then the coupling of each hadronic field to the spin J closed string fields has the form

$$\kappa_J \int d^5x\sqrt{-g}\, e^{-\Phi} h_{a_1\cdots a_J}\Upsilon\nabla^{a_1}\cdots\nabla^{a_J}\Upsilon\,. \tag{2.26}$$

Notice that in principle different types of hadrons will have a different coupling κ_J. The transverse condition on the spin J field guarantees that this coupling is unique up to derivatives of the dilaton field, which are subleading in the Regge limit.

The amplitude for $m_1m_2 \to m_1m_2$ scattering through exchange of a spin J field in the t-channel may now be computed in the dual theory. In the Regge limit we have

$$\begin{aligned}\mathcal{A}_J(k_i) = -\kappa_J\kappa'_J \int d^5X d^5X' \sqrt{-g}\sqrt{-g'} e^{-\Phi-\Phi'} \\ \left(\Upsilon_1\partial_-^J\Upsilon_3\right)\Pi^{-\cdots-,+\cdots+}(X,X')\left(\Upsilon'_2\partial_+'^J\Upsilon'_4\right),\end{aligned} \tag{2.27}$$

where $X = (z,x)$ and $X' = (z',x')$ are bulk points and fields with a prime are evaluated at X', e.g. $\Phi' \equiv \Phi(z')$. We use this notation throughout. We expect the spin J field propagator to obey an equation of the type

$$\begin{aligned}&(\mathcal{D}\Pi)_{a_1\cdots a_J,b_1\cdots b_J}(X,X') = \\ &ie^{2\Phi} g_{a_1(b_1}\cdots g_{|a_J|\,b_J)}\delta_5(X,X') - \text{traces}\,,\end{aligned} \tag{2.28}$$

for some differential operator $\mathcal{D}$. We are interested in the $+\cdots+, -\cdots-$ component of this equation, for which the differential operator $\mathcal{D}$ can be read from (2.19).

Some algebra shows the amplitude (2.27) simplifies to

$$\begin{aligned}\mathcal{A}_J(s,t) = iV\frac{\kappa_J\kappa'_J}{(-2)^J}\, s\int dzdz' e^{3A+3A'-\Phi-\Phi'} \\ |\upsilon_1|^2|\upsilon'_2|^2\left(se^{-A-A'}\right)^{J-1} G_J(z,z',t)\,,\end{aligned} \tag{2.29}$$

where V is the boundary volume. The function

$$G_J(z,z',t) = \int d^2l_\perp e^{-iq_\perp\cdot l_\perp} G_J(z,z',l_\perp)\,, \tag{2.30}$$

is the Fourier transform of

$$\begin{aligned}G_J(z,z',l_\perp) = i(-2)^J e^{(1-J)(A+A')} \\ \frac{1}{2}\int dw^+dw^-\Pi_{+\cdots+,-\cdots-}(z,z',w)\,,\end{aligned} \tag{2.31}$$

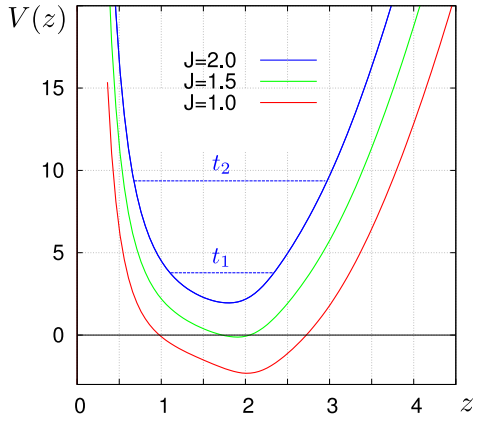

Figure 2.3: Effective potential for different values of spin J. The first 2^{++} glueball states are also shown.

where $w = x - x' = (w^+, w^-, l_\perp)$ and $l_\perp = x_\perp - x'_\perp$. From the $+\cdots+,-\cdots-$ component of (2.28), as defined by (2.19), it follows that $G_J(z, z', l_\perp)$ is an Euclidean scalar propagator in the three-dimensional transverse space of the dual scattering process ($dx^+ = dx^- = 0$ in (2.2)), i.e.

$$\left[\Box_3 - 2e^{-2A(z)}\dot{\Phi}\partial_z - e^{-2A(z)}\left(2\dot{A}^2 + \ddot{A} - 2\dot{A}\dot{\Phi}\right) - \frac{\Delta(\Delta-4)}{L}\right] G_J(z, z', l_\perp) = -e^{2\Phi}\delta_3(x, x')\,, \tag{2.32}$$

where here $x = (z, x_\perp)$ and $x' = (z', x'_\perp)$. Writing

$$G_J(z, z', t) = e^{\Phi(z) - \frac{A(z)}{2}}\psi(z)\,, \tag{2.33}$$

the homogeneous solution to (2.32) is exactly given by the Schrodinger problem of (2.23) and (2.24). Moreover, using $\sum_n \psi_n(z)\psi_n^*(z') = \delta(z - z')$, we conclude that the propagator $G_J(z, z', t)$ can be written in the spectral representation

$$G_J(z, z', t) = e^{\Phi - \frac{A}{2} + \Phi' - \frac{A'}{2}} \sum_n \frac{\psi_n(z)\psi_n^*(z')}{t_n(J) - t}\,. \tag{2.34}$$

Note the eigenvalues t_n and functions ψ_n depend on J.

2.3.4 Regge theory

We will sum all even spin J exchanges with $J \geq 2$ using a Sommerfeld-Watson transform

$$\frac{1}{2}\sum_{J\geq 2}\left(s^J + (-s)^J\right) \to -\frac{\pi}{2}\int \frac{dJ}{2\pi i}\frac{s^J + (-s)^J}{\sin(\pi J)}\,, \tag{2.35}$$

which requires the analytic continuation of the amplitude $\mathcal{A}_J(s,t)$ to the complex J-plane. Then, the amplitude for the exchange off all even spin J fields becomes

$$\mathcal{A}(s,t) = iV \int dz dz' e^{3(A+A')} |\upsilon_1|^2 |\upsilon_2'|^2 \sum_n \chi_n \,, \tag{2.36}$$

where $\chi_n = \chi_n(z,z',s,t)$ is given by

$$\chi_n = -\frac{\pi}{2} \int \frac{dJ}{2\pi i} \frac{s^J + (-s)^J}{\sin(\pi J)} \frac{\kappa_J \kappa_J'}{2^J} e^{-(J-\frac{1}{2})(A+A')} \frac{\psi_n(z)\psi_n^*(z')}{t_n(J) - t} \,.$$

We assume the J-plane integral can be deformed from the poles at even values of J, to the poles $J = j_n(t)$ defined by $t_n(J) = t$. In the scattering domain of negative t these poles are along the real axis for $J < 2$. Thus we can write

$$\chi_n = s^{j_n(t)} \Big[-\frac{\pi}{2} \left(\cot \frac{\pi j_n}{2} + i \right) \frac{\kappa_{j_n} \kappa_{j_n}'}{2^{j_n}} e^{-(j_n - \frac{1}{2})(A+A')} \frac{dj_n}{dt} \psi_n(z) \psi_n^*(z') \Big] \,,$$

where $j_n = j_n(t)$ and we remark that the wave functions ψ_n are computed at $J = j_n(t)$. It is clear that for large s the amplitude (2.36) will be dominated by the Regge pole with highest $j_n(t)$, in accord with the Regge behavior (2.1).

We now specify to the model considered in this chapter, which is determined by the effective Schrödinger potential (2.24). Since we are interested in the region $J < 2$, we can use the model introduced in (2.21) for the curve $\Delta = \Delta(J)$. Figure 2.3 shows the potential for several value of J. The energy levels for $J = 2$ are shown and compute the mass of the spin 2 glueball masses. As J decreases the energy levels will eventually cross the zero energy value. This will be the value of the intercept for the n-th Reggeon. Figure 2.4 shows the curves $j_n(t)$, which clearly show that $n = 1$ is the leading Regge pole. The curves are approximately straight so we can also define a Regge slope. Note that the model considered in this chapter allows us to investigate the region of real $J < 2$ and find the Regge poles. This differs from previous approaches based on Regge trajectories (see for instance [48]).

2.4 Results

Finally we can test to which degree we are reproducing QCD physics. We consider first the leading Regge pole. We vary l_s, introduced in (2.21), to fix the Pomeron intercept to the value given in [7], as an optimal fit for total cross sections. For the value $l_s = 0.178$ GeV^{-1}, and independently of our choice of Λ_{QCD}, we obtained $\alpha_0 = 1.08$. The value of the slope is then fixed by the choice of Λ_{QCD}. We obtained

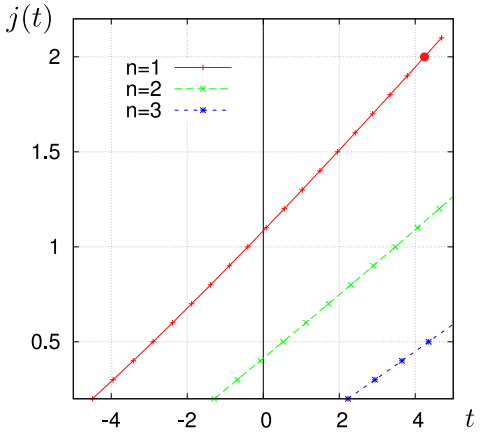

Figure 2.4: The first Regge trajectories that result from solving the Schrödinger problem for discrete values of J. Here t is in GeV^2.

$\alpha'\Lambda_{QCD}^2 = 0.018$. If we fix $\Lambda_{QCD} = 0.292$ GeV as in [43,44], such that the first glueball mass $m_{0^{++}} = 1.475$ GeV, one obtains $\alpha' = 0.21$ GeV^{-2}. If, on the other hand, we require the measured value of $\alpha' = 0.25$ GeV^{-2} [49], we obtain $\Lambda_{QCD} = 0.265$. This is consistent with having the 2^{++} glueball of the Pomeron trajectory with a mass of 1.9 GeV, which is a known possibility [23, 50].

Let us remark that we could fix l_s to reproduce the intercept obtained in lattice simulations of $SU(3)$ pure Yang-Mills [3]. In this case, for $l_s = 0.192$ GeV^{-1} one has $\alpha_0 = 0.93$. Then, setting $\Lambda = 0.292$, which is fixed to reproduce $m_{0^{++}} = 1.475$ GeV of the same lattice simulations, we obtained a slope $\alpha' = 0.25$ GeV^{-2}. This is exactly the slope obtained by the lattice simulations [3].

For the second pole we obtained an intercept of 0.433, which is consistent with the value used in [7]. We ran fits to $p\,\bar{p}$ total cross section data [51] and found that the second pole is necessary and needs to be in a narrow range of $\approx 0.35 - 0.55$. We determined this range by fitting an expression of the form

$$\sigma = g_0(\alpha' s)^{\alpha_0} + g_1(\alpha' s)^{\alpha_1}\,, \tag{2.37}$$

using g_0 and g_1 as parameters, and varying α_1. We fit this to $p\,\bar{p}$ scattering data with $\sqrt{s} > 10\,\text{GeV}$. The above range is fixed by the requirement that $\chi^2_{d.o.f.}$ be of order 1 or less. Our results can be seen in figure 2.5. As can be seen there, using just the leading Pomeron exchange fails to fit the data satisfactorily. The second pole in [7] corresponds to several degenerate meson trajectories, while here it represents a next-to-leading glueball trajectory. Thus, our work points to the possibility that in this range there is a glueball trajectory as well. In fact, at least some of the f_2 states are

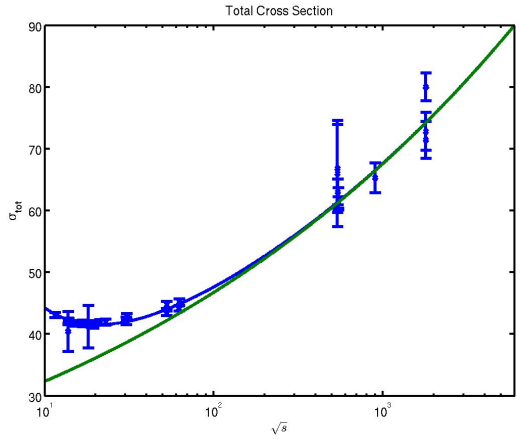

Figure 2.5: A fit to $p\bar{p}$ total cross section data using the exchange of the first two Regge poles in our model. The green line represents the leading Pomeron exchange, and fails to fit the data at moderate values of $\sqrt{s}$.

known to correspond to glueballs (see [52] and references therein for recent results).

2.5 Conclusion

Soft pomeron physics is still beyond the current analytic understanding of QCD. The best one can do at weak coupling is to start from the BFKL approach and then introduce the running of the coupling, therefore breaking conformal symmetry. As a consequence, the branch cut of the BFKL pomeron becomes a set of poles in the J-plane [11]. This approach can be used to fit DIS data for hard scattering, keeping a very large number of poles. However, it is not applicable to the case of soft probes. In general we expect to have a description of soft pomeron exchange as a Regge pole, in agreement with the phenomenological approach pioneered by Donnachie and Landshoff [7]. Such description was proposed in [13], based on scattering of closed strings in a dual confining background. In particular, that work anticipated that for confining theories with a negative β function, the pomeron described as the graviton Regge trajectory becomes a Regge pole. Our work confirms this expectation by extending the holographic QCD model of [43, 44] to scattering processes dominated by soft pomeron exchange, bringing a new insight to soft pomeron physics.

Let us finish with a caveat and two open questions. It has been claimed that a soft Pomeron pole is not enough to describe the new LHC data [53]. This is somewhat expected, since it is known that at very high energies such a Regge pole would violate

the Froissart-Martin bound, and other effects need to be included, for example multi-Pomeron exchange. However, this does not invalidate the great experimental successes of soft Pomeron exchange up to LHC energies, as well as the necessity to understand the subleading trajectories.

The first question is related to the spectrum of the spin J field, at integer values. It would be very nice to reconstruct the spin J equation in this domain, such that it reproduces perturbative QCD results. The second question concerns the relation between hard and soft pomerons. Several studies in gauge/gravity duality reproduce a plethora of low-x processes using the graviton Regge trajectory as the dual trajectory of the QCD Pomeron [14–18]. In these cases one observes a running of the intercept with the size of the probes. It would be very interesting if we could embed these results within the present model, therefore unifying both pomerons. This task will be addressed in the next chapter where, in oposition with what we made in this chapter, we will identify the leading trajectory with the Hard Pomeron and the first subleading one with the Soft Pomeron, and we will see that at least two daughter trajectories more are needed in order to explain the latest Deep Inelastic Scattering data.

3

Unity of the Pomeron from gauge/gravity duality

This chapter is based in [21]. We develop a formalism where the hard and soft pomeron contributions to high energy scattering arise as leading Regge poles of a single kernel in holographic QCD. The kernel is obtained using effective field theory inspired by Regge theory of a 5-d string theory. It describes the exchange of higher spin fields in the graviton Regge trajectory that are dual to glueball states of twist two. For a specific holographic QCD model we describe Deep Inelastic Scattering in the Regge limit of low Bjorken x, finding good agreement with experimental data from HERA. The observed rise of the effective pomeron intercept, as the size of the probe decreases, is reproduced by considering the first four pomeron trajectories. In the case of soft probes, relevant to total cross sections, the leading hard pomeron trajectory is suppressed, such that in this kinematical region we reproduce an intercept of 1.09 compatible with the QCD soft pomeron data. In the spectral region of positive Maldelstam variable t the first two pomeron trajectories are consistent with current expectations for the glueball spectrum from lattice simulations.

3.1 Introduction

Deep inelastic scattering (DIS) is another process where Regge theory is important. In this case we consider the imaginary part of the amplitude for $\gamma^* p \to \gamma^* p$, at zero momentum transfer ($t = 0$), which gives the total cross section for the scattering of an off-shell photon with a proton. Single Reggeon exchange then predicts a total cross section determined by the intercept, $\sigma \sim s^{j(0)-1}$. However this story is bit more evolved. Recall the kinematical quantities defined in section 1.1.5 virtuality of the photon Q^2 and the Bjorken x in the $\gamma^* p$ system, which in the Regge limit is related

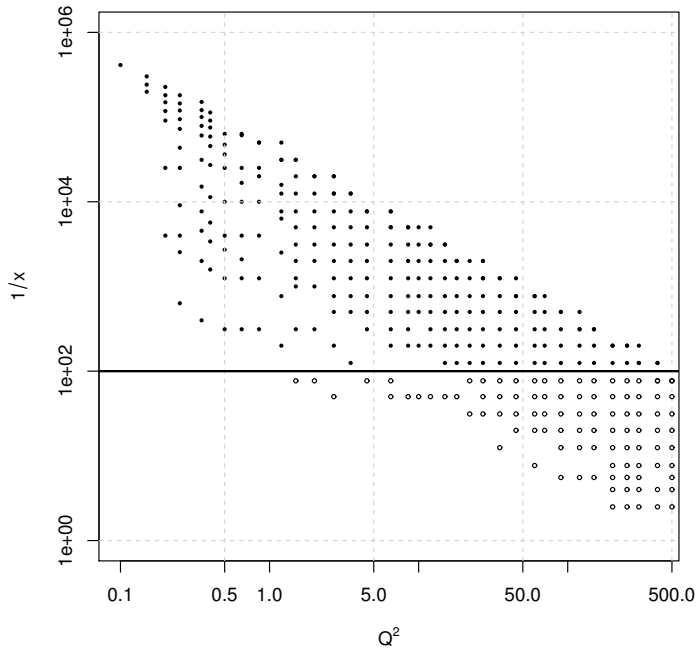

Figure 3.1: Values of x and $Q^2(\mathrm{GeV}^2)$ for the data points analysed in this chapter [2]. Regge kinematics restricts this domain to $x < 0.01$, above the horizontal line.

to s by $s = Q^2/x$, with $x \ll 1$. When HERA data for DIS scattering came out, it was somehow surprising to observe that the rise of the cross section with $1/x$ was actually faster than that predicted by the soft pomeron. The main difference is that, instead of using two soft probes for the scattering process, the off-shell photon virtuality can be well above the QCD confining scale. What is actually observed is a growth of the intercept with Q^2 from about 1.1 to 1.4. More concretely, if we write the total cross section as

$$\sigma\big(x, Q^2\big) = f\big(Q^2\big)\, x^{-\epsilon(Q^2)}\,, \tag{3.1}$$

then the exponent ϵ grows with Q^2. Figure 3.1 shows the latest data points from HERA experiment, restricted to the region of low x where Regge kinematics holds. In figure 3.2 we see the observed behaviour of the exponent $\epsilon(Q^2)$.

The behaviour of the exponent $\epsilon(Q^2)$ for low Q^2 is consistent with the observed intercept of the soft pomeron for soft probes, but for hard probes (larger Q^2) this is no longer the case, suggesting the existence of another trajectory with a bigger intercept, the so called hard pomeron. The nature of both pomerons, and in particular their relation, remains an unsolved problem in QCD. Are the soft and hard pomerons the

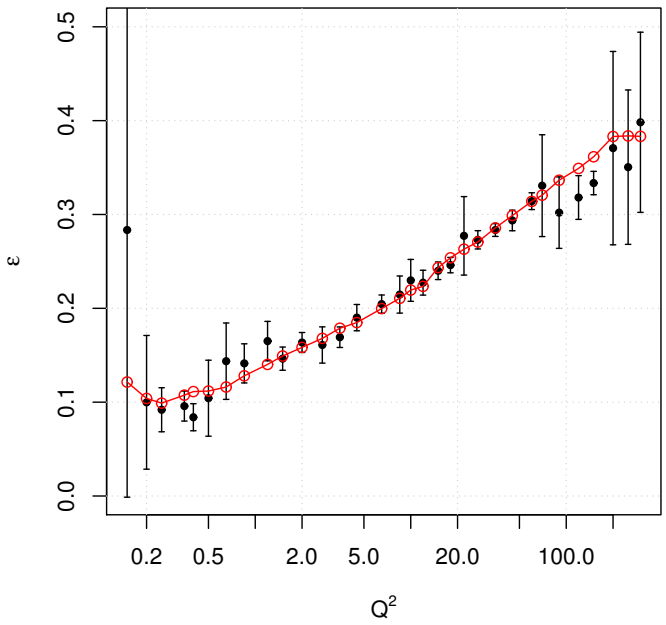

Figure 3.2: The effective exponent $\epsilon(Q^2)$ in DIS. Black dots are obtained by extrapolating the log of the cross section at fixed $Q^2(\mathrm{GeV}^2)$ with a straight line in $\log x$. The corresponding error bars are at 3σ. The red curve is our prediction for the effective exponent using the model proposed in this work.

same or distinct trajectories? Our main motivation in this work is to use holography to shed light into this problem.

A very interesting proposal to resolve the above puzzle was again put forward by Donnachie and Landshoff [5, 53–56]. They proposed that the hard and soft pomerons are distinct trajectories, with the hard pomeron intercept around 1.4. The soft pomeron would be dominant in the soft region, since it is already well established to explain all soft processes, and the hard pomeron with a bigger intercept would dominate in the hard processes. More concretely, the idea is to write the cross section as

$$\sigma\big(x, Q^2\big) = \sum_n f_n\big(Q^2\big)\, x^{-\epsilon_n}\,, \tag{3.2}$$

where the sum runs over distinct trajectories. Then the effect of summing over several trajectories, which compete with each other as one varies the virtuality Q^2, has the desired effect of producing a varying effective exponent $\epsilon(Q^2)$, as shown in figure 3.2. We shall follow this perspective and see that it follows naturally using the gauge/string

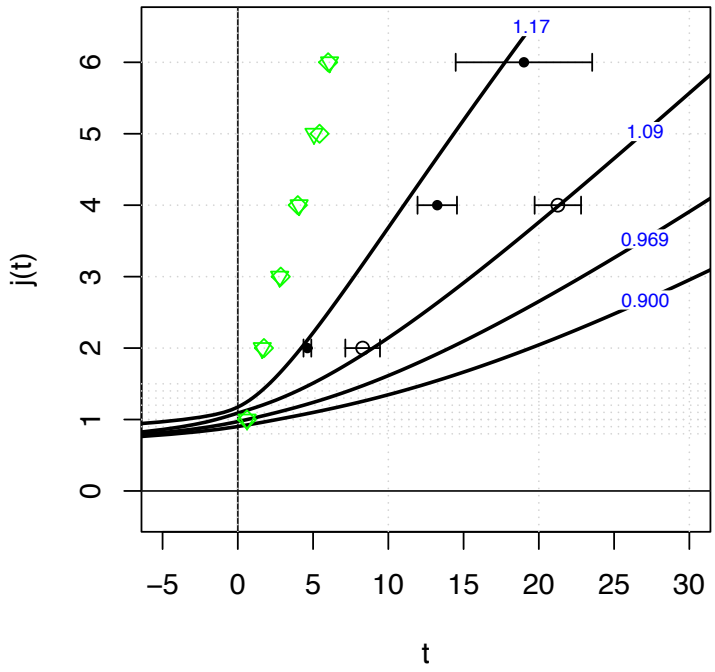

Figure 3.3: The first four pomeron trajectories found in this chapter. The blue labels are the intercepts of each one. Shown are also the square of the masses of the higher spin glueballs from lattice QCD data [3,4], which clearly seem to belong to the hard and soft pomeron trajectories. In green we plotted the masses of vector mesons, which also contribute to DIS, but are expected to have a lower intercept than the first pomeron trajectories considered in this chapter. Horizontal axis is in GeV^2.

duality as a tool to study QCD strongly coupled phenomena.

In this chapter we shall explore the above Regge theory ideas for DIS in the new framework of the gauge/string duality. We shall test our predictions using the specific holographic QCD model. Our main findings are summarized in figures 3.2 and 3.3. We show that low x DIS data, and in particular the running of the effective exponent $\epsilon(Q^2)$, can be reproduced considering only the first four pomeron trajectories arising from the graviton trajectory in holographic QCD. The glueball trajectories shown in figure 3.3 are fixed by DIS scattering data, but they are also consistent with results of higher spin glueballs from lattice simulations [3, 4].

This chapter is organized as follows. In section 3.2, we redo the computation by

Donnachie and Landshoff that tries to reproduce DIS data with a hard and a soft pomeron, determining the functions $f_n(Q^2)$ in (3.2) from data analysis. Quite remarkably if we translate these functions into the proper gauge/string duality language, they are nothing but wave functions describing the normalizable modes of the graviton Regge trajectory. Section 3.3 presents the necessary formulae to study DIS using the gauge/string duality. The discussion is standard and already scattered in existing literature. In section 3.4 we focus on the pomeron trajectory, and in particular in constructing the analytic continuation of the spin J equation that describes string fields in the graviton Regge trajectory. This discussion extends that already presented in the previous chapter. In section 3.5 we do the data analysis, fitting low x DIS data in the very large kinematical range of $0.1 < Q^2 < 400$ GeV^2. Our best fit has a χ^2 per degree of freedom of 1.7, without removing presumed outliers existing in data. This leads us to the pomeron Regge trajectories shown in figure 3.3.

3.2 What is DIS data telling us about holographic QCD?

The physics of the pomeron in the gauge/string duality was uncovered in [13] where pomeron exchange was identified with the exchange of string states in the graviton Regge trajectory. The amplitude for a $2 \to 2$ scattering process in the Regge limit is then of the general form:

$$A(s,t) = \int dz d\bar{z}\, \phi_1(z)\phi_3(z)\, \mathcal{K}_P(s,t,z,\bar{z})\, \phi_2(\bar{z})\phi_4(\bar{z})\,, \tag{3.3}$$

where the functions $\phi_k(z)$ represent the external scattering waves functions for a given process and $\mathcal{K}_P(s,t,z,\bar{z})$ is the so-called kernel of the pomeron which represents the tree level interchange of the aforementioned string states. Leaving aside technicalities which will be discussed in section 3.3, the pomeron kernel has the following dual representation

$$\mathcal{K}_P(s,t,z,\bar{z}) = \sum_n f_n\, s^{j_n(t)-1} \psi_n\big(j_n(t),z\big)\psi_n^*\big(j_n(t),\bar{z}\big)\,, \tag{3.4}$$

where the sum runs over the graviton Regge trajectories $j_n(t)$ that arise from quantising string states in the "AdS" box. The quantum number n plays a important role in this work, since the contribution of the first few pomeron trajectories will be vital to reproduce the DIS cross section. The prefactor f_n depends on $j_n(t)$, it factorizes in

z and z', and it has a functional form that depends on the specific QCD holographic dual. We shall see that in general it has the form

$$f_n = g\big(j_n(t)\big)\, e^{(1-j_n(t))A(z)} e^{B(z)}\, e^{(1-j_n(t))A(\bar{z})} e^{B(\bar{z})}\,, \tag{3.5}$$

where A is the usual conformal function in the 5D dual metric and the function B will be determined by the background fields, for instance by the dilaton field Φ. For the specific holographic model used in this chapter we will have $B = \Phi - A/2$.

The function $\psi_n(z)$ in (3.4) is the n-th excited wave function of a Schrödinger problem. We shall see that this fact follows from the spectral representation of the propagator of spin J string fields in the graviton Regge trajectory that are exchanged in the dual $5D$ geometry, analytically continued to $J = j_n(t)$. This is a highly non-trivial statement that can be checked by looking at an amplitude of the form (3.3) and fitting it to data. Once the external state functions ϕ_k and the specific functional form (3.5) are fixed, we can use data to confirm, or disprove, this fact. More concretely, if we consider a process dominated in the Regge limit by pomeron exchange and choose a specific holographic QCD model, we can test this model since the data should *know* about the underlying Schrödinger problem formulated in the dual theory.

We consider DIS, for which the $p + \gamma^* \to X$ total cross section can be computed, through the optical theorem, from the imaginary part of the amplitude (3.3) for $p + \gamma^* \to p + \gamma^*$ at zero momentum transfer. In this case two of the external state functions, say $\phi_{1,3}(z)$, represent the off-shell photon which couples to the quark bilinear electromagnetic current operator, which is itself dual to a bulk $U(1)$ gauge field. The insertion of a current operator in a correlation function is then described by a non-normalizable mode of this bulk gauge field. The other two functions, $\phi_{2,4}(\bar{z})$, describe the target proton in terms of a bulk normalizable mode. We recall that, in QCD language, the functions $\phi_k(z)$ are known as dipole wave functions of the external states.

We wish to find out if the available experimental data is compatible with the holographic recipe, leaving aside technicalities which will be discusses in section 3.3. As it is well known, the imaginary part of the amplitude (3.3) at $t = 0$ is related to the structure function $F_2(Q^2, x)$. Here Q is the offshellness of the spacelike probe photon, whose dependence enters through the external state wave functions $\phi_{1,3}(z)$. The Maldelstam variable s is related to x by the usual expression $s = Q^2/x$, so we are in the low x regime. As a first approximation, the integration over the variable z in the amplitude (3.3) can be done by considering a Dirac delta function centred at $z \sim 1/Q$. This is a good approximation only for large Q, i.e. near the AdS boundary at $z \to 0$,

but it will be enough for the purpose of this section. In any case it is a quick way to gain some insight about the shape of the kernel and the compatibility of our proposal with the experimental data. The $\bar{z}$ integral can simply be done because the expression factorizes and the external wave functions $\phi_{2,4}(\bar{z})$ are normalizable, therefore affecting the contribution of each Regge pole by an overall multiplicative constant. After these steps the expression for F_2, as we will see in the next section, drastically simplifies to

$$F_2(Q^2,x) = x\sum_n c_n \left(\frac{Q^2}{x}\right)^{j_n} e^{(-j_n+\frac{1}{2})A(1/Q)} e^{\Phi(1/Q)} \psi_n(1/Q)\,, \tag{3.6}$$

where the c_n do not depent neither on x nor on Q, and we denoted by j_n the intercept values of each Reggeon $j_n(t=0)$. Here we are keeping the right warp factor and dilaton dependence, but if one takes the conformal limit, $A(z) = -\log(z)$ and $\Phi = const$, the qualitative result would be the same. Thus we predict a structure function of the form

$$F_2(Q^2,x) = \sum_n f_n(Q^2)\, x^{1-j_n}\,, \tag{3.7}$$

where $f_n(Q^2)$ is the product of known functions and a Schrödinger wave function with quantum number n (the n-th excited state). More concretely, a generic confining potential would produce wavefunctions where its number of nodes can be used to label them: the ground state would have one node, the first excited state would have two nodes and so on.

Let us now focus on the QCD side of the problem. Using Regge theory arguments Donnachie and Landshoff [54] proposed that the structure function has precisely the form (3.7). We can do the same reasoning as them. In order to know more about the functions $f_n(Q^2)$ the simplest thing to do is to first consider some fixed values of the j_n that are physically reasonable, like $j_0 = 1.43$ and $j_1 = 1.08$. These are reasonable values for the intercepts of the hard and soft pomeron, that are now unified in a single framework, since they appear as distinct Regge trajectories of the dual graviton trajectory in a confining background. Next, for a fixed value of Q^2 we find the best coefficients f_0 and f_1 that match the data with the formula $f_0\, x^{1-j_0} + f_1\, x^{1-j_1}$, then we can see how these coefficients evolve with Q^2. This was already done for a different set of data in [54], which served as a starting point for the authors' proposal for the $f_{0,1}(Q^2)$ functional dependence. Of course the shape of the functions depends on the choice of the intercepts but it is well motivated, given the vast experimental evidence to fix the soft pomeron intercept around $j_1 = 1.08$. Regarding j_0 we should be open to different values, but the expectation is that it will be responsible for the faster growth observer in DIS at higher values of Q^2. The left panel of figure 3.4 shows the result of

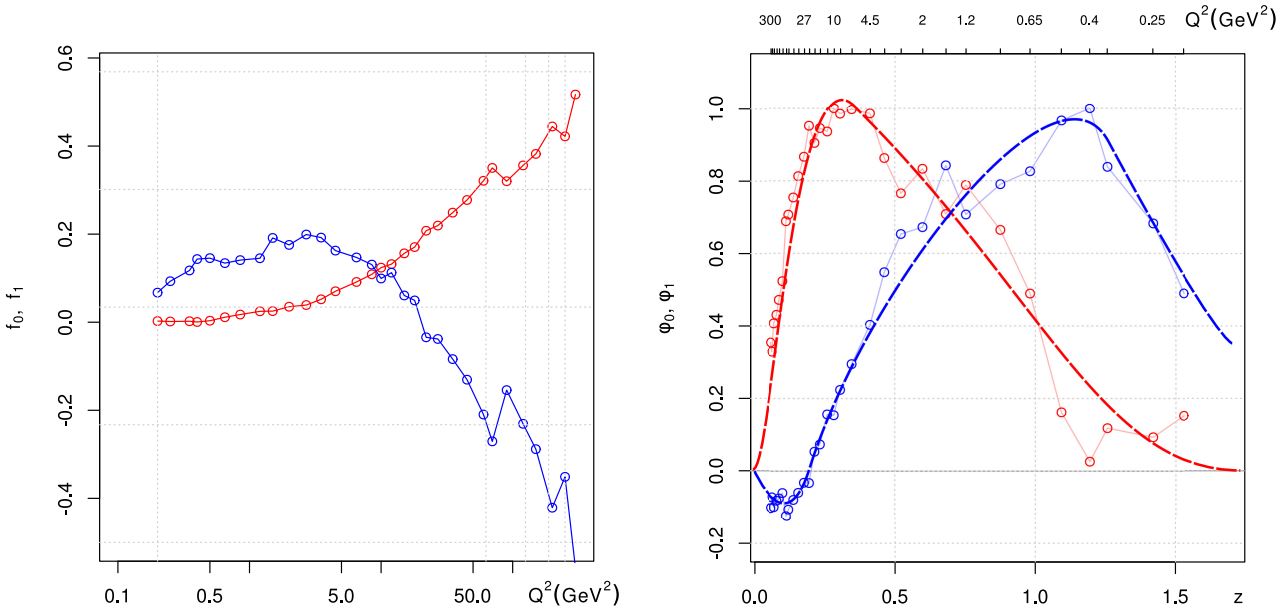

Figure 3.4: Hard (red) and soft (blue) pomerons guess from data. Left panel presents the plots of $f_{0,1}(Q)$ similar to [5]. The right panel shows the associated wavefunctions $\psi_{0,1}(z)$, after considering the prefactor suggested by the gauge/gravity duality. The values $j_0 = 1.26$, $j_1 = 1.08$ have been used, close to what we find later in the paper. Clearly the shape of the wave functions is that of a ground state and of a first excited state of some Schrödinger operator.

this procedure for the values $j_0 = 1.26$ and $j_1 = 1.08$, close to what we will show to be the intercepts that give the best fit in our model. The point we want to emphasize is that apparently not much is learned from the shape of these functions.

However, if we divide the functions $f_{0,1}(Q^2)$ by the appropriate functions, as given by (3.6), the putative wave functions $\psi_{0,1}(z = 1/Q)$ of the Schrödinger problem emerge. This remarkable fact is shown in the right panel of figure 3.4, which clearly meets our expectations. We should remark that if we use instead $j_1 = 1.43$, as first suggested by Donnachie and Landshoff, we do not observe the oscillatory behavior expected for ψ_1, suggesting perhaps that this value is unphysical. In fact it is known that recent data suggests a smaller j_0 [53]. Indeed, as soon as we get below certain threshold value for j_1 the oscillatory behaviour becomes evident with the first node of ψ_1 localized very close to the boundary. Moreover, the form of the wavefunctions in our kernel will be very similar to the dashed lines in the figure. We take this as a strong evidence that the DIS data has encoded the dynamics suggested by holographic QCD. In the next sections we will proceed to phenomenologically construct the effective Schrödinger potential that leads to the wavefunctions $\psi_n(z)$ that fit best the data.

The discussion of this section was oversimplified, but it brings out the main idea. In practice, the integral over z in the dual representation of the amplitude (3.3) is not localized, since we also consider lower values of Q^2. Also, to get a reasonable fit to the data we need to include the first four pomeron Regge trajectories. This is fine because those trajectories will be dominant with respect to the $1/s$ corrections to the leading hard pomeron trajectory. Eventually one would also need to include the exchange of meson Regge trajectories, but that is for now left out of our work, since those trajectories are presumably still suppressed with respect to the first four Pomerons.

3.3 Low x DIS in holographic QCD

In this section we present the essential ingredients of the effective field theory description for low x DIS in holographic QCD. First we briefly describe the kinematics of DIS and its connection to the forward Compton scattering amplitude via the optical theorem. Then we present the holographic description of that amplitude, in the Regge limit, via the exchange of higher spin fields. We finish the section deriving a formula similar to (3.7) which encodes the Regge pole contribution to the DIS structure functions.

3.3.1 Kinematics

The structure function $F_2(x, Q^2)$ is related to the total cross-section of the inelastic $\gamma^* p \to X$ process. As already explained in chapter 1, we have

$$\sigma_T + \sigma_L = \frac{4\pi^2\alpha}{Q^2} F_2(x, Q^2)\,, \tag{3.8}$$

where α is the fine structure constant and σ_T and σ_L are the total cross-sections for the process $\gamma^* p \to X$ with γ^* having transverse and longitudinal polarizations respectively. Through the optical theorem, these total cross-sections can be related to the imaginary part of the amplitude of the correspondent elastic forward Compton scattering $\gamma^* p \to \gamma^* p$ process, thus

$$F_2(x, Q^2) = \frac{Q^2}{4\pi^2\alpha} \frac{1}{s} \operatorname{Im} \mathcal{A}(s, t = 0)\,, \tag{3.9}$$

where $\mathcal{A} \equiv \mathcal{A}_T + \mathcal{A}_L$, s and t are the usual Mandelstam variables (in the low x regime, $s = Q^2/x$). We will compute this amplitude using the AdS/QCD prescription as

described below. In light-cone coordinates $(+,-,\perp)$, for the external off-shell photon with virtuality Q^2 we take

$$k_1 = \left(\sqrt{s}, -\frac{Q^2}{\sqrt{s}}, 0\right), \qquad -k_3 = \left(\sqrt{s}, \frac{q_\perp^2 - Q^2}{\sqrt{s}}, q_\perp\right), \tag{3.10}$$

while for the target hadron of mass M we take

$$k_2 = \left(\frac{M^2}{\sqrt{s}}, \sqrt{s}, 0\right), \qquad -k_4 = \left(\frac{M^2 + q_\perp^2}{\sqrt{s}}, \sqrt{s}, -q_\perp\right). \tag{3.11}$$

The Regge limit corresponds to $s \gg t = -q_\perp^2$ and the case $t = 0$ corresponds to forward Compton scattering. Recall that $q = k_1 = -k_3$ and $P = k_2 = -k_4$. The possible polarization vectors for the incoming and outgoing vector fields are

$$n^\mu(\lambda) = \begin{cases} (0, 0, \epsilon_\lambda), & \lambda = 1, 2, \\ (\sqrt{s}/Q, Q/\sqrt{s}, 0), & \lambda = 3, \end{cases} \tag{3.12}$$

where ϵ_λ is just the usual transverse polarization vector.

3.3.2 Regge theory in holographic QCD

In DIS there are two interesting limits that are usually considered. The first is the Bjorken limit, where $Q^2 \to \infty$ with x fixed. In this limit perturbative QCD provides a good description of the experimental data in terms of partonic distribution functions. The second interesting case is the limit of $s \to \infty$, the so-called Regge limit of DIS, for which Q^2 is fixed and $x \approx -Q^2/s$ is very small. In this limit the hadron becomes a dense gluon medium so that the picture of the hadron made of weakly interacting partons is no longer valid. As explained in section 3.2, in this chapter we investigate DIS in the Regge limit (low x) from the perspective of the pomeron in holographic QCD, which encodes the dynamics of the dense gluon medium. We develop a five dimensional model for the graviton Regge trajectory for a family of backgrounds dual to QCD-like theories in the large-N limit. Our formalism leads to the existence of a set of leading Regge poles describing DIS in the Regge limit, the first two interpreted as the hard and soft pomerons.

Let us now consider the computation of the forward Compton scattering amplitude in holographic QCD. We are interested in elastic scattering between a virtual photon and a scalar particle with incoming momenta k_1 and k_2, respectively. As explained, we will extract the DIS structure functions from the forward Compton amplitude. First we define with generality the holographic model that may be used. We need to define

the external states in DIS and the interaction between them that is dominated by a t-channel exchange of higher spin fields (those in the graviton Regge trajectory). Later on, to compare with the data, we will use a specific holographic QCD model [43, 44], but for now we will write general formulae that can be used in other models.

The string dual of QCD will have a dilaton field and a five-dimensional metric that are, respectively, dual to the Lagrangian and the energy-momentum tensor. We use the same background dynamic as in chapter 2. The warp factor $A(z)$ is defined with respect to the string frame metric.

In DIS the external photon is a source for the conserved $U(1)$ current $\bar{\psi}\gamma^{\mu}\psi$, where the quark field ψ is associated to the open string sector. The five dimensional dual of this current is a massless $U(1)$ gauge field A. We shall assume that this field is made out of open strings and that is minimally coupled to the metric, so its effective action is the one described in section 1.2.5 with $\beta = 0$[1]. In the next chapter a detailed consideration of the case $\beta \neq 0$ will be done, we omit it here since the discussion is considerably technical and different.

For the target we consider a scalar field Υ that represents an unpolarised proton. This hadronic state is described by a normalizable mode of the form

$$\Upsilon(x,z) = e^{iP\cdot x}\upsilon(z)\,. \tag{3.13}$$

The specific details will not be important. We will simply assume that we can make the integration over the point where this field interacts with the higher spin fields. The effect of such an overall factor can be absorbed in the coupling constant.

The next step in our construction is to introduce the higher spin fields $h_{b_1\ldots b_J}$ that will mediate the interaction terms between the external fields of the scattering process. As already pointed out, these fields are dual to the spin J twist two operators made of the gluon field that are in the leading Regge trajectory. There are also other twist two operators made out of the quark bilinear. However, as we shall see, the corresponding Regge trajectories are subleading with respect to the first pomeron trajectories here considered. Noting that the higher spin field is in the closed string sector, and that the external fields are in the open sector, we shall consider the minimal coupling

$$\kappa_J \int d^5X\sqrt{-g}\,e^{-\Phi}\left(F_{b_1 a}D_{b_2}\ldots D_{b_{J-1}}F^{a}_{\ b_J}\right)\,h^{b_1\ldots b_J}\,, \tag{3.14}$$

[1]Only in the body of this chapter the photon polarization vector is denoted by ξ to keep the discussion in line with [21].

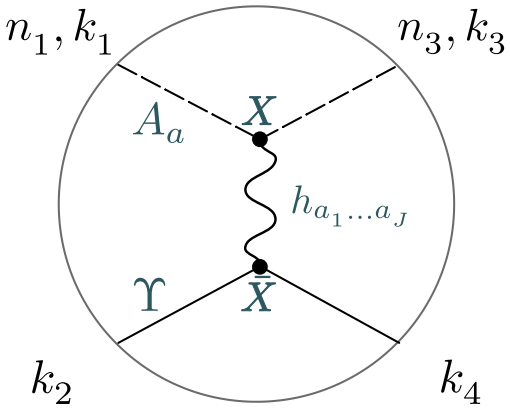

Figure 3.5: Tree level Witten diagram representing spin J exchange in a $12 \to 34$ scattering.

for the gauge field A_a and

$$\bar{\kappa}_J \int d^5X \sqrt{-g}\, e^{-\Phi}\, (\Upsilon D_{b_1} \ldots D_{b_J} \Upsilon)\, h^{b_1 \ldots b_J}\,, \tag{3.15}$$

for the scalar field Υ. The higher spin field $h_{b_1 \ldots b_J}$ is totally symmetric, traceless and satisfies the transversality condition $\nabla^{b_1} h_{b_1 \ldots b_J} = 0$. The latter fact implies we do not need to worry in which external fields the derivatives in (3.14) and (3.15) act. However, there can be other couplings to the derivatives of the dilaton field and also to the curvature tensor. Here we consider only this leading term in a strong coupling expansion (that is, the first term in the derivative expansion of the effective action). Below we simply assume that the higher spin field has a propagator, without specifying its form. In the next section we focus on the dynamics of this field in detail.

In the Regge limit, the amplitude describing the spin J exchange between the incoming gauge field $A_a^{(1)} \sim e^{ik_1 \cdot x}$ and scalar field $\Upsilon^{(2)} \sim e^{ik_2 \cdot x}$ can be written as

$$\begin{aligned} A_J\left(k_1, k_2, k_3, k_4\right) = (i\kappa_J)\,(i\bar{\kappa}_J) \int d^5X \int d^5\bar{X} \sqrt{-g(z)}\, e^{-\Phi(z)} \sqrt{-g(\bar{z})}\, e^{-\Phi(\bar{z})} \\ \times \left(F_{-\,a}{}^{(1)}(X) \partial_-^{J-2} F^a{}_{-}{}^{(3)}(X)\right)\, \Pi^{-\cdots-,+\cdots+}(X, \bar{X})\, \left(\Upsilon^{(2)}(\bar{X}) \bar{\partial}_+^J \Upsilon^{(4)}(\bar{X})\right). \end{aligned} \tag{3.16}$$

The correspondent Witten diagram is shown in figure 3.5. The fields $A_a^{(3)} \sim e^{ik_3 \cdot x}$ and $\Upsilon^{(4)} \sim e^{ik_4 \cdot x}$ represent the outgoing gauge and scalar fields. The tensor $\Pi^{a_1 \ldots a_J, b_1 \ldots b_J}(X, \bar{X})$ represents the propagator of the spin J field. After some algebra the amplitude takes the form

$$\begin{aligned} A_J\left(k_1, k_2, k_3, k_4\right) = iV \left(\frac{4}{s}\right) \frac{\kappa_J \bar{\kappa}_J}{2^J} \int dz \int d\bar{z} \sqrt{g_3(z)} e^{-\Phi(z)} \sqrt{g_3(\bar{z})} e^{-\Phi(\bar{z})} \\ \times F_{-\,a}\left(k_1, z\right) F^a{}_{-}\left(k_3, z\right) \Upsilon\left(k_2, \bar{z}\right) \Upsilon\left(k_4, \bar{z}\right) \left[S(z, \bar{z})\right]^J \left[e^{A(z)} e^{A(\bar{z})} G_J(z, \bar{z}, t)\right], \end{aligned} \tag{3.17}$$

where $V = (2\pi)^4\delta^4(\sum k_i)$ and $g_3(z)$ is the determinant of the 3-d transverse metric given by $ds_3^2 = e^{2A(z)}\left[dz^2 + dx_\perp^2\right]$. This is the metric on the transverse space of the dual scattering process. The local energy squared for the dual scattering process is given by $S(z,\bar{z}) = s\, e^{-A(z)}e^{-A(\bar{z})}$. The function $G_J(z,\bar{z},t) = \int d^2l_\perp e^{-iq_\perp\cdot l_\perp}G_J(z,\bar{z},l_\perp)$ is the Fourier transform of the integrated propagator for a field of even spin J,

$$G_J(z,\bar{z},l_\perp) = i\,2^J\left[e^{A(z)}e^{A(\bar{z})}\right]^{1-J}\int\frac{dw^+dw^-}{2}\Pi_{+\cdots+,-\cdots-}(w^+,w^-,\ell_\perp,z,\bar{z})\,, \tag{3.18}$$

and the light-cone coordinates $w^\pm$ are defined by the relation $x-\bar{x} = (w^+,w^-,l_\perp)$ with $l_\perp = x_\perp - \bar{x}_\perp$. For the case of forward Compton scattering we have that $k_1 = -k_3 = q$, $k_2 = -k_4 = P$ and $t = 0$. Summing over the contribution of the fields with spin $J = 2,4,\ldots$ and taking the imaginary part, we find using 3.9

$$F_2\left(x,Q^2\right) = 8\pi Q^2\int dzd\bar{z}\,P_{13}\left(Q^2,z\right)P_{24}\left(P^2,\bar{z}\right)\mathrm{Im}\big[\chi(s,t=0,z,\bar{z})\big], \tag{3.19}$$

where we have defined

$$\begin{aligned} P_{13}\left(Q^2,z\right) &= \sqrt{g_3(z)}e^{-\Phi(z)}e^{-2A(z)}\left[f^2 + \frac{1}{Q^2}\left(\partial_z f\right)^2\right], \\ P_{24}\left(P^2,\bar{z}\right) &= \sqrt{g_3(\bar{z})}e^{-\Phi(\bar{z})}\,\Upsilon^2\left(P^2,\bar{z}\right), \end{aligned} \tag{3.20}$$

and $\chi(s,t,z,\bar{z})$ is the eikonal phase defined by

$$\chi(s,t,z,\bar{z}) = -\left(\frac{\pi}{4s}\right)\int\frac{d\,J}{2\pi i}\frac{[S(z,\bar{z})]^J + [-S(z,\bar{z})]^J}{\sin(\pi J)}\frac{\kappa_J\bar{\kappa}_J}{2^J}\,e^{A(z)+A(\bar{z})}G_J(z,\bar{z},t)\,. \tag{3.21}$$

In (3.21) we used a Sommerfeld-Watson transform to convert the sum in $J = 2,4,\ldots$ into an integral in the complex J-plane.

3.3.3 Regge poles

In the next section we will describe the dynamics of a higher spin field $h_{a_1\ldots a_J}$. In particular, we shall see how the propagator $G_J(z,z',t)$ admits a spectral representation associated to a Schrödinger problem that describes massive spin J glueballs. Assuming that such Schrödinger potential admits an infinite set of bound states for fixed J, we will show that

$$G_J(z,\bar{z},t) = e^{B(z)+B(\bar{z})}\sum_n\frac{\psi_n(J,z)\,\psi_n^*(J,\bar{z})}{t_n(J)-t}\,. \tag{3.22}$$

The function $B(z)$ depends on the particular holographic QCD model and will be obtained below for backgrounds of the form (2.2). The eigenfunctions and eigenvalues

of the Schrödinger equation are $\psi_n(J,z)$ and $t_n(J)$, respectively. Plugging this result in (3.21) and deforming the contour integral, so that we pick up the contribution from the Regge poles $j_n(t)$, we find that [2]

$$\chi(s,t,z,\bar{z}) = -\left(\frac{\pi}{4s}\right) e^{A(z)+A(\bar{z})+B(z)+B(\bar{z})} \times \sum_n \frac{\kappa_{j_n(t)}\bar{\kappa}_{j_n(t)}}{2^{j_n(t)}} \left[\cot\left(\frac{\pi}{2}j_n(t)\right)+i\right] [S(z,\bar{z})]^{j_n(t)} j_n'(t)\, \psi_n\big(j_n(t),z\big)\, \psi_n^*\big(j_n(t),\bar{z}\big)\,. \tag{3.23}$$

In DIS this result implies that the structure functions $F_1(x,Q^2)$ and $F_2(x,Q^2)$ take the Regge form

$$F_2\left(x,Q^2\right) = \sum_n g_n\, x^{1-j_n(0)} Q^{2j_n(0)} \bar{P}_{13}{}^n\big(Q^2\big)\,, \tag{3.24}$$

where we have defined the functions

$$\bar{P}_{13}{}^n\big(Q^2\big) = \int dz\, P_{13}\left(Q^2,z\right) e^{(1-j_n(0))A(z)} e^{B(z)} \psi_n\big(j_n(0),z\big)\,, \tag{3.25}$$

and the couplings

$$g_n = -2\pi^2 \frac{\kappa_{j_n(0)}\bar{\kappa}_{j_n(0)}}{2^{j_n(0)}}\, j_n'(0) \int dz\, P_{24}\big(P^2,z\big)\, e^{(1-j_n(0))A(z)} e^{B(z)} \psi_n^*\big(j_n(0),z\big)\,. \tag{3.26}$$

Notice that in (3.24) we have already used the relation $s = Q^2/x$, valid in the Regge limit of DIS. The couplings g_n include our ignorance of the hadron dual wave function, which appears in the integrand of (3.26), as well as the local couplings in the dual picture between the external fields and the spin J field. The formula (3.24) has the expected form (3.7) advocated by Donnachie and Landshoff.

3.4 Pomeron in holographic QCD

In the large s scattering regime the lowest twist two operators dominate in the OPE of the currents appearing in the computation of the hadronic tensor. Therefore we consider here the interchange of the gluonic $\mathcal{O}_J$ twist 2 operators of the form

$$\mathcal{O}_J \sim \mathrm{tr}\left[F_{\beta\alpha_1} D_{\alpha_2} \ldots D_{\alpha_{J-1}} F^{\beta}_{\ \alpha_J}\right], \tag{3.27}$$

where D is the QCD covariant derivative. In the singlet sector there are also twist 2 quark operators of the form $\bar{\psi}\gamma_{\alpha_1} D_{\alpha_2} \cdots D_{\alpha_J}\psi$, but these are subleading because the corresponding Regge trajectory has lower intercept. From a string theory perspective

[2] This procedure is standard in Regge Theory (see e.g. [23]).

the equations of motion for the higher spin fields dual to $\mathcal{O}_J$ should come by requiring their correspondent vertex operator to have conformal weights $(1,1)$ in the background dual to the QCD vacuum. We shall follow an effective field theory approach, proposing a general form of the equation in a strong coupling expansion, and then use the experimental data to fix the unknown coefficients. The proposed equation will obey two basic requirements, namely to be compatible with the graviton's equation for the case $J = 2$ and to reduce to the well known case in the conformal limit (pure AdS space with constant dilaton), as already explained in the previous chapter.

Let us consider first the conformal case ($A(z) = \log(L/z)$ and constant dilaton). In AdS space the spin J field obeys the equation

$$\left(\nabla^2 - M^2\right) h_{a_1 \cdots a_J} = 0\,, \qquad\qquad (LM)^2 = \Delta(\Delta - 4) - J\,, \tag{3.28}$$

where L is the AdS length scale and Δ is the dimension of $\mathcal{O}_J$. Note that this field is symmetric, traceless ($h^b{}_{ba_3 \cdots a_J} = 0$) and transverse ($\nabla^b h_{ba_2 \cdots a_J} = 0$). This equation is invariant under the gauge transformation $\delta h_{a_1 \ldots a_J} = \nabla_{a_1} \Lambda_{a_2 \ldots a_J}$ with $\nabla^2 \Lambda_{a_2 \ldots a_J} = 0$, but we will modify this in such a way that this gauge symmetry will be broken, as expected for a dual of a QFT with no infinite set of conserved currents. This is trivially achieved by changing the value of M in (3.28) away from the unitarity bound $\Delta = J + 2$. The transversality condition allows us to consider as independent components only the components $h_{\alpha_1 \ldots \alpha_J}$, along the boundary direction. These can be further decomposed into irreducible representations of the Lorentz group $SO(1,3)$, so that the traceless and divergenceless sector $h^{TT}_{\alpha_1 \ldots \alpha_J}$ decouple from the rest and describe the $\mathcal{O}_J$ in the dual theory. Finally note that we can analyse the asymptotic form of the spin J equation of motion (3.28) near the boundary, with the result

$$h_{\alpha_1 \ldots \alpha_J} \sim z^{4-\Delta-J} \mathcal{J} + \ldots + z^{\Delta - J} \langle \mathcal{O}_J \rangle + \ldots \tag{3.29}$$

where $\mathcal{J}$ denotes the source for $\mathcal{O}_J$. Since under the rescaling $z \to \lambda z$ the AdS field $h_{\alpha_1 \ldots \alpha_J}$ has dimension J, we conclude that the operator $\mathcal{O}_J$ and its source have, respectively, dimension Δ and $4 - \Delta$, as expected. In the case that concerns us, since QCD is nearly conformal in the UV, we can do a similar analysis near the boundary.

Next let us consider the case $J = 2$, where we have some control. This is the case of the energy-momentum tensor dual to the graviton. To describe the TT metric fluctuations we need to assume what is the dynamics of this field. The simplest option is to consider an action for the metric and dilaton field of the form

$$S = M^3 N_c^2 \int d^5X \sqrt{-g}\, e^{-2\Phi} \left[R + 4\left(\partial\Phi\right)^2 + V(\Phi)\right]\,, \tag{3.30}$$

where we work in the string frame. Our goal is to write a two derivative equation for the spin J fields using effective field theory arguments in an expansion in the derivatives of the background fields. The arguments are in the line of the ones already discussed in section 2.3.2, the new ingredients in the proposed equation of motion for the spin J field are the addition of already discussed possible terms related to α' corrections in string theory. After decomposing this field in $SO(1,3)$ irreps, the TT part $h^{TT}_{\alpha_1\cdots\alpha_J}$ decouples from the other components and describes the propagating degrees of freedom. The proposed equation has the form

$$\Big(\nabla^2 - 2\,e^{-2A}\dot{\Phi}\nabla_z - \frac{\Delta(\Delta-4)}{L^2} + J\dot{A}^2 e^{-2A} + \\ (J-2)e^{-2A}\left(a\,\ddot{\Phi} + b\left(\ddot{A} - \dot{A}^2\right) + c\,\dot{\Phi}^2\right)\Big) h^{TT}_{\alpha_1\ldots\alpha_J} = 0\,, \tag{3.31}$$

where a, b and c are constants. Several comments are in order: (i) For $J = 2$ this equation reduce sto the graviton equation (2.14); (ii) In the AdS case all terms in the second line vanish and the equation reduces to (3.28) for the TT components; (iii) The second term comes from the tree level coupling of a closed string, as appropriate for the graviton Regge trajectory in a large N approximation; (iv) This action contains all possible terms of dimension inverse squared length compatible with constraints (i) and (ii) above. Notice that the term $\dot{\Phi}\dot{A}$ is absent because it reduces to other two derivative terms of A and Φ by the equations of motion. Also, note that the terms with two z derivatives are accompanied by a metric factor $g^{zz} = e^{-2A}$ from covariance of the 5-d theory. The exception is the first term, which itself includes the 5-d metric $\nabla^2 = g^{ab}\nabla_a\nabla_b$, and the third that is a mass term related to the dimension of the dual operator, which requires a length scale L.

It is important to realize that (3.31) is not supposed to work for any J. Instead, we are building the analytic continuation of such an equation, which we want to use around $J = 2$. We expect this to be the case for large coupling, which is the case for the dense gluon medium observed in the low x regime. In practice, we will look at the first pomeron poles that appear between $0.6 \lesssim J \lesssim 1.5$ (for $t = 0$, as required in the computation of the total cross section).

Finally let us consider the third term in (3.31). This mass term is determined by the analytic continuation of the dimension of the exchanged operators $\Delta = \Delta(J)$. We will write the following formula

$$\frac{\Delta(\Delta-4)}{L^2} = \frac{2}{l_s^2}\,(J-2)\left(1 + \frac{d}{\sqrt{\lambda}}\right) + \frac{1}{\lambda^{4/3}}(J^2-4)\,, \tag{3.32}$$

where $\lambda = e^{\Phi}$ is the 't Hooft coupling, d is a constant and l_s is a length scale set

by the QCD string, which will be one of our phenomenological parameters. The first term follows directly from the diffusion limit (2.17), relating the scales L and l_s via $\mathcal{D}$. We are considering a strong coupling expansion, so it is natural that the dimension of the operators gets corrected in an expansion in $1/\sqrt{\lambda}$. This is the reason for adding the second term in (3.32), following exactly what happens in $\mathcal{N}=4$ SYM [57, 58]. This term can be added to correct the IR physics, but it is still subleading in the UV, when compared with the last term. The effect of this correction is to make the scale l_s dependent of the energy scale, while keeping the general shape of curve $\Delta=\Delta(J)$ in figure 2.2. The last term in (3.32) was added simply to reproduce the correct free theory result that is necessary to be obeyed near the boundary in the UV. More concretely, in order to obtain a scaling of the form (3.29), with the free dimension $\Delta=J+2$, we need this last term. This follows by considering the asymptotic value of the background fields and then analysing our spin J equation near the boundary to obtain $h^{TT}_{+\cdots+}\sim z^2$. This behaviour is important since it implies Bjorken scaling at the UV. We can regard (3.32) as an interpolating function between the IR and UV that matches the expected form of the dimension of the spin J operator in both regions. This is the same type of approach followed in phenomenological holographic QCD models.

To sum up, we shall consider the effective Reggeon equation (3.31), with (3.32), to describe the exchange of all the spin J fields in the graviton Regge trajectory. This equation contains 5 parameters that will be fixed by the data, namely the constants a, b, c, d and l_s.

We finish the analysis of the spin J equation with a remark. In the same lines of [42] we can try to write a quadratic effective action for the spin J symmetric, traceless and transverse field, such that its $SO(1,3)$ irrep TT part obeys the proposed free equation. Such an action would have the form

$$I=\frac{1}{2}\int d^5X\sqrt{-g}\,e^{-2\Phi}\Big[\nabla_b h_{a_1\ldots a_J}\nabla^b h^{a_1\ldots a_J}-M^2(z)h_{a_1\ldots a_J}h^{a_1\ldots a_J}+\ldots\Big], \qquad (3.33)$$

where the dots represent terms quadratic in $h_{a_1\ldots a_J}$ that are higher in the derivatives of either $h_{a_1\ldots a_J}$ or the background fields. Since in the QCD vacuum only scalars under the $SO(1,3)$ irrep decomposition are allowed to adquire a vev, the mass term in (3.33) includes all such possibilities. We are also treating the dilaton field in a special way, by allowing a very specific coupling in the overall action. In particular, other scalar

fields could also have a non-trivial coupling to the kinetic term [3]. It is simple to see that our proposal (3.31), with (3.32), corresponds to setting

$$M^2(z) = -J\, e^{-2A}\dot{A}^2 + m^2(z)\,, \tag{3.34}$$

with

$$m^2(z) = (J-2)\left[\frac{2}{l_s^2}\left(1+\frac{d}{\sqrt{\lambda}}\right) + \frac{J+2}{\lambda^{4/3}} + e^{-2A}\left(a\,\ddot{\Phi} + b\left(\ddot{A}-\dot{A}^2\right) + c\,\dot{\Phi}^2\right)\right]. \tag{3.35}$$

3.4.1 Effective Schrödinger problem

The amplitude (3.16) computes the leading term of the Witten diagram describing the exchange of the spin J field in the Regge limit, whose propagator obeys the equation

$$(\mathcal{D}\Pi)_{a_1\cdots a_J, b_1\cdots b_J}(X,X') = ie^{2\Phi} g_{a_1(b_1}\cdots g_{|a_J|\,b_J)}\delta_5(X,X') - \text{traces}\,, \tag{3.36}$$

for some second order differential operator $\mathcal{D}$ whose action on the TT part of the spin J field is defined by (3.31). For Regge kinematics, however, we are only interested in the component $\Pi_{+\cdots+,-\cdots-}$ of the propagator, in the limit where the exchanged momentum has $q_+ = O(1/\sqrt{s}) \sim 0$, as can be seen from the kinematics of the external photons (3.10). Thus, we can take $\partial_+ h^{TT}_{+\cdots+} = 0$, which implies that the $+\cdots+$ component of (3.31) decouples from the other components, taking the following form [4]

$$\left\{\left[\partial_z + 2\dot{A} - 2\dot{\Phi}\right]\left[\partial_z - \dot{A}\right] + \nabla_\perp^2 - m^2(z)e^{2A}\right\} e^{(1-J)A} h^{TT}_{+\cdots+} = 0\,. \tag{3.37}$$

This equation can be re-casted as a 1-d quantum mechanics problem, that is, setting

$$h^{TT}_{+\cdots+} = e^{iq\cdot x} e^{(J-1)A} e^{B(z)}\psi(z)\,, \tag{3.38}$$

with $q_+ = 0$, and choosing $B(z) = \Phi - A/2$ to cancel the term linear in the derivative ∂_z, equation (3.37) takes the Schrödinger form

$$\left[\partial_z^2 + t - V(z)\right]\psi(z) = 0\,, \tag{3.39}$$

[3] Since we write a 5-d action, one could also have fields with a vev proportional to the 5-d metric η_{ab}. An example is the background Riemann tensor that can couple to the spin J field (for instance, the metric fluctuations do). However, for traceless fields only mass terms of the type written in (3.33) will survive.

[4] For example, the bulk Laplacian projected in the boundary indices gives $\nabla^2 h_{\alpha_1\ldots\alpha_J} = \left(e^{JA(z)}\nabla_0^2 e^{-JA(z)} - JA'(z)^2\, e^{-2A(z)}\right) h_{\alpha_1\ldots\alpha_J} + O(1/\sqrt{s})$, where ∇_0^2 is the bulk scalar Laplacian. More details on appendix C.

where $t = -q_\perp^2$ and the potential V is given by

$$V(z) = \frac{3}{2}\left(\ddot{A} - \frac{2}{3}\ddot{\Phi}\right) + \frac{9}{4}\left(\dot{A} - \frac{2}{3}\dot{\Phi}\right)^2 + m^2(z)e^{2A}\,. \tag{3.40}$$

The energy spectrum for each integer J quantises $t = t_n(J)$, therefore yielding the glueball masses (although we only expect the proposed equation to be a good approximation for analytically continued values of J around $J = 2$, and certainly not in the asymptotic regime of large J). As expected, for $J = 2$ this potential reduces to the one obtained from linearized Einstein equations, since $m^2(z) = 0$ for $J = 2$.

Finally we can consider the integrated propagator $G_J(z, z', l_\perp)$ defined in (3.18). This is the scalar propagator obtained from integrating the component $\Pi_{+\cdots+,-\cdots-}$ of the full propagator along the light-rays. From the differential equation (3.37) if follows that

$$\left[\Delta_3 - e^{-2A(z)}\left(2\dot{\Phi}\partial_z + 2\dot{A}^2 + \ddot{A} - 2\dot{A}\dot{\Phi}\right) - m^2(z)\right] G_J(z, z', l_\perp) = -e^{2\Phi}\delta_3(x, x')\,, \tag{3.41}$$

where here $x = (z, x_\perp)$ and $\bar{x} = (\bar{z}, \bar{x}_\perp)$ are points in the scattering transverse space with metric $ds_3^2 = e^{2A(z)}\left[dz^2 + dx_\perp^2\right]$, and Δ_3 is the corresponding Laplacian. It is now clear that writing

$$G_J(z, \bar{z}, t) = e^{B(z)}\psi(z)\,, \tag{3.42}$$

the homogeneous solution to (3.41) is exactly given by the Schrödinger problem of (3.39). Moreover, using the spectral representation $\sum_n \psi_n(z)\psi_n^*(\bar{z}) = \delta(z - \bar{z})$, we conclude that

$$G_J(z, \bar{z}, t) = e^{B(z)+B(\bar{z})}\sum_n \frac{\psi_n(z)\psi_n^*(\bar{z})}{t_n(J) - t}\,. \tag{3.43}$$

This result was used in subsection 3.3.3 to derive the contribution of Regge poles to the DIS structure functions. Notice that both the eigenvalues t_n and the functions ψ_n depend on J.

3.5 Fit of DIS data in IHQCD

In this section we will test the previous phenomenological model for DIS against the combined H1-ZEUS data points for $x < 0.01$ from [2], as shown in figure 3.1. We will look for the optimal values of the free parameters in the structure function $F_2(x, Q^2)$ given in (3.24). This function depends on the couplings g_n to each Reggeon, given by (3.26), and on the parameters l_s, a, b, c and d in (3.35) that characterize the analytic

continuation of the graviton Regge trajectory. At the end of the day we will fix the shape of the first glueball Regge trajectories, which then can be compared with the known higher spin glueball data obtained from lattice computations. Not only we are able to fit DIS data, we shall see that our results are also compatible with the most recent results we have found so far for the higher spin glueball spectrum [3, 4]. This is expected, although a very non-trivial test, since the spectral and scattering data ought to be connected consistently.

Although we kept in the previous sections our discussion of pomeron physics general, we need to use a specific holographic QCD model to test our ideas. As the previous chapter 2, we shall consider the Improved Holographic QCD (IHQCD) model proposed in [44]. The QCD vacuum is described by a dilaton gravity theory with an action of the form (3.30). The potential $V(\Phi)$ is then judicially chosen such that the theory reproduces the QCD beta function in the UV and confines in the IR. In our fit we will consider data points with Q^2 as large as 400 MeV. For this reason we need to start close to the AdS boundary at $z_{min} \equiv e^{-A_0} = 0.0067$ with $\lambda_0 = 0.0337462$. These initial values of $A(z)$ and $\lambda(z)$ are consistent with the choice of $\Lambda_{QCD} = 0.292GeV$ which gives the value of the lowest mass of the spin 2 glueball proposed originally in [44]. For the maximum value of the holographic variable we chose $z_{max} = 6$. Eventually we have changed z_{max} to a bigger value, the results showing no sensitivity. [5]

Next we need to compute the non-normalizable modes associated to the current operator sourced by the off-shell photon, as explained in section 1.2.5. This is done by solving the equation for the $U(1)$ gauge field in the bulk for each of the Q^2 available in the data. The dependence of the structure function $F_2(x, Q^2)$ on the external probe arises from the shape of the function ${P_{13}}^{(2)}(Q^2, z)$ defined in (3.20), since this function is then integrated along z in (3.25). In figure 3.6 we plot the function ${P_{13}}^{(2)}(Q^2, z)\, Q^2 e^{-2A}$ for several values of Q^2.

At this point we can confirm that the approximation of the external photon wave functions to the integral (3.25) by a Dirac delta function, as assumed in section 3.2, only works for large values of Q^2. Writing the integrand in (3.25) as ${P_{13}}^{(2)}(Q^2, z)\, Q^2 e^{-2A} \times function(z)$, it is simple to see that the first function behaves as a delta function for large Q, while the $function(z)$ is smooth enough such that the integral gets no contribution from the boundary at $z = 0$. This is the reason why we kept our discussion of section 3.2 at a more qualitative level, since in the reconstruction of the

[5] For the interested reader we released our spectral code under a MIT License, which you can find at github `https://github.com/rcarcasses/schrodinger`. A discussion about one of the methods used, the Numerov's method, can be found in appendix D.

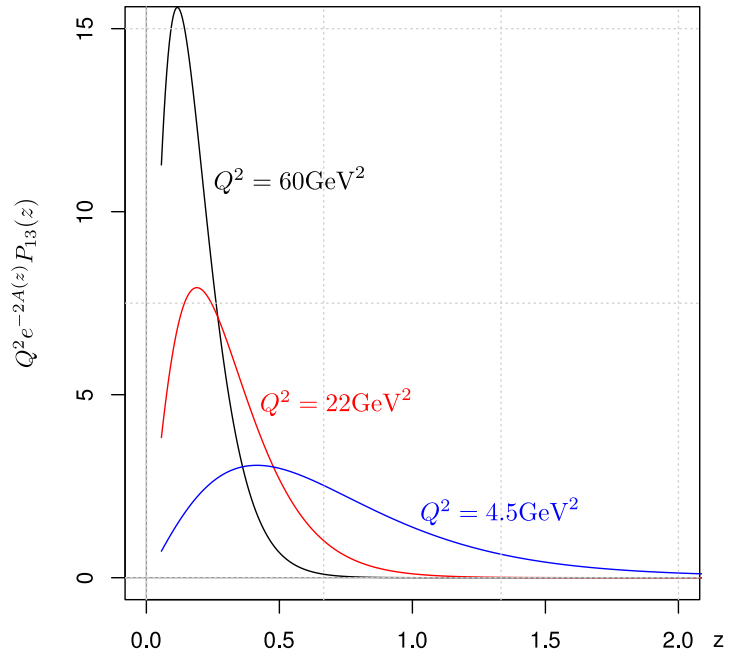

Figure 3.6: The function previously approximated to a delta function in section 3.2. The quality of the approximation clearly decreases as Q^2 becomes smaller.

wave functions in figure 3.4 we did the replacement $z \sim 1/Q$. Clearly such replacement is a gross approximation for many of the values of Q we are considering. [6] An honest computation would involve solving numerically an integral equation for the $\psi_{0,1}$ given the experimental $f_{0,1}(Q)$, with a kernel of the form shown in figure 3.6. Nevertheless we would expect that this correction will not introduce any new extreme point for the wavefunction but to deform it in a non trivial way in the region where the delta function approximation is bad, giving still the right number of nodes for each ψ, which is really the point we wanted to emphasize in section 3.2.

Let us remark that, in contrast with the external off-shell photon with varying virtuality Q^2, the target proton wave function does not require a detailed description of the holographic dual $\Upsilon(P^2, z)$. The dependence on that normalizable mode was carried by $P_{24}(P^2, z)$ and absorbed in the coupling constants g_n, as shown in (3.26).

Following our program we define an error function depending of the phenomenological parameters α_i. This defines a optimization problem where we wish to find the values

[6] In fact it is puzzling how such approximation, which leads to a closed formula for F_2 using a hard wall model [16], works very well with results comparable to those presented in this chapter.

of α_i that minimize the quantity

$$\chi^2 \equiv \sum_{k=1}^{N} \left(\frac{F_2(Q_k^2, x_k; \alpha_i) - F_2^{exp}(Q_k^2, x_k)}{\sigma_k} \right)^2, \tag{3.44}$$

which is just a weighted least square fit where the weight is the inverse of the error in the measurement, such that quantities with bigger error affect less the result. A widely accepted criteria for the quality of a fit is that the quantity $\chi^2_{d.o.f.} \equiv \chi^2/(N - N_{par})$, where N_{par} is the number of parameters to be fitted, is close to one.

3.5.1 The fit

We proceed to find the optimal values for the phenomenological parameters. As explained in the introduction and shown in figure 3.1 we consider data points with $x < 0.01$ to be in the limit of Regge kinematics. Let us remind ourselves that in our derivation we have dropped terms of order $1/s$. Such terms are sub-leading with respect to the first trajectories as long as their intercept does not differ from the leading one at most by unit. This validates our choice of retaining the first daughter trajectories.

We have found that with only two trajectories it is possible to provide a good fit for the DIS data, but unfortunately the second intercept does not correspond to the soft pomeron. As explained before, it is desirable that the second intercept matches that of the soft pomeron given the experimental evidence from total cross sections of soft probes. We have also found that fixing the intercept of the second trajectory to $1.08 \sim 1.09$, and performing the fit with only two Pomerons, does not provide a good fit.

Thus the most reasonable thing to do is to fix the soft pomeron intercept and include a third or a fourth trajectory in our fit, similar to [54], but in our case these trajectories are associated to glueballs instead of mesons. The reason we stopped at the fourth trajectory is that it is enough to obtain a good quality fit. We found that these trajectories still have an intercept above the mesons one , i.e. $j_n > 0.55$, so they are important and should be taken into account[7]. Figure 3.7 shows our best fit from which we obtained $\chi^2_{d.o.f.} = 1.7$. The corresponding parameters are listed in the table 3.1 and more details can be found in the appendix E.

[7]This is subtle: if the meson trajectories bend in the same way as the glueball ones then their intercepts will raise. We plan to analyze mesons' contribution in a future work.

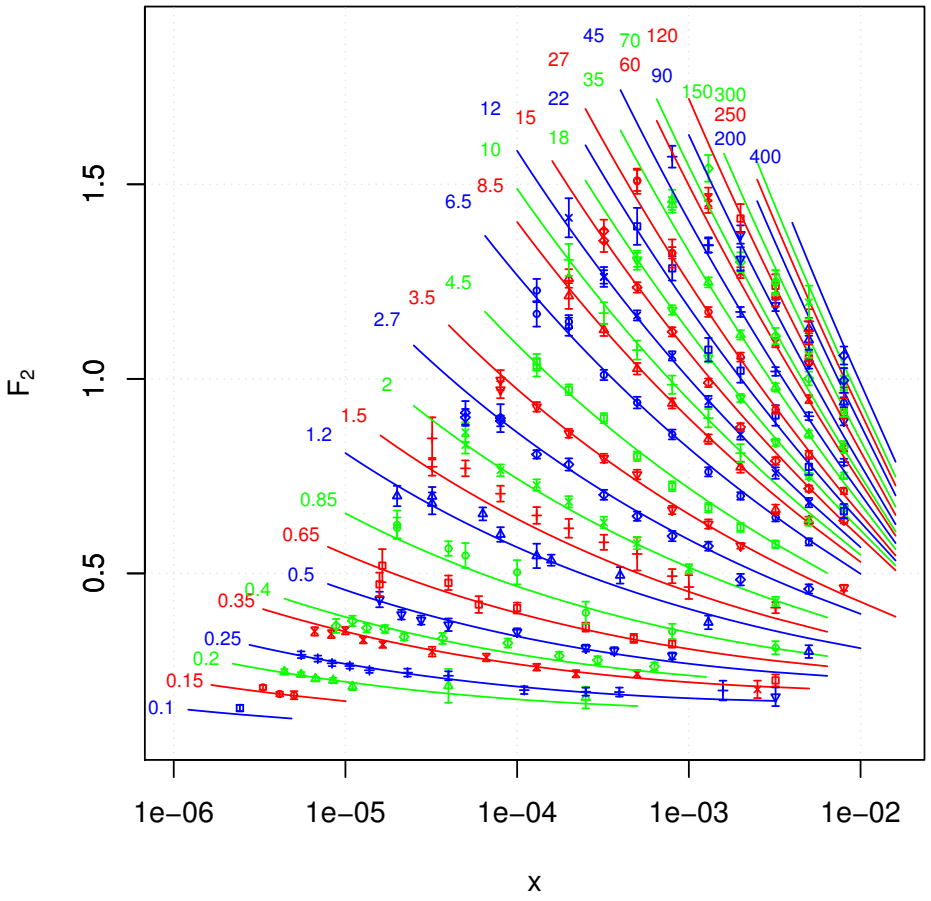

Figure 3.7: Plot of the experimental F_2 data versus the prediction of our model. We cover a very large kinematical window with $x < 0.01$ and $0.1 < Q^2 < 400$ in GeV^2, in a total of 249 points. The $\chi^2_{d.o.f.}$ of this fit is 1.7.

In figure 3.8 we show, for each pomeron, the wave function and corresponding potential in the associated Schrödinger problem. As anticipated the wavefunctions resemble those of section 3.2 with some sort of deformation, specially for large z, due to the use of the right functions for the external off-shell photon. Recall that, as we vary the spin J in the Reggeon equation (3.39), the intercept of the n-th trajectory is given by the value of J for which the energy of the n-th excited state crosses zero. Thus the wave function shown in each figure is the zero energy state for the potential shown in the same figure. We see that as J decreases the potential spreads to the IR region. This fact is at the heart of the decrease of the effective intercept with a decreasing virtuality

Pomeron equation coefficients	coupling	Intercept
$a = -4.35$	$g_0 = 0.175$	$j_0 = 1.17$
$b = 1.41$	$g_1 = 0.121$	$j_1 = 1.09$
$c = 0.626$	$g_2 = 0.297$	$j_2 = 0.969$
$d = -0.117$	$g_3 = -1.63$	$j_3 = 0.900$
$l_s = 0.153$	–	–

Table 3.1: The nine parameters for our best fit. As an output we also show the intercept of the first four pomeron trajectories (in fact we forced the second trajectory to have the soft pomeron value, so only the other values are a prediction of the model).

Q^2 shown in figure 3.2 in the introduction. In other words, as the process becomes more localized in the IR the wave function of the hard-pomeron is very suppressed, leading to more important contributions from the other daughter trajectories. The potential also shows a very sharp minimum near the UV, that localizes the hard pomeron wave function near the boundary. However, we do not fully understand the two minima behaviour exhibited by the potential. For instance, it could be that this is just an artifact of the specific interpolation between the IR and UV physics in the holographic QCD background considered here. Nevertheless, we believe the most important fact here is that the wave functions are smooth and are more spread across the IR in the case of the daughter trajectories.

3.5.2 Regge trajectories

The power of Regge theory relies on the fact that spectrum and scattering physics are related in a very natural way. In the conventional approach one organizes the spectrum in Regge trajectories $J = j(M^2)$, for integer J. Then one considers processes where particles in a given trajectory $j_n(t)$ are exchanged. Regge theory predicts that the contribution of the trajectory $j_n(t)$ to the cross section behaves as $s^{j_n(t)}$, where the function $j_n(t)$ is analytically continued to negative t.

Here we are following a similar strategy. First we construct a phenomenological model and then fix the unknown coefficients by confronting the model to scattering data. In fact, since we consider a total cross section for an inelastic process, the scattering data we used is directly related to the value of each Regge trajectory at $t = 0$. We can then look how each Regge trajectory behaves for positive and negative t. The plot of the first four pomeron Regge trajectories considered in this work was presented in figure

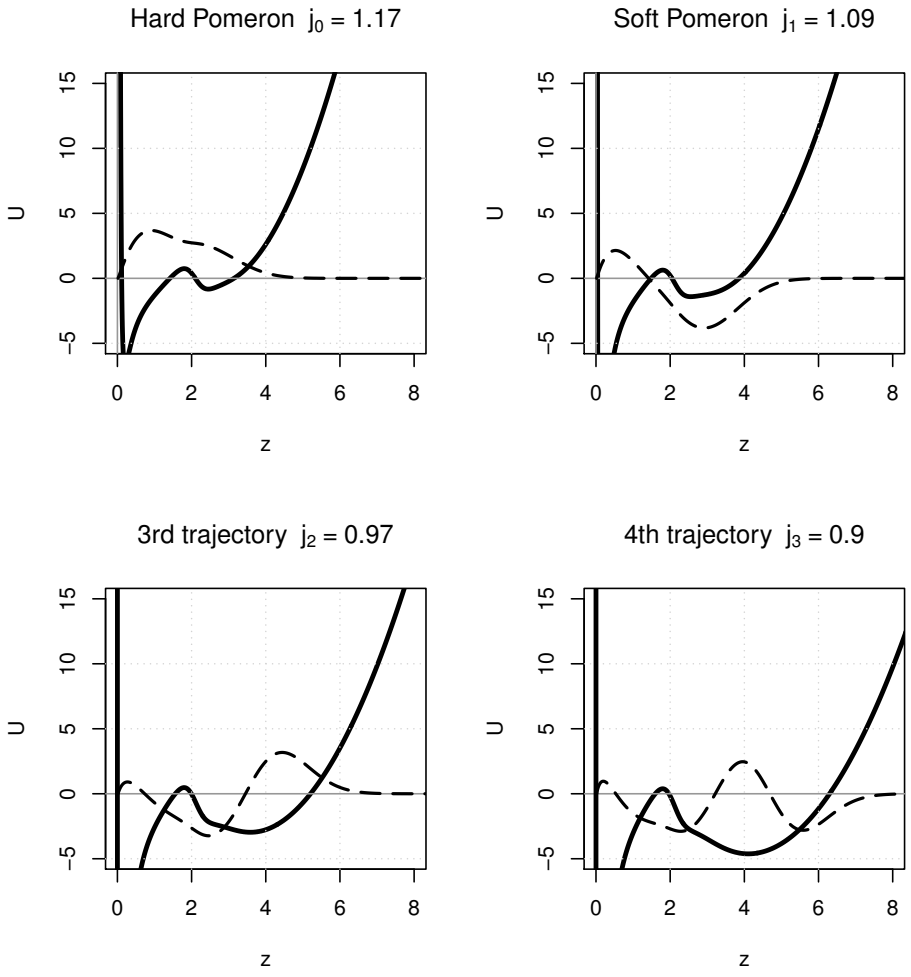

Figure 3.8: Wavefunctions and corresponding potential for optimal phenomenological values for the hard and soft pomerons, and also for the other daughter trajectories considered in the fit. The normalized wavefunctions have been scaled by 5 in this figure.

3.3 in the introduction. It is rewarding to see that the first two trajectories, that is the hard and soft pomeron, pass reasonably well through the known lattice QCD data for the masses of the higher spin glueballs. One should keep in mind, though, that we are using a phenomenological holographic QCD model, and also that this lattice data refers to pure glue with SU(3) gauge group.

An interesting feature of our leading Regge trajectories is that they coincide in shape with what was recently proposed to be the universal behaviour for weakly coupled theories with massive higher spin fields [59], where the authors argue that $j(t) \sim t + ...$ for large positive t and that $j(t) = const$ for large negative t. Another interesting fact

of figure 3.3 is that the trajectories are very close to each other in the scattering region of $t < 0$. We comment on possible implications to elastic differential cross sections of soft probes in the conclusions.

3.6 Conclusions

In this chapter we have shown how holographic QCD can be effectively used to address an essentially non-perturbative problem in QCD, that of the pomeron Regge trajectories. The construction is general, but to test it against experimental data we have considered the Improved Holographic QCD background proposed in [43, 44, 60]. More specifically we have been able to explain satisfactory DIS data in the $x < 0.01$ region, covering a large region for the photon virtuality Q^2. Moreover, the same Regge trajectories that describe DIS data are compatible with the lattice data for the higher spin glueball spectrum.

There is a natural parameter one could have chosen to tune, which is Λ_{QCD}. In IHQCD this is equivalent to choose some A_0 and λ_0 at a given value of $z = z_0$. This parameter was left fixed to the same value the authors of [43, 44] suggest, since in the original papers it was fixed such that the mass of the scalar glueball coincides with that of lattice QCD. In our case changing it would lead simply to a rescaling of all dimensionful quantities in the model, like for instance the unknown coefficients we were fitting, and it has the effect of shrinking/expanding the t axis of figure 3.3. Since we are also confronting our model with spectral data, we decided not to change that number. At most we could match exactly the mass of the lightest spin two glueball, but our hard pomeron trajectory already passes very close to that point as can be see from figure 3.3, so we decided not to use such extra freedom.

Our works points towards the solution of a long standing problem in QCD, namely the nature of the hard and soft pomeron. In our framework both arise as distinct Regge trajectories made of glueballs. In the dual picture they originate from the graviton trajectory, which degenerates in many trajectories once it is quantized in the asymptotically AdS space (which can be thought as a gravitational box). The way these trajectories appear in DIS data, by means of a wave function of a Schrödinger problem, clearly calls for a reconstruction of the holographic dual of QCD. Somehow this is what we have done for the graviton Regge trajectory associated with higher spin glueballs. We considered a holographic QCD model that describes the QCD vacuum, and then used effective field theory arguments to reconstruct the analytic continuation

of the spin J equation of motion that best fits the data.

An important point that pops up from the analysis of figure 3.3 is that eventually meson trajectories will also contribute to the scattering (either in DIS, as we vary the virtuality Q^2, or in differential cross sections for elastic processes, as we vary t). This was well noticed in the work of Donnachie and Landshoff and we expect that including the dynamics of the higher spin fields dual to the mesons might improve the quality of our fit.

Requiring several trajectories to explain the DIS data is also compatible with the picture of having a branch cut structure in the J-plane that turns into a set of poles due to the breaking of conformal invariance. In fact, DIS data was also successfully reproduced using a hardwall model with a conformal pomeron [16]. Moreover, the perturbative approach that uses the BFKL pomeron also breaks conformal invariance and then considers several daughter trajectories [11]. However, in that case one needs to consider a very large number of trajectories, leading to a very large number of free parameters in the model and even so, this approach leaves out the low Q^2 region of the data. We believe holographic QCD is better suited to address pomeron physics, because the whole construction is better suited to study strongly coupled phenomena.

In the next chapter we will consider other possible couplings between the spin J fields and the spin 1 gauge field considered here as the dual of the hadronic current operator $\bar{\psi}\gamma_\mu\ \psi$. We will see that there exist more possibilities in which the bulk coupling constants are dimensionful and that its consideration lead to considerable improvements in the fit of DIS.

4

Non-minimal coupling contribution to DIS at low x in Holographic QCD

We consider the effect of including a non-minimal coupling between a $U(1)$ vector gauge field and the graviton Regge trajectory in holographic QCD models. This coupling describes the QCD interaction between the quark bilinear electromagnetic current and the Pomeron. We test this new coupling against DIS data at low Bjorken x and obtain an excellent fit with a chi squared of 1.1 over a very large kinematical range in the photon virtuality $Q^2 < 400$ GeV^2 and for $x < 10^{-2}$. The scale of the new dimension full coupling, which arises from integrating higher spin fields, is of order 6 GeV. This value matches precisely the expectations from effective field theory, which indicate that such corrections are controlled by the mass gap between the spin two and spin four glueballs that are described holographically by the graviton and spin four field in the graviton Regge trajectory, respectively.

4.1 Introduction

As we have already saw, the observation that the Pomeron is dual to the graviton Regge trajectory [13] opened an entirely new approach to the analysis of QCD processes dominated by Pomeron exchange. In this chapter we focus on low x DIS again, extending the results of the previous chapter. Here we shall extend the analysis of chapter 3 by allowing for a non-minimal coupling between this gauge field and the higher spin fields in the graviton Regge trajectory. We shall fit the same set of data as in chapter 3, more concretely we fit 249 data points, covering the very large kinematical range of $x < 10^{-2}$ and $Q^2 < 400$ GeV^2, where x is the Bjorken x and Q^2

the photon virtuality. As a result, we manage to improve the quality of our fit from a chi squared per degree of freedom of 1.7 in chapter 3 to an excellent value of 1.1.

The existence of such non-minimal coupling between the bulk $U(1)$ gauge field and the graviton Regge trajectory is expected. Starting from the UV high energy limit, the OPE expansion of the two currents, $J_\mu(x)J_\nu(y)$, contains two OPE coefficients for each spin J symmetric traceless operator associated with the glueballs on the pomeron trajectory, $\mathcal{O}_J \sim \mathrm{tr}(F_{\mu\alpha_1} D_{\alpha_2} \cdots D_{\alpha_{J-1}} F_{\alpha_J}{}^{\mu})$. Holographically, and for pure AdS space, this amounts to precisely the same counting when coupling a vector gauge field to the graviton, or to the higher spin fields in the gravity Regge trajectory. Thus we shall consider such non-minimal coupling. In fact, since QCD is not a conformal theory, there is actually more freedom in the choice of such couplings in holographic QCD which, as we shall see, are very much model dependent. For concreteness we shall consider one such coupling, which arises in an effective field theory expansion in the dual QCD string tension. After obtaining the new expression for the DIS structure function $F_2(x, Q^2)$ in generic AdS/QCD models, we focus on the specific holographic QCD model of [43, 44, 60]. This allows us to put numbers in our expressions that are then tested against available low x DIS data.

4.2 Holographic computation of F_2 structure function

We shall compute the DIS F_2 structure function using the framework of AdS/QCD, following the same logic and kinematic definitions of chapter 3, using the same holographic dual. First we present general formulae and then specify to a particular model. We are interested in the Regge limit where the amplitude is dominated by the exchange of the graviton Regge trajectory, which includes fields of even spin J. The corresponding Witten diagram for such exchange is shown in figure 4.1. The upper part of the diagram is related to the incoming and outgoing virtual photons, whereas the bottom part to the proton target. We will work with the string frame metric as usual.

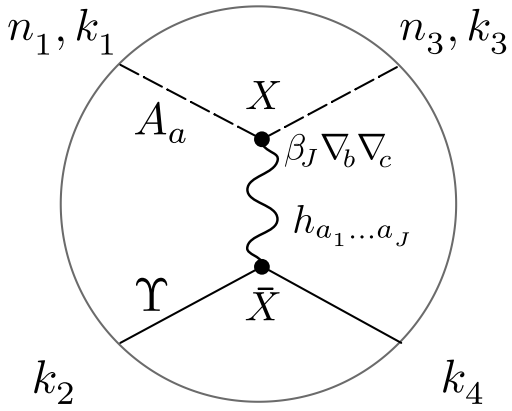

Figure 4.1: Tree level Witten diagram representing spin J exchange in a $12 \to 34$ scattering. Here we consider a non-minimal coupling in the upper vertex in opposition to the computation of chapter 3.

4.2.1 Non-minimal coupling

To compute the Witten diagram of figure 4.1, we need to consider the interaction between the external scattering states and the spin J fields in the graviton Regge trajectory. Thus, the higher spin field comes from the closed string sector while the external fields come from the open sector.

First we consider the coupling between the $U(1)$ gauge field and the graviton. In Einstein-Maxwell theory, and for AdS or flat space, it is well known that there are only two possible cubic couplings between these fields, namely

$$F^{ac}F^{b}{}_{c}h_{ab}\,, \quad F^{ac}F^{bd}\nabla_c\nabla_d h_{ab}\,, \tag{4.1}$$

where h_{ab} is the metric fluctuation. The present case, however, is less restrictive because we have an additional scalar field and also because space-time is not maximally symmetric. To understand this better, let us linearize the action (1.69) around the background metric, that is, we write $g_{ab} = \bar{g}_{ab} + h_{ab}$. Setting $h = h^{a}{}_{a} = 0$ we have the cubic couplings

$$\begin{aligned}\delta S = -\frac{1}{2}\int d^5X\sqrt{-\bar{g}}\,e^{-\Phi}\Big(&F^{ab}F^{c}{}_{b}h_{ac} \\ &+ \frac{\beta}{2}h_{ap}\bar{R}^{p}_{bcd}F^{ab}F^{cd} - \beta F^{ac}F^{bd}\bar{\nabla}_a\bar{\nabla}_b h_{cd}\Big)\,.\end{aligned} \tag{4.2}$$

To study the graviton Regge trajectory in the background (2.2) we need to decompose the metric in $SO(1,3)$ irreducible representations. We will be only interested in the

graviton TT components $h_{\alpha\beta}$, satisfying $\partial^\alpha h_{\alpha\beta}=0$ and $h^\alpha{}_\alpha=0$, and we set $h_{z\alpha}=0=h_{zz}$. Using that $R_{\alpha\mu\beta\nu}=\dot{A}^2e^{2A}(\eta_{\alpha\nu}\eta_{\mu\beta}-\eta_{\alpha\beta}\eta_{\mu\nu})$ and $R_{\alpha z\beta z}=-\ddot{A}e^{2A}\eta_{\alpha\beta}$ in the background (2.2), and computing the covariant derivatives, we obtain

$$\begin{aligned}\delta S=-\frac{1}{2}\int d^5X\sqrt{-\bar{g}}\,e^{-\Phi}\Big[&F^{\alpha\mu}F^{\beta}{}_{\mu}\big(1-\beta e^{-2A}\dot{A}\partial_z\big)\\&-\beta F^{\alpha\mu}F^{\beta\nu}\partial_\mu\partial_\nu-2\beta F^{\alpha z}F^{\beta\nu}\big(\partial_z-2\dot{A}\big)\partial_\nu\\&+F^{\alpha z}F^{\beta}{}_{z}\Big(1-\beta e^{-2A}\big(\partial_z^2-3\dot{A}\partial_z+2\dot{A}^2\big)\Big)\Big]h_{\alpha\beta}\,.\end{aligned}\tag{4.3}$$

Notice that in the AdS case ($A=-\log z$) these couplings reduce to the two allowed couplings in (4.1). However, in the present case there are more possibilities. For example, other contractions with the Riemann tensor will give different functions multiplying the same tensor structures in the couplings. We may also use derivatives of the scalar field to contract with the field strength. For simplicity, the approach we follow in this work will be to focus on the coupling given by the action (1.69). Our aim is to test whether this type of corrections are important in describing DIS using holographic QCD.

Next we wish to generalize the previous coupling to case of the cubic interaction between the gauge field and a symmetric, transverse and traceless spin J field, $h_{a_1\ldots a_J}$. The pomeron trajectory includes such higher spin fields of even J. Again there are several possibilities, but we shall focus on the simplest extension of the two couplings to the graviton considered above. The first term is the minimal coupling term, which can be generalized to

$$\kappa_J\int d^5X\sqrt{-\bar{g}}\,e^{-\Phi}F^{a_1b}\bar{\nabla}^{a_2}\ldots\bar{\nabla}^{a_{J-1}}F^{a_J}{}_{b}h_{a_1\ldots a_J}.\tag{4.4}$$

The transverse condition of $h_{a_1\ldots a_J}$ guarantees that this term is unique up to dilaton derivatives. For the non-minimal coupling we will write

$$\begin{aligned}\beta_J\int d^5X\sqrt{-\bar{g}}e^{-\Phi}\Big(&F^{ca_1}\bar{\nabla}^{a_2}\ldots\bar{\nabla}^{a_{J-1}}F^{a_Jd}\bar{\nabla}_c\bar{\nabla}_d\\&+\frac{1}{2}F^{a_1b}\bar{\nabla}^{a_2}\ldots\bar{\nabla}^{a_{J-1}}F^{cd}R^{a_J}{}_{bcd}\Big)h_{a_1\ldots a_J}\,.\end{aligned}\tag{4.5}$$

We remark that in both expressions (4.4) and (4.5) the way we distribute the covariant derivatives acting on the field strength is important. After integrating by parts such a covariant derivative, we are left with an extra term in the derivative of the background dilaton field. However, these terms will have a component of the higher spin field along the z direction, which can be dropped in the case of the pomeron.

Next we need to decompose the spin J fields in $SO(1,3)$ irreducible representations. In the Regge limit we are only interested in the TT components of these fields, that

is in $h_{\alpha_1\ldots\alpha_J}$ with $\partial^\nu h_{\nu\alpha_2\ldots\alpha_J}=0$ and $h^\nu{}_{\nu\alpha_3\ldots\alpha_J}=0$. From now on we will assume these two conditions. Thus for the minimal coupling (4.4) we obtain simply

$$\kappa_J\int d^5X\sqrt{-\bar{g}}\,e^{-\Phi}\Big(F^{\alpha_1\mu}\partial^{\alpha_2}\ldots\partial^{\alpha_{J-1}}F^{\alpha_J}_{\ \mu} +F^{\alpha_1 z}\partial^{\alpha_2}\ldots\partial^{\alpha_{J-1}}F^{\alpha_J}_{\ z}\Big)h_{\alpha_1\ldots\alpha_J}. \tag{4.6}$$

For the non-minimal coupling (4.5) we obtain after a cumbersome computation

$$\begin{aligned}&\beta_J\int d^5X\sqrt{-\bar{g}}e^{-\Phi}\Big[F^{z\alpha_1}\partial^{\alpha_2}\cdots\partial^{\alpha_{J-1}}F^{\alpha_J}_{\ z}\mathcal{D}^J_{\parallel}+\\ &F^{\mu\alpha_1}\partial^{\alpha_2}\cdots\partial^{\alpha_{J-1}}F^{\alpha_J\nu}\left(e^{2A}\mathcal{D}^J_{\perp}\eta_{\mu\nu}+\partial_\mu\partial_\nu\right)+\\ &2F^{\mu\alpha_1}\partial^{\alpha_2}\cdots\partial^{\alpha_{J-1}}F^{\alpha_J z}\left(\partial_z-J\dot{A}\right)\partial_\mu\Big]\,h_{\alpha_1\cdots\alpha_J}\,,\end{aligned} \tag{4.7}$$

where

$$\begin{aligned}\mathcal{D}^J_{\perp}&=e^{-2A}\dot{A}\left(\partial_z-(J-2)\,\dot{A}\right),\\ \mathcal{D}^J_{\parallel}&=e^{-2A}\left(\partial_z^2-(2J-1)\,\dot{A}\partial_z-(J-2)\,\ddot{A}+J\,(J-1)\,\dot{A}^2\right).\end{aligned} \tag{4.8}$$

For $J=2$ this coupling reduces to the graviton non-minimal coupling given in (4.3).

For the scalar field Υ we will consider a minimal coupling with spin J closed string fields

$$\bar{\kappa}_J\int d^5X\sqrt{-g}\,e^{-\Phi}\ (\Upsilon\nabla^{a_1}\ldots\nabla^{a_J}\Upsilon)\ h_{a_1\ldots a_J}\,. \tag{4.9}$$

Again, this coupling is unique up to derivatives of the dilaton field that are subleading in the Regge limit. Focusing on the TT part of the spin J field, we are left with the single coupling

$$\bar{\kappa}_J\int d^5X\sqrt{-g}\,e^{-\Phi}\ (\Upsilon\partial^{\alpha_1}\ldots\partial^{\alpha_J}\Upsilon)\ h_{\alpha_1\ldots\alpha_J}\,. \tag{4.10}$$

4.2.2 Witten diagram in Regge limit

The scattering amplitude will have a contribution from the minimal and the non-minimal coupling. The contribution of the minimal coupling to the structure function F_2 is presented and described in the previous chapter. Here we shall compute the contribution of the non-minimal coupling (4.7) to the exchange of a spin J field, corresponding to the Witten diagram in figure 4.1. Using the Regge kinematics and

taking as external states $F_i^{ab}(X)$ for $i = 1, 3$ and $\Upsilon_j(\bar{X})$ for $j = 2, 4$, we obtain for forward scattering the expression

$$\beta_J \bar{\kappa}_J \sum_{\lambda=1}^{3} \int d^5X d^5\bar{X} \sqrt{-g}\sqrt{-\bar{g}}\, e^{-\Phi} e^{-\bar{\Phi}} \Upsilon_2 \big(\bar{\partial}^-\big)^J \Upsilon_4$$
$$\times \left[F_1^{+z} \left(\partial^+\right)^{J-2} F_{3\,z}^{+} \mathcal{D}_{\parallel}^J + F_1^{+\mu} \left(\partial^+\right)^{J-2} F_{3\,\mu}^{+} \mathcal{D}_{\perp}^J \right] \Pi_{+\cdots+,-\cdots-}(X, \bar{X}) \,, \tag{4.11}$$

where bars denote quantities evaluated at $\bar{X}$. Notice that the couplings involving derivatives along the boundary in (4.7) vanish for forward scattering. Using (1.87) and (**??**) for the external states and performing the sum over polarisations we find

$$- \beta_J \bar{\kappa}_J s^J \int d^5X d^5\bar{X} \sqrt{-g}\sqrt{-\bar{g}}\, e^{-\Phi-\bar{\Phi}-2(J+1)A-2J\bar{A}}$$
$$\times \upsilon_m^2(\bar{z}) \left(f_Q^2(z) \mathcal{D}_{\perp}^J + \frac{\dot{f}_Q^2(z)}{Q^2} \mathcal{D}_{\parallel}^J \right) \Pi_{+\cdots+,-\cdots-} \,. \tag{4.12}$$

We remark that the terms with $\mathcal{D}_{\perp}^J$ and with $\mathcal{D}_{\parallel}^J$ are, respectively, the leading contribution arising from the transverse and longitudinal polarizations, therefore justifying our notation.

Performing the change of variable $w = x - \bar{x}$, setting $l_\perp = x_\perp - \bar{x}_\perp$, $t = -q_\perp^2$ and defining the transverse propagator at zero momentum transfer by

$$\int \frac{dw^+ dw^- d^2 l_\perp}{2} \Pi_{+\cdots+,-\cdots-}(w, z, \bar{z}) = -\frac{i}{2^J} e^{(J-1)(A+\bar{A})} G_J(z, \bar{z}, t = 0), \tag{4.13}$$

we finally obtain

$$i \frac{\beta_J \bar{\kappa}_J s^J}{2^J} V \int dz d\bar{z} e^{-\Phi-\bar{\Phi}-2J(A+\bar{A})+3A+5\bar{A}} \upsilon_m^2(\bar{z}) \tag{4.14}$$
$$\times \left(f_Q^2(z) \mathcal{D}_{\perp}^J + \frac{\dot{f}_Q^2(z)}{Q^2} \mathcal{D}_{\parallel}^J \right) \left[e^{(J-1)(A+\bar{A})} G_J(z, \bar{z}, 0) \right],$$

where the space-time volume V comes from the delta function momentum conservation that we imposed from the beginnig on the external particles. Now we proceed as in the previous chapter and write a spectral representation for the transverse propagator

$$G_J(z, \bar{z}, t) = e^{B+\bar{B}} \sum_n \frac{\psi_n(J, z)\, \psi_n^*(J, \bar{z})}{t_n(J) - t} \,, \tag{4.15}$$

where $\psi_n(J, z)$ are the normalizable modes associated to the spin J fields. The function $B(z)$ depends on the particular holographic QCD model. We will fix it later in order to perform fits to data.

4.2.3 Regge Theory

In order to get the total amplitude we need to sum over even spin J fields with $J \geq 2$. Then we can apply a Sommerfeld-Watson transform

$$\frac{1}{2}\sum_{J\geq 2}\left(s^J+(-s)^J\right) = -\frac{\pi}{2}\int \frac{dJ}{2\pi i}\frac{s^J+(-s)^J}{\sin \pi J}\,, \tag{4.16}$$

which requires analytic continuation of the amplitude for spin J exchange to the complex J-plane. We assume that the J-plane integral can be deformed from the poles at even J, to the poles $J = j_n(t)$ defined by $t_n(J) = t$. The scattering domain of negative t contains these poles along the real axis for $J < 2$. The scattering amplitude for $t = 0$ is then

$$\mathcal{A}(s,0) = \sum_n h_n s^{j_n}\int dz\, e^{-\Phi}e^{A(-2j_n+3)}\times \tag{4.17}$$
$$\left(f_Q^2\mathcal{D}_\perp^{j_n(0)} + \frac{\dot{f}_Q^2}{Q^2}\mathcal{D}_\parallel^{j_n(0)}\right)\left[e^{A(j_n(0)-1)}e^{B}\psi_n\big(j_n(0),z\big)\right],$$

with h_n defined as

$$h_n = -\frac{\pi}{2}\frac{\beta_{j_n(0)}\bar{\kappa}_{j_n(0)}}{2^{j_n(0)}}\left(i+\cot\frac{\pi j_n(0)}{2}\right)j_n'(0) \tag{4.18}$$
$$\times\int d\bar{z}\, e^{\bar{A}(4-j_n(0))}e^{-\bar{\Phi}}e^{\bar{B}}\upsilon_m^2(\bar{z})\,\psi_n^*\big(j_n(0),\bar{z}\big)\,. \tag{4.19}$$

Finally, the action of the differential operators on the functions of z allows us to rewrite the forward scattering amplitude as

$$\mathcal{A}(s,0) = \sum_n h_n s^{j_n}\int dz\, e^{-(j-2)A+B-\Phi}\left(f_Q^2\tilde{\mathcal{D}}_\perp^{j_n(0)} + \frac{\dot{f}_Q^2}{Q^2}\tilde{\mathcal{D}}_\parallel^{j_n(0)}\right)\psi_n\big(j_n(0),z\big)\,, \tag{4.20}$$

with

$$\tilde{\mathcal{D}}_\perp = e^{-2A}\left(\dot{A}\partial_z + \dot{A}^2 + \dot{A}\dot{B}\right), \tag{4.21}$$
$$\tilde{\mathcal{D}}_\parallel = e^{-2A}\left(\partial_z^2 - \big(\dot{A}-2\dot{B}\big)\partial_z + \ddot{B} + \ddot{A} + \dot{B}^2 - \dot{A}\dot{B}\right).$$

4.2.4 F_2 structure function

The DIS structure function can be written in Regge theory in the following form

$$F_2(x,Q^2) = \sum_n\left(f_n^{\mathrm{MC}}(Q^2) + f_n^{\mathrm{NMC}}(Q^2)\right)x^{1-j_n}\,, \tag{4.22}$$

where we separated the contributions from the minimal and non-minimal couplings between the graviton trajectory and the $U(1)$ current that arise from the holographic computation. In chapter 3, for $B = \Phi - A/2$, we showed that

$$f_n^{\rm MC}(Q^2) = g_n Q^{2j_n} \int dz\, e^{-\left(j_n-\frac{3}{2}\right)A} \left(f_Q^2 + \frac{\dot{f}_Q^2}{Q^2} \right) \psi_n \,. \tag{4.23}$$

Using the definitions (3.8) and (3.9), we may take the imaginary part of the forward scattering (4.20), to obtain the contribution from the non-minimal coupling

$$f_n^{\rm NMC}(Q^2) = \tilde{g}_n Q^{2j_n} \int dz\, e^{-\left(j_n-\frac{3}{2}\right)A} \left(f_Q^2 \tilde{\mathcal{D}}_\perp + \frac{\dot{f}_Q^2}{Q^2} \tilde{\mathcal{D}}_\parallel \right) \psi_n \,, \tag{4.24}$$

where $\tilde{g}_n = {\rm Im}(h_n)/(4\pi^2\alpha)$. Both constants g_n and $\tilde{g}_n$ are used as fitting parameters in our setup, thus the details of holographic wave function for the proton are not important in the fit. Notice that the g_n and $\tilde{g}_n$ do not have the same dimensions, indeed comparing both couplings we see that $[\tilde{g}_n/g_n] = L^2$. Formula (4.24) is one of the main results of this chapter.

4.2.5 Improved Holographic QCD

To test the above ideas against experimental data we need to consider a concrete QCD holographic model. As in chapter 3, we shall consider the improved holographic QCD model introduced in [43,44,60]. This fixes the background fields $A(z)$ and $\Phi(z)$, which give an approximate dual description of the QCD vacuum.

Next we need to consider the equation of motion for the spin J fields that are dual to the twist two operators, whose exchange gives the dominate contribution in DIS at low x. This equation is then analytically continue in J, in order to do the Sommerfeld-Watson transform in Regge theory. Again, this procedure was described in detail in the previous chapter, so we will not repeat it here.

The constants l_s, a, b, c and d are used as fitting parameters and will be adjusted such that the best match with $F_2(x, Q^2)$ data is achieved. In particular, from the low energy effective string theory perspective, l_s is related to the string tension; d is related to the anomalous dimension curve of the twist 2 operators, or it can also be thought as encoding the information of how the masses of the closed strings excitations are corrected in a slightly curved background; the constants a, b and c encode the first order derivative expansion of a presumed string field theory lagrangian.

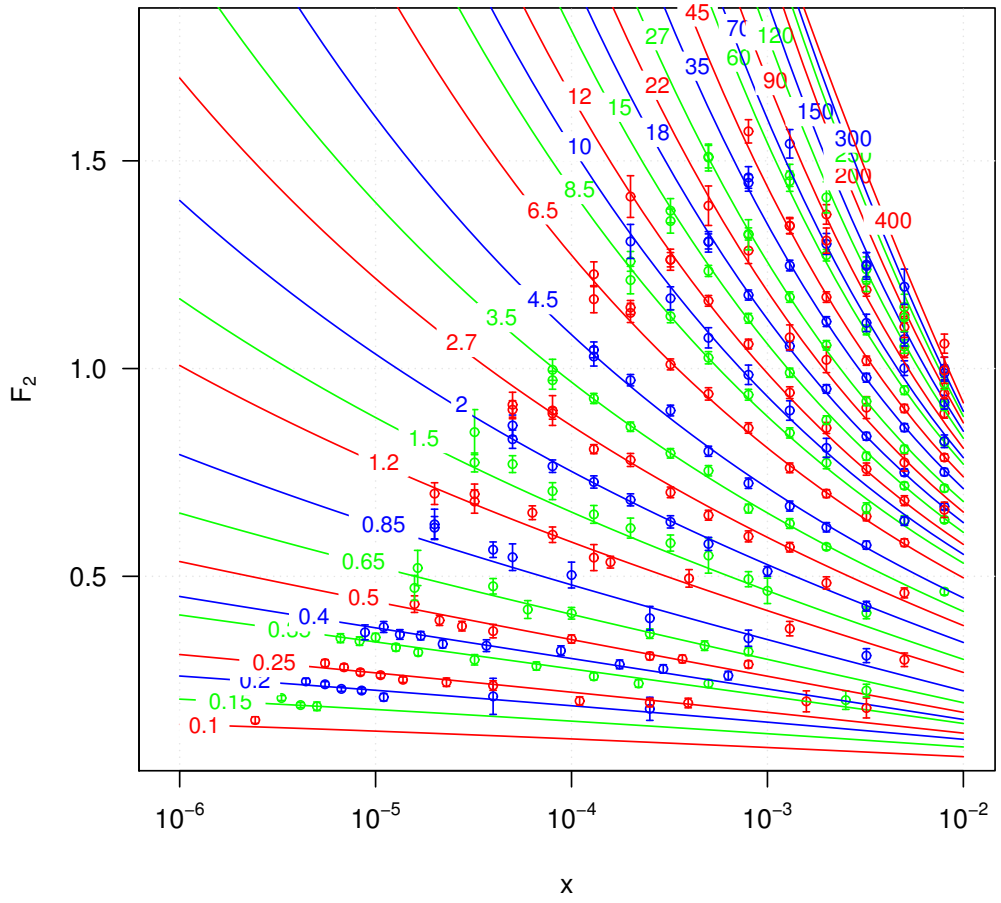

Figure 4.2: Structure function $F_2(Q^2, x)$. Experimental points vs prediction of this work with a $\chi^2_{d.o.f} = 1.1$. Each line corresponds to a given Q^2 (GeV^2) as indicated.

4.3 Data analysis

With the previously described setup we proceed to find the best values for the potential parameters l_s, a, b, c and d, as well as for the coupling values β, g_n and $\tilde{g}_n$ that better fit the data. We look, as usual, for the best set of parameter values such that the sum of the weighted difference squared between experimental data and model predicted values is minimum, using as weight the inverse of the experimental uncertainty. Since this is a highly non trivial numerical optimization problem in which we do not known explicitly the gradient of the function to be optimized, we use the Nelder-Mead algorithm, using R language, and try with different starting points in the parameter space. We

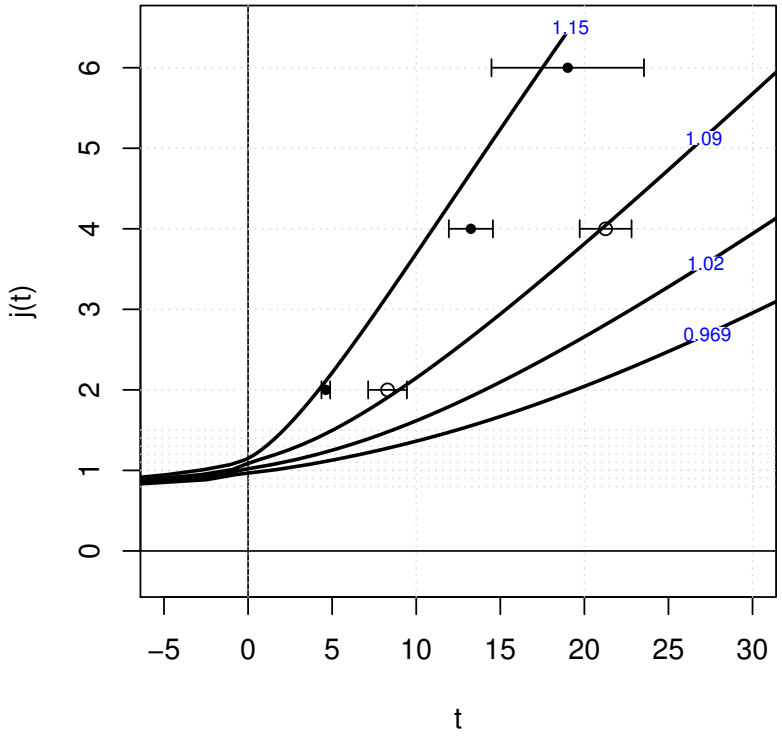

Figure 4.3: Regge trajectories compared with the square of glueball masses from lattice simulations [3, 4], t units are GeV^{2}2. Shown are also the values we obtained for the intercept of each trajectory. Configurations that give the soft pomeron intercept $j_1 = 1.09$ were favoured in the fitting process.

have found that the inclusion of the non-minimal coupling contribution considerable decreases the convergence ratio of the minimizing routine compared with the case where only the minimal coupling case is used, consistent with the fact that the new function to optimize has a much rougher landscape. Our best fit results for $F_2(x, Q^2)$ are presented in figure 4.2. In this fit we considered values of x in the range $x < 10^{-2}$, and of the photon virtuality $Q^2 < 400$ GeV^2. This gives a total number of 249 data points. The $\chi^2_{d.o.f}$ for this fit is 1.13. As in the previous chapter, aiming to make a consistent model for the Soft Pomeron, we have forced the intercept of the second trajectory to be around $j_1 = 1.09$. This is achieved penalizing those set of parameters which give a different second intercept by adding a term of the type $10^4(j_1 - 1.09)^2$ to the function to be optimized. The correspondent Regge trajectories can be seen in figure 4.3.

The values of the parameters that give the best fit are summarized in table 4.1. We would like to understand the scale defined by the non-minimal coupling. The best fit fixes the value of this coupling in the equation of motion (1.70) for the $U(1)$ gauge field to be $\beta = 0.026$ GeV^{-2}. This numerical value correspond to an energy of 6 GeV and therefore the energy scale associated with this correction is in the range of $1-10$ GeV. We may also look at the ratio between the constants g_n and $\tilde{g}_n$, given by,

$$\frac{\tilde{g}_n}{g_n} = \frac{\beta_{j_n(0)}}{\kappa_{j_n(0)}}, \tag{4.25}$$

which has dimensions $length^2$. This follows from taking the imaginary part of (4.19) and from the fact that g_n has a similar expression, as defined in chapter 3. Looking at table 4.1 it is simple to see that the ratio $\tilde{g}_n/g_n$, for each n, is also in the energy range of $1-10$ GeV. The scale of the non-minimal coupling should be associated with the mass gap between the spin 2 and spin 4 glueballs, that arise from the spectrum of the bulk graviton and spin 4 field, respectively. Indeed this is precisely the size of the gap observed in the glueball spectrum in figure 4.3.

Table 4.1: Values of the parameters for the best fit found. All parameters are dimensionless except for $[l_s] = L$, $[\beta] = L^2$ and $[\tilde{g}_i] = L^2$. Numerical values are expressed in GeV units.

parameter	value	couplings	value	couplings	value $\times 10$
l_s^{-1}	6.93	g_0	-0.154	$\tilde{g}_0$	0.707
a	-4.68	g_1	-0.424	$\tilde{g}_1$	-0.378
b	4.85	g_2	2.12	$\tilde{g}_2$	-2.48
c	0.665	g_3	-0.721	$\tilde{g}_3$	3.63
d	-0.328				
β	-0.026				

4.4 Conclusion

In this chapter we considered the contribution of a non-minimal coupling between the $U(1)$ gauge field and the higher spin fields in the graviton Regge trajectory to the holographic computation of the DIS structure function $F_2(x, Q^2)$. These non-minimal couplings are expected to be present and to play an important role in theories with higher spin fields. Such terms are controlled by the gap between the graviton and the next higher spin field [61]. Our results are consisten with this expectation since the

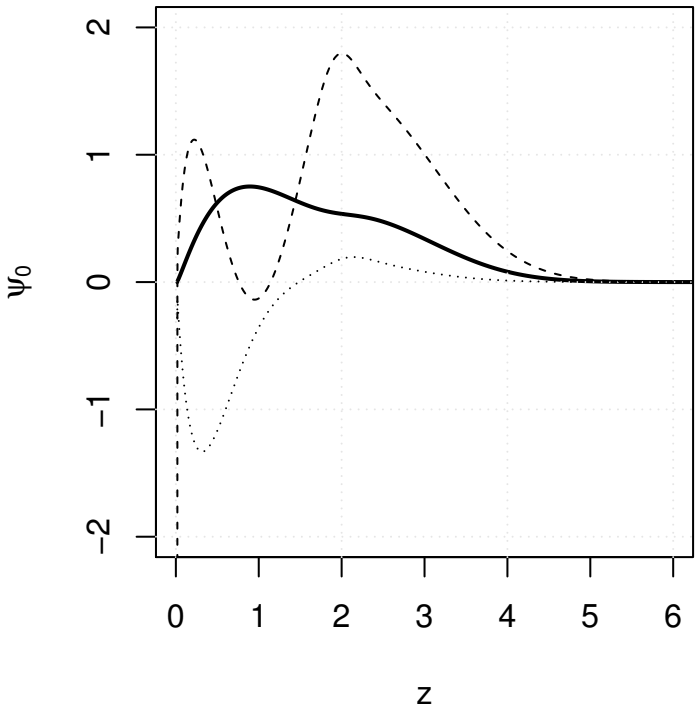

Figure 4.4: Hard Pomeron wave function for the best fit found and for its intercept value $J = j_0$. The dotted and dashed line represent the action of the operator $\tilde{\mathcal{D}}_\perp$ and $\tilde{\mathcal{D}}_\parallel$ on the Hard Pomeron wave function $\psi_0(z)$ respectively. In this plot all the functions have been scaled by a factor of 10.

scale we obtained for the non-minimal coupling has the correct order of magnitude that reproduces the mass difference between the spin 2 and spin 4 glueballs.

With the inclusion of the new coupling the quality of our fit to low x DIS data has improved considerably. In the previous chapter, that considered only the minimal coupling, a $\chi^2_{d.o.f}$ of 1.7 was obtained. With the new coupling we improved this result to a $\chi^2_{d.o.f}$ of 1.1. We believe this is an important improvement that validates the holographic approach to low x physics. We are reproducing data over a very large kinematical range in the two variables x and Q^2, fitting a total of 249 points.

One can draw some intuition on how the inclusion of the non-minimal coupling improves the fit to physical data by looking at the Reggeon wave functions. These functions are shown for the hard and soft pomerons, for the corresponding values of

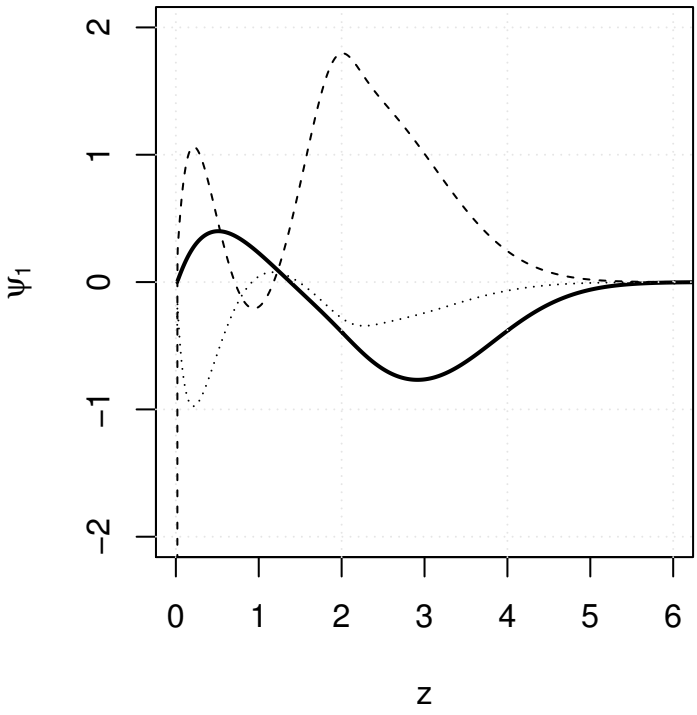

Figure 4.5: Same as figure 4.4 but for the Soft Pomeron and for its intercept value $J = j_1$.

the intercept, in figures 4.4 and 4.5, respectively. These waves functions are the ground state and first excited state of the associated Schrödinger problem. For the minimal coupling they control the dependence of the structure function in the photon virtuality Q^2 as can be seen from (4.23). For the non-minimal coupling they also control the Q^2 dependence but now the action of the differential operators $\tilde{\mathcal{D}}_\perp$ and $\tilde{\mathcal{D}}_\parallel$ in (4.24) changes such dependence to a more oscillating behaviour, as can be seen from figures 4.4 and 4.5. What is not a priori trivial is that this freedom can be used to better fit the data, yielding for the scale of non-minimal coupling precisely the expected order of magnitude (due to the oscillations it could be that this order of magnitude was much smaller, which would seem to contradict the expected value of the gap for higher spin glueballs).

It seems we are getting closer to a very satisfactory holographic description of low x data. There are two immediate questions that we believe deserve some further

attention. As a working example we have been considering the improved holographic QCD model of [43,44,60]. We take this model as our QCD vacuum, and then introduce higher spins fields for which we do Regge theory. Clearly we should study to which extent other models can also be used to reproduce the data here analysed. Our expectation is that holography is very appropriate to study processes dominated by Pomeron exchange, so that other models that are close enough to QCD should give similar results. Another interesting point is to extend this analysis to other processes than DIS. Previous studies of deeply virtual Compton scattering (DVSC) and vector meson production could now be revisited, including the non-minimal coupling here considered, to attain better fits. For example, in the case of DVSC the cross section depends on three kinematical quantities, namely x, Q^2 and momentum transfer. Extending the contribution of the non-minimal coupling terms to non-vanishing t gives a very non-trivial dependence that deserves to be looked at.

Next chapter will be devoted to the study of DVCS process, considering as a first step just the minimal coupling as in chapter 3.

5

Deeply Virtual Compton Scattering and the holographic Pomeron

We have seen in the previous chapters that it is possible to have a holographic description of the Pomeron's physics with a few free parameters which can be fixed such that we maximize our model proposed likelihood function against the experimental values. From the breakthrough of BPST work [13] to nowadays, there have been many works [14–19, 21, 62–81] in which much evidence has been gathered about how to bring the mainstream theoretical ideas of AdS/CFT down and test them agaist real experimental data where Pomeron exchange is supposed to dominate. There is however, a lack of consistence between these works since each one of them basically create models for the Pomeron tailored to specific processes or kinematic regimes. A true candidate for holographic description of the Pomeron, should be able to successfully explain all the known processes physics dominated by Pomeron exchange in their respective kinematic regimes. Ideally its shape should be narrowed by contrasting its predictions against all the experimental data available among different processes. In this chapter we present our current progress towards the solution of this problem by considering another process, Deeply Virtual Compton Scattering (DVCS) , showing that it is possible to fit both batch of datas available for the process, the total and differential cross-section ones, with a *single* holographic model for the Pomeron. Our ultimate goal would be to include all the known processes, like for instance Deep Inelastic Scattering and Vector Mesons Production, which are supposed to be dominated by Pomeron's exchange into a single model in the future. In the present chapter we present our current progress towards this goal up to the time of the writing of this thesis. The results here presented are not yet published.

5.1 Deeply Virtual Compton Scattering and the gauge/gravity duality

The Compton scattering where the incoming photon has a high virtuality is known as Deeply Virtual Compton Scattering, or DVCS. It is an exclusive process that has been extensively studied by the H1 and ZEUS collaborations at DESY, and also at JLAB. Generalized parton distribution functions (GDP) [82, 83], which encode information about the correlations between the transverse and longitudinal momentum of quarks and gluons inside the nucleon [82], are accessible through DVCS.

Gauge/gravity duality has been already used in the construction of models which explain DVCS data, this include conformal and hard wall Pomerons [17] and holographic dipole-dipole scattering [84]. DIS and DVCS are tightly related through the hadronic tensor, which enters in the computations of the different observables of both processes, so to a great extend the analysis in the present chapter follows closely the one made in chapter 3. We will show that a suitable choice of the parameters that define the kernel of the Pomeron constructed in chapter 3, together with a few parameters more which encode the holographic wave function of the proton and the coupling dependence with the spin, allows to explain all the data simultaneously.

5.2 Holographic computation of the amplitudes

In this section we use the model for the holographic Pomeron introduced in chapter 3 to compute σ and $d\sigma/dt$ for the DVCS process. We will also rewrite the amplitude for the process $\gamma^* p \to \gamma^* p$ already computed in chapter 3 in a new way more suited to the DVCS computation.

For DVCS, the reported data is on the form of the cross-sections of the process $\gamma^* p \to \gamma p$, which is basically the same process that appears in DIS with the difference that the final photon is *on-shell*. The associated Witten diagram is show in figure 5.1. To put the final photon *on-shell* we consider first the amplitude of $\gamma^* p \to \gamma^* p$ and take $Q^3 \equiv k_3^2 \to 0$.

We will use the same kinematical definitions as in chapters 3 and 4 so we omit them here. We will consider the minimal coupling between the spin 1 gauge field and the

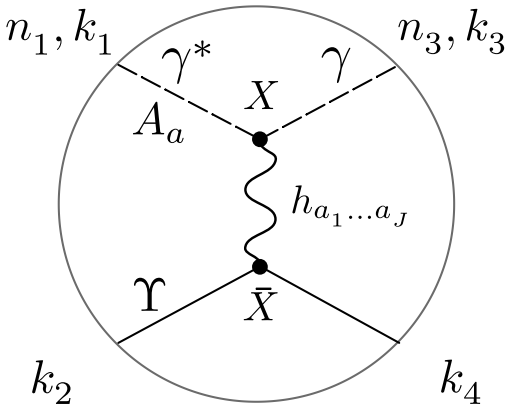

Figure 5.1: Tree level Witten diagram associated with the computation of the amplitude $\mathcal{A}_J^{\lambda_1 \lambda_3}$ of the DVCS process $\gamma^* p \to \gamma p$. The bottom lines represent the proton modeled by a scalar Υ.

higher spin field $h_{a_1 \ldots a_J}$

$$k_J \int d^5X \sqrt{-g} e^{-\Phi} F_{b_1 a} D_{b_2} \ldots D_{b_{J-1}} F^a_{b_J} h^{b_1 \ldots b_J}, \tag{5.1}$$

and the coupling of the scalar field to be

$$\bar{k}_J \int d^5\bar{X} \sqrt{-\bar{g}} e^{-\bar{\Phi}} \bar{\Upsilon} \bar{D}_{b_1} \ldots \bar{D}_{b_J} \bar{\Upsilon} \bar{h}^{b_1 \ldots b_J}. \tag{5.2}$$

The computation of these cross-sections is very close to the computation we already made in chapter 3, so we will not repeat it here and instead will write the final result

$$\mathcal{A}^{\gamma^* \gamma}(s,t) = \sum_n I\left(j_n(t)\right) \bar{I}\left(j_n(t)\right), \tag{5.3}$$

where

$$I^{\gamma^* \gamma}(J) \equiv s^J \int dz e^{-(J-\frac{3}{2})A} f_Q \psi_n(J), \qquad \bar{I}(J) \equiv h(J) \frac{dJ}{dt} \int d\bar{z} e^{(-J+\frac{7}{2})\bar{A}} \bar{v}_2 \bar{v}_4 \bar{\psi}_n(J), \tag{5.4}$$

$$h(J) \equiv H(J) \left(i + \cot\left(\frac{\pi J}{2}\right)\right) \qquad H(J) \equiv 2^{-J-1} \pi \kappa_J \bar{\kappa}_J. \tag{5.5}$$

The last amplitude is the one where both photons have transverse polarizations, other combinations are subleading in s. To obtain this expression we have used the fact that $\lim_{Q_3 \to 0} f_{Q_3}(z) = 1$.

To make predictions with this model we will need a recipe to compute the integral over $\bar{z}$ that captures the physics. The proton, as other baryons, in the context of the

gauge/gravity duality is expected to be dual to a configuration of three open strings attached to a D-brane [85, 86]. In opposite to the mesons case, phenomenological holographic QCD approaches for explaining baryons spectrum are scarce, probably due to the technicalities of the three string vertex. In this work we have modeled the proton as a scalar field in the bulk. To be a good holographic description for the proton this field would have, for instance, a spectrum that matches the proton mass as well as all the other composite particles lying on the same trajectory. As we do not have any concrete proposals in the context of the Improved Holographic QCD model we follow a phenomenological approach and we will evaluate the integral in $\bar{I}(J)$ doing a delta function approximation. This will be a gross approximation, yet it should catch to a good extend how the integral in $\bar{I}(J)$ depends on J. The idea is that the combination $e^{3A-\Phi}\upsilon_2\upsilon_4$ is a function with a single extreme, which goes to zero in both integral limits, and evaluates to 1 since it is the integrand of the norm of the υ function. Thus the integrand in $\bar{I}(J)$ is the overlap of this function with the remaining parts. Concretely, we will replace $e^{3A-\Phi}\upsilon_2\upsilon_4$ by $\delta(z-z^*)$. The position of the maximum z^* has to be related, by dimensional analysis, to the inverse of the mass of the proton and we will leave it as a fitting parameter.

We will also need to know the $H(J)$ function defined in (5.5), at least a good approximation of it within the range of interest for the J values, which is $0.6 \lesssim J \lesssim 1.3$. In the next section we will motivate the ansatz for $H(J)$ that will be used in the fitting procedure.

5.3 Ansatz for $H(J)$

Let us write the amplitude for the process $\gamma^* p \to \gamma^* p$, which was already found in chapter 3, using now the new definitions, the result is

$$F_2(x,Q^2) = \frac{Q^2}{4\pi^2\alpha s}\mathrm{Im}\mathcal{A}^{\gamma^*\gamma^*}(s,t=0) = \sum_n I^{\gamma^*\gamma^*}(j_n(0)), \mathrm{Im}\bar{I}(j_n(0)). \tag{5.6}$$

where

$$I^{\gamma^*\gamma^*}(J) \equiv \frac{Q^{2J}}{4\pi^2\alpha}x^{1-J}\int dz e^{-(J-\frac{3}{2})A}\left(f_Q^2 + \frac{(\partial_z f_Q)^2}{Q^2}\right)\psi_n(J). \tag{5.7}$$

If we compare this with the expression (3.24) for $F_2(x,Q^2)$ and recalling the definition (3.26), then we see that the g_n which gives the best fit of DIS data are related to the values of $\bar{I}(J)|_{J=j_n(t)}$

$$g_n = g_n(t=0), \qquad g_n(t) = H(J)\int d\bar{z} e^{(-J+\frac{7}{2})\bar{A}}\bar{\upsilon}_{24}\bar{\psi}_n(J)\frac{dJ}{dt}|_{J=j_n(t)}. \tag{5.8}$$

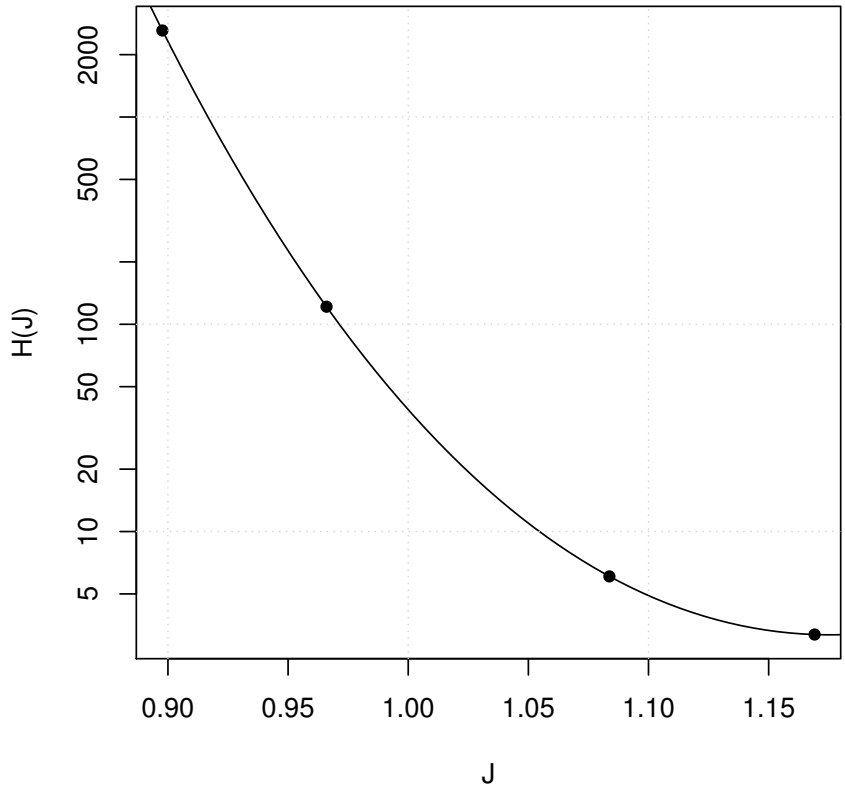

Figure 5.2: Reconstruction of the $H(J)$ function using the best parameters found in chapter 3 and $z^* = 0.565$. The solid line represents the function $\exp\left(a_0 + a_1(J-1) + a_2(J-1)^2\right)$ with $a_0 = 3.70$, $a_1 = -30.3$ and $a_2 = 89.1$.

By considering the above described approximation $e^{3A-\Phi}\upsilon_2\upsilon_4 \sim \delta(z-z^*)$ and inverting the relation we can find a relation between $H(J)$ and the g_n

$$H(j_n(t)) = \frac{g_n(t)}{e^{(-j_n(t)+\frac{1}{2})A^*}\psi_n^*(j_n(t))\frac{dj_n(t)}{dt}} \tag{5.9}$$

Now we can use the values of g_n, j_n and ψ_n found in chapter 3 with the previous formula to reconstruct $H(J)$ with the hope to learn at least some qualitative aspect of this function. We start by choosing a z^* value around 1, to be consistent with the inverse proton mass scale, and change this value noticing in a logarithmic plot that the $\log H$ can be well approximated in the range of interest by a quadratic curve in J, say $\log H(J) = a_0 + a_1(J-1) + a_2(J-1)^2$ with a_i some unknown coefficients. We choose therefore z^* to the value such that we get the best match with such quadratic

curve, which we found to be $z^* = 0.565$. The result is shown in figure 5.3, the black dots represent the actual reconstructed values of $H(J)$ for each n.

This curve has as salient aspects a steep decay with J and non zero or extrema presents. Now we would like to known whether if this is a realistic physical picture or not. We can try to guess the shape of this function by considering the shape of the $\kappa(J)$ and $\bar{\kappa}(J)$ functions with J, at least in the sharp region for values of J of interest. In the dual picture, these couplings are related to the coefficient of a spin J operator in the OPE of two spin 1 operators. In the UV fixed point it should be possible to compute this exactly since the theory would be free $SU(N)$ and therefore the computation only involves Wick contractions. Then as we move from the fixed point perturbative corrections should appear. We will not carry on such computation here but instead we will argue that a similar theory in the UV fixed point and for which the computation has been done [87], the $O(N)$ vector model, gives an $H(J)$ with precisely the same qualitative behavior. Indeed, if we take the results of [87] for the three-point bulk vertex coupling of type A minimal higher-spin theory in AdS_{d+1} of massless higher spin field of spin $s_1 = 1$, $s_2 = 1$ and $s_3 = J$, compute the $H(J)$ function defined before and plot it in the range of interest then we see that precisely this is a very steep decreasing function of J with no extrema or zeros in general, consistent with our reconstructed results. Moreover if we replace the gamma functions appearing there by its approximate version using the Stirling formula and expand quadratically around $J = 1$, we get precisely an $H(J)$ consistent with our ansatz. Of course this similarity has to be taken with caution since we are comparing different theories, but our point is that overall function shapes matches, and beyond the fixed point, corrections may be well captured in suitable redefinitions of the coefficients a_i in our ansatz. Whether this capture some physics or not can be only said by confronting our predictions against experimental data, which is what we do in the next section.

5.4 Results

In this section we will find the best fit for the free parameters in our model such that our model matches the best the experimental data. We will have two process observables: the total and differential cross-section data for DVCS from combined H1-ZEUS points reported in [88, 89]. We define the global χ^2_g as the sum of the χ^2 of each one of the process observables considered:

$$\chi^2_g = \chi^2_{\sigma_t} + \chi^2_{\frac{d\sigma(t)}{dt}}. \tag{5.10}$$

For a given observable $O \in \{\sigma_t, \frac{d\sigma(t)}{dt}\}$, the respective χ^2 function is defined as usual

$$\chi^2_O \equiv \sum_n \left(\frac{O_n^{\text{pred}} - O_n}{\delta O_n} \right)^2 \tag{5.11}$$

with O^{pred} the predicted theoretical value and δO the experimental uncertainty and the sum goes over the available experimental points.

In term of the amplitudes defined in the previous section the differential cross section for DVCS is

$$\frac{d\sigma}{dt} = \frac{1}{16\pi s^2} \frac{1}{2} \sum_{\lambda_1,\lambda_3=1}^{2} \left| A^{\lambda_1,\lambda_3}(s,t) \right|^2 = \frac{1}{16\pi^2 s^2} |\mathcal{A}^{\gamma^*\gamma}(s,t)|^2, \tag{5.12}$$

where we average over the incoming photon polarization. The total cross-section is just the integral of the above

$$\sigma_t = \int_{-1}^{0} dt \frac{d\sigma(t)}{dt}. \tag{5.13}$$

The range $-1 \leq t \leq 0$ comes from the data.

We use our `R` developed package `HQCDP` to run the optimization problem for the χ^2_g function defined in (5.10) respect to the 9 parameters to be fitted. We compute our kernel wave functions with $N = 400$ Chebyshev points and to compute the total cross-section we split the interval $-1 \leq t \leq 0$ in parts of length 0.05, compute the predicted differential cross-section for each one of these values and then we construct an interpolation function using splines to get the predicted $d\sigma(t)/dt$ in the given interval with high precision. Our code includes a cache system using `REDIS` *in memory* database which store the most expensive computations so they can be easily reused. We also optimized our code for parallel computing by serializing the computation of many integrals, using multiple cores if available. The present results were found using a node in a High Performance Computing (HPC) cluster with 16 cores.

With the previously described setup we found a fit with a global $\chi^2_{d.o.f,} \sim 1.5$. To get an idea of what is the performance of this global fit in the individual datasets we compute $\chi^2_{d.o.f.}$ separately, first for the total and then for the differential cross-section experimental data, and got 1.8 and 1.3 respectively, showing that the description per process is good as well. The best values found are shown in table 5.1. In figures 5.4 and 5.3 the theoretical predictions and the experimental values for the total and differential cross-sections of DVCS are shown.

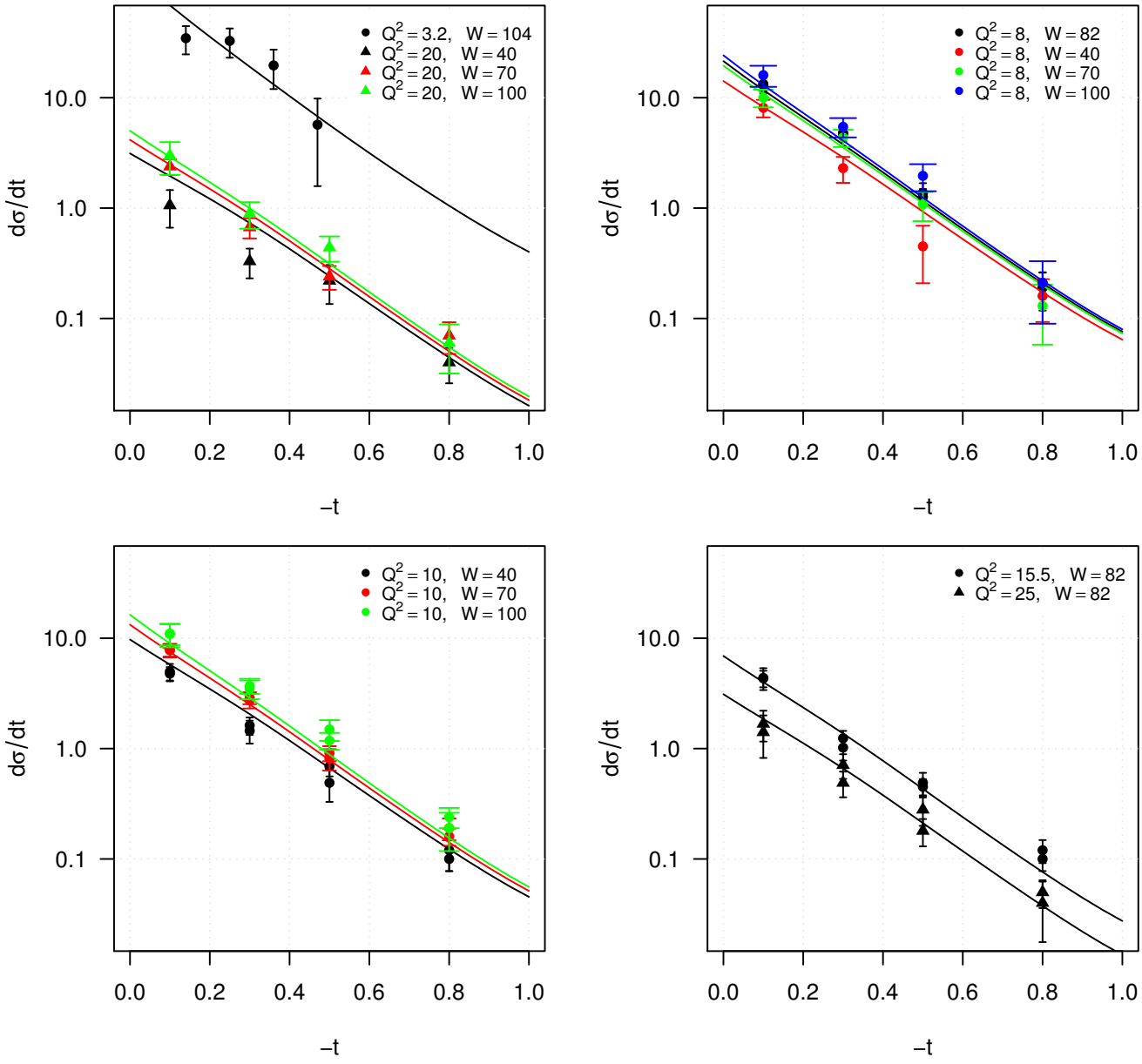

Figure 5.3: Predicted vs. experimental values of the differential cross-section $\frac{d\sigma(t)}{dt}$ for DVCS. Different gray levels correspond to different combinations of Q^2 and W as described in the legends. Here Q^2 and t are in GeV^2, W in GeV and $\frac{d\sigma}{dt}$ is in $\frac{\text{nb}}{\text{GeV}^2}$.

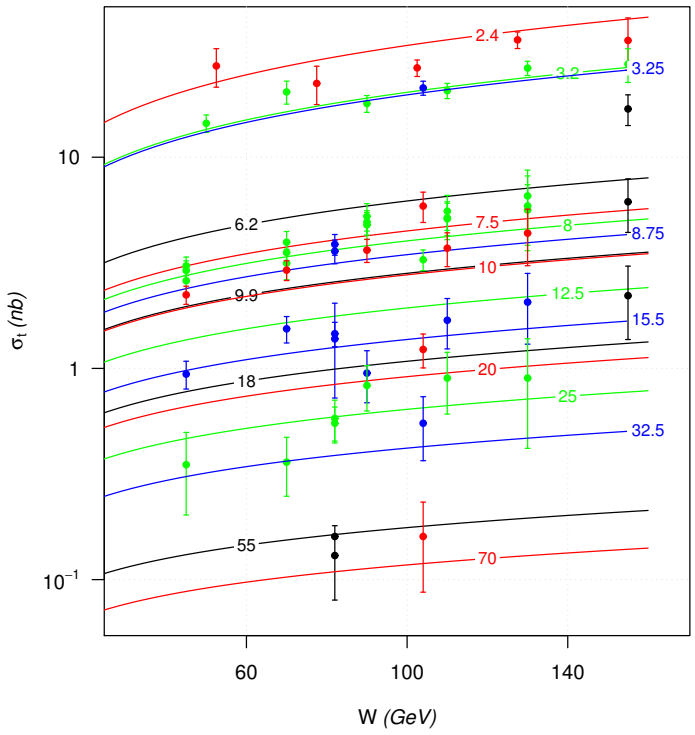

Figure 5.4: Predicted vs. experimental values of the total cross-section σ_t of DVCS. Small numbers attached to lines and points of the same grey level indicate the respective value of Q^2 in GeV.

Kernel parameters	Extra parameters	Intercepts
$a = -4.55$	$h_0 = 4.74$	$j_0 = 1.24$
$b = 0.980$	$h_1 = -35.9$	$j_1 = 1.13$
$c = 0.809$	$h_2 = 142$	$j_2 = 1.08$
$d = -0.160$	$z^* = 0.296$	$j_3 = 1.05$
$l_s = 0.153$	–	–

Table 5.1: The 9 parameters for our best fit and the intercept of the first four pomeron trajectories. All parameters are dimensionless except z^* and l_s which are in GeV^{-1}.

5.5 Conclusions

In this chapter we show that is possible to have a quantitative explanation of the H1-ZEUS latest data of total and differential cross-sections of DVCS using the same kernel for the holographic Pomeron for both experimental datasets. With this, we give our first steps towards a single model for the holographic Pomeron across different process known to be dominated by Pomeron's exchange. We should remark however, that we are presenting here preliminary results which can potentially be improved. If we predict DIS data with the model found in this chapter we get a large $\chi^2_{d.o.f}$. This is somehow expected since looking at table 5.1 we see that the intercepts differ considerably from those in table 3.1, and we know that F_2 depends sensitively on those. Nevertheless, comparing the kernel parameters found here with those which gives the best fit in chapter 3, we see that their relative difference is not large: 4.6%, 30.5%, 29.2% and 36.8% for a, b, c and d while l_s coincide. This supports the idea that using a different ansatz for $H(J)$ or actually performing the $\bar{z}$ integral may lead to a successful joint fit of DVCS and DIS data.

Since our kernel is built on top of bottom-up holographic QCD models, this may serve as well as a check point for such models. For such task, we are releasing together with this work an `R` package that can take as input different solutions of dilaton-gravity equations, say a list of values of z and the correspondent values of $A(z)$ and $\Phi(z)$. It may be well the case that the kernel representing the twist 2 fermion operators may be needed, as suggested by Donnachie and Landshoff [5]. We will have further discussion about this in the final conclusions.

6 Conclusions

In this thesis we have explored the idea of realizing the Pomeron in the context of bottom up approaches to holographic QCD. In chapter 2 we show how to deform the known spin J field equations in AdS, considering the diffusion limit, and how this can lead to explain the Soft Pomeron trajectory.

In chapter 3 we go one step further and, following the suggestion of Donnachie and Landshoff, show that it is possible to explain the raise in the effective exponent of the $F_2(x, Q)$ structure function with Q by considering the exchange of multiple Pomeron trajectories which are part of a single kernel. This is a concrete realization of the idea suggested by AdS/CFT that both Soft and Hard Pomeron are part of the same object. We saw how the $f_{0,1}(Q^2)$ encode the wave function of the kernel of the holographic Pomeron and how these wave functions can be reconstructed, obtaining for them shapes which look like solutions of a quantum mechanic problem. At this point we realized that the terms considered in chapter 2 in the strong coupling expansion of $\Delta_J(\lambda)$ were not enough so further terms, proportional to $J-2$, are needed in the kernel construction. From the perspective of the gauge/string duality this means that α' corrections are important. We considered such α' corrections by adding all the possible terms of the dynamical fields allowed by dimensional analysis and we let the coefficients to be fixed by the fitting against experimental data procedure. Moreover we saw that after the fitting procedure the Regge trajectories obtained are in great agreement with the known lattice QCD data for the masses of the higher spin glueballs, and also that its asymptotic behaviors are the one expected for a realistic QFT.

In chapter 4 we consider a different type of coupling between the higher spin fields belonging to the graviton's trajectory and the spin 1 gauge field in the bulk that represent the hadronic current in the dual theory. In AdS there are only two possible

couplings, but once we break conformal invariance more richer structures are allowed, making a systematic analysis more complex. We consider a specific type of vertex and show that considering such coupling can lead to an improvement in the fit of Deep Inelastic Scattering data.

Finally in chapter 5 we explore the possibility of having a realistic realization of the holographic Pomeron, beyond tailored models per specific processes. With this in mind we show that is possible to make a global fit of total σ_t and differential cross-sections $d\sigma(t)/dt$ experimental data from Deeply Virtual Compton Scattering processes.

As output of all this research, together with the papers produced, we release all our code available at:

`https://github.com/rcarcasses/HQCD-P`

This has the form of an `R` language package. We have chosen `R` since it provides an easy interface with `C` and `C++`, so bottleneck computation can actually speed up, it produces paper ready quality graphs, is free, is a beautiful functional language, has a highly active community and it contains many optimization routines by default. From our perspective `R` is greatly suited for the tasks we carried on in this thesis since it just glue together many well established `FORTRAN` and `C` routines in a transparent way, allowing at the same time a simple and efficient manipulation of their output. With the release of this code we put our research to the reach of anyone, in the public domain. There are many reasons we believe this is the right thing to do. Firstly our result can be easily per reviewed by other experts, which can potentially spot errors or mistakes and therefore can contribute to its improvement. Secondly, we may potentially have contributions from other specialist which can also enrich the library. Thirdly, we are living in an age where testability of scientific results have become a problem, and we believe is a good practice to publish the code used in research that involves numerical computations, contributing this way to an easy spread of knowledge. We hope to continue to develop this package in the future for it to become a reference in the subject, allowing future users to predict with ease what would be for instance the predicted behavior of $F_2(x, Q^2)$ at some x and Q given as input certain holographic model, say a list with z and $A(z)$ values produced in `Mathematica` for instance, or a certain shape for the potential that define the kernel, or to consider many kernels, etc.

We would like to discuss now the perspectives of this work. The result found in the global fit of DVCS data is encouraging and suggest as natural next step to put together with these processes the Vector Meson Production and DIS ones. The last is currently

under development and seems plausible since there exist already phenomenological global fits with VMP and DVCS data using, for example, the fact that the data exhibit geometrical scaling, see for example the recent paper [90].

As we have already pointed out in the conclusions of chapter 3, it seems natural to include also in the computation of the scattering amplitude not only the kernel associated with the glue sector of the gauge theory, which is known to give the leading contribution, but also the holographic kernel associated with the exchange of fermion twist 2 operators. The last are subleading in $1/N$, but beyond the leading order eventually they have to be considered and its trajectories may overlap with the 3 and 4 pomerons in the region near $|t| \sim 0$ as the graph 3.3 suggest. It could well be the case that the observed behavior of F_2 data with Q and x comes from the combined effect of the first two trajectories from the gluon sector and the first two from the fermion sector, as suggested by the work of Donnachie and Landshoff [5, 55]. In their work they consider the exchange of the mesons ρ and a families which are supposed to be created by these fermion twist 2 operators. According with a linear extrapolation for these trajectories their intercepts are in the range $0.5 \sim 0.9$, precisely where our third and four pomerons are. If one expect a slight bending of these trajectories as to become flatter near $|t| \sim 0$, just like what happens for the pomeron's trajectories, then these intercept values should be even higher.

To proceed in this line we need to follow a similar logic as in chapter 2: starting with the dual field of the operator $\bar{\psi}\gamma^{\mu}\psi$, which is a spin 1 gauge field in the bulk, we then should try to analytically extend its equation of motion such that its extension satisfies the same principles described in section 2.3.2, consider α' corrections and find the associated kernel by resumming the tree level exchange of all the fields described by such equation of motion. To get a consistent picture from the Regge theory perspective, the normalizable modes of the dual field to the operator $\bar{\psi}\gamma^{\mu}\psi$ should give the mass spectrum of the ρ mesons in the radial quantum number n. Then our analytic continuation should lead to the right spectrum dependence with the spin quantum number J as well as to a kernel, which combined with the gluon sector one, allows to explain scattering data. We are currently developing this line and hope to get some insights soon.

Finally we would like to revisit the elastic $pp \to pp$ (proton-proton) process, whose differential cross-section data we would like to include in our global fit in the near future as well. One of the reasons we would like to include this process is because there is plenty of data which we can use to refine holographic models. This process seems to be dominated by Pomeron's exchange [53], but it also seems to require multipomeron

exchanges to explain the data if one assume a linear trajectory for the Soft and Hard Pomerons. This is interesting because we know that single Pomeron exchange should violate the Froissart bound, but we do not know at which scale this occurs, so this process may be pointing out the value for s_0 in formula (1.12). But, on the other hand in our proposal the argument of Donnachie and Landshoff is not valid since our trajectories are not linear, so we can potentially explaining the observed data without considering further Pomeron exchanges. Nevertheless from the holographic perspective we still have to develop a more realistic model that describe the proton's wave functions in the radial coordinate. Baryons are expected to be described by the dynamic of the vertex of three open strings, a picture that comes intuitively from considering the three valence quarks inside the baryon interacting through color flux tubes. More precisely in the context of AdS/CFT, baryons appear when three strings, each with a free end, have their other end terminating on the same place in a D-brane. This is the top-down picture. But for concreteness in our computations we will need to develop a bottom-up approach considering a pair of bulk spinors to describe the boundary Dirac spinor, following for instance [91]. Then we will need to review as well how these spinors can couple to the higher spin fields from graviton's trajectory, particularly which are the relevant vertices in the Regge limit, and which components survive. This is an exciting subject we hope we can address as well. This thesis ends here.

Appendix

A

Mandelstam variables

Mandelstam variables are particularly useful in the analysis of 2 vs 2 scattering. Consider the s-channel scattering $1+2 \to 3+4$ as shown in the figure A.1.

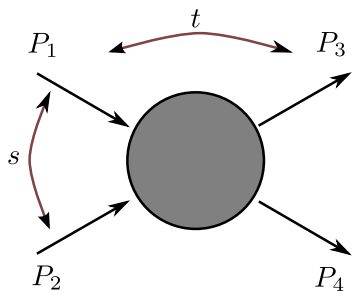

Figure A.1: 2 vs 2 scattering process.

The Mandelstam variables, which are Lorentz invariant by construction, are

$$s = (P_1 + P_2)^2 \,, \tag{A.1}$$

$$t = (P_1 - P_3)^2 \,, \tag{A.2}$$

$$s = (P_1 - P_4)^2 \,, \tag{A.3}$$

where four momentum conservation implies $s + t + u = \sum_i m_i^2$, thus only two are independent, usually s and t are taken. The scattering amplitude can be written then as $\mathcal{A}(s,t,u) = \mathcal{A}(s,t)$, for example. By reversing the sign of some of the four momenta the amplitudes in the t and u channel are obtained: the figure A.1 represent the scattering $1+2 \to 3+4$ but changing the sign of P_3 and P_2 one gets the scattering $1+\bar{3} \to \bar{2}+4$, which is the t-channel scattering amplitude where the bar denotes an antiparticle, and similarly for the u-channel. This *crossing symmetry* property implies

$$\mathcal{A}_{1+2\to 3+4}(s,t,u) = \mathcal{A}_{1+\bar{3}\to\bar{2}+4}(t,s,u) = \mathcal{A}_{1+\bar{4}\to\bar{2}+3}(u,t,s) \,. \tag{A.4}$$

In the center of mass frame

$$P_1 = (E_1, \vec{p}_1) \qquad P_2 = (E_2, -\vec{p}_1)\,, \tag{A.5}$$

$$P_3 = (E_3, \vec{p}_3) \qquad P_4 = (E_4, -\vec{p}_3)\,. \tag{A.6}$$

Notice that these P_i are not the ones in the figure A.1 but the transformations of those in the center of mass frame. Momentum conservation demands $P_1 + P_2 = P_3 + P_4$ which implies $s = (P_1 + P_2)^2 = (E_1 + E_2)^2 = (E_3 + E_4)^2$. In this frame

$$E_1 = \frac{1}{2\sqrt{s}}\left(s + m_1^2 - m_2^2\right) \qquad E_2 = \frac{1}{2\sqrt{s}}\left(s + m_2^2 - m_1^2\right), \tag{A.7}$$

$$E_3 = \frac{1}{2\sqrt{s}}\left(s + m_3^2 - m_4^2\right) \qquad E_4 = \frac{1}{2\sqrt{s}}\left(s + m_4^2 - m_3^2\right), \tag{A.8}$$

$$\vec{p}_1^{\,2} = \frac{1}{4s}\left[s - (m_1 + m_2)^2\right]\left[s - (m_1 - m_2)^2\right], \tag{A.9}$$

$$\vec{p}_3^{\,2} = \frac{1}{4s}\left[s - (m_3 + m_4)^2\right]\left[s - (m_3 - m_4)^2\right], \tag{A.10}$$

thus the three Mandelstam variables are

$$\begin{aligned} s &= (E_1 + E_2)^2 \\ t &= m_1^2 + m_3^2 - 2\left(E_1 E_3 - |\vec{p}_1|\,|\vec{p}_3|\cos\theta_s\right) \\ u &= m_1^2 + m_4^2 - 2\left(E_1 E_4 + |\vec{p}_1|\,|\vec{p}_3|\cos\theta_s\right) \end{aligned}$$

where θ_s is the scattering angle in the center of mass frame. The physical region for the s-channel is

$$s \geq (m_1 + m_2)^2 \qquad -1 \leq \cos\theta_s \leq 1. \tag{A.11}$$

For equal masses $m_i = m$

$$\begin{aligned} s &= 4\left(p^2 + m^2\right), \\ t &= -2p^2\left(1 - \cos\theta_s\right), \\ u &= -2p^2\left(1 + \cos\theta_s\right), \end{aligned}$$

where $p = |\vec{p}_1| = |\vec{p}_3|$. The physical regions for the different channels are

$$s \geq 4m^2 \quad t \leq 0 \quad u \leq 0 \qquad s\text{-channel}, \tag{A.12}$$

$$t \geq 4m^2 \quad s \leq 0 \quad u \leq 0 \qquad t\text{-channel} \tag{A.13}$$

$$u \geq 4m^2 \quad s \leq 0 \quad t \leq 0 \qquad u\text{-channel}. \tag{A.14}$$

It is possible to do a pictorial representation of the physical region for each channel by considering fact that the sum of the distances from a point on a plane to the sides of a triangle does not depend on the position of the point. In particular choosing an equilateral triangle and identifying s, t and u with the distance of a point to each one of the sides of the triangle, then each point of the plane satisfy $s + t + u = 4m^2$, and the physical regions will be those shadowed in the figure A.2.

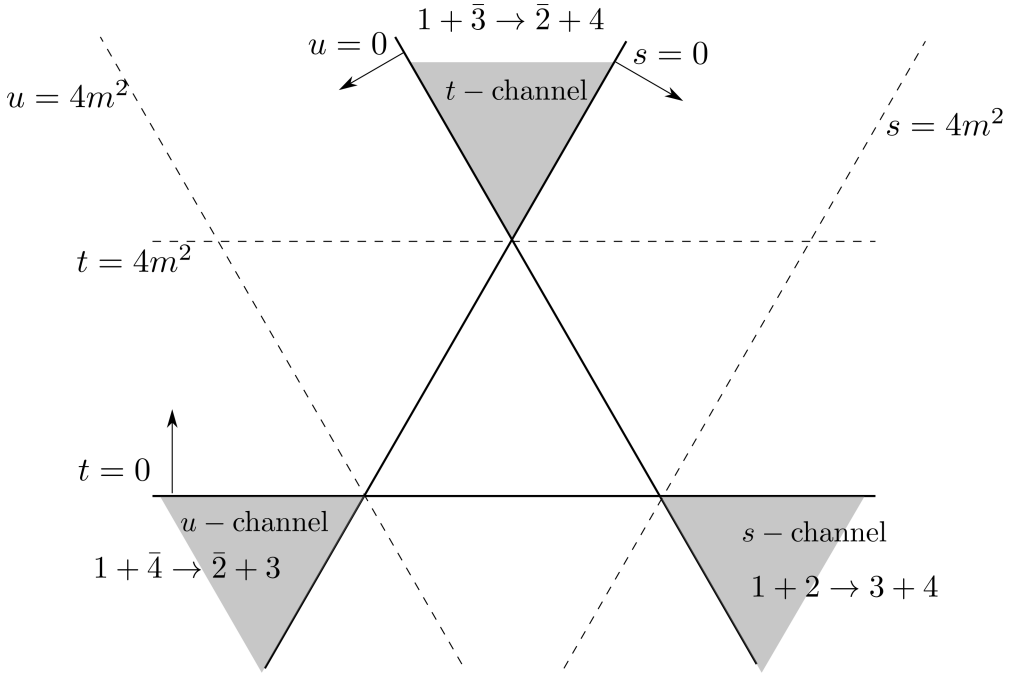

Figure A.2: A geometrical representation of the physical regions for each channel.

B

Some remarks about the BPST Pomeron

In this section a few explicit computations relative to the BPST Pomeron are presented in detail.

B.1 Saddle point of the integrand

This is almost a trivial computation. The extreme points of a function can be computed by deriving it and equaling to zero, the same applies for complex variables, one have just to be careful enough and keep in mind that in this notation w and $\bar{w}$ are independent variables

$$\begin{aligned}\frac{d}{dw}\left(w^{-4-\frac{\alpha'}{2}t}\left(1-w\right)^{-4-\frac{\alpha'}{2}s}f\left(\bar{w}\right)\right) &= w^{-4-\frac{\alpha'}{2}t}\left(1-w\right)^{-4-\frac{\alpha'}{2}s}\times, \\ &\times \left(\left(-4-\frac{\alpha'}{2}t\right)\frac{1}{w}+\left(-4-\frac{\alpha'}{2}s\right)\frac{-1}{1-w}\right)=0.\end{aligned}$$

This is equivalent to

$$\left(-4-\frac{\alpha'}{2}t\right)\frac{1}{w}=\left(-4-\frac{\alpha'}{2}s\right)\frac{1}{1-w}, \tag{B.1}$$

which for $s,t\to\infty$ becomes

$$t-tw=sw\to w=\frac{t}{s+t}. \tag{B.2}$$

B.2 Regge limit amplitude integral

In this section the integral (1.89) is compute as detailed as possible given its importance. As noticed by the authors the integral converges only for $-4>\alpha' t>-8$,

and the expression for *the amplitude* for other values of t is obtained by analytic continuation of these results, this is, the same expression but now with a bigger domain of possible values of t.

Noticing that

$$|w|^{-4-\frac{\alpha'}{2}t} = \frac{1}{\Gamma\left(2+\frac{\alpha'}{4}t\right)}\int_0^\infty dx x^{1+\frac{\alpha'}{4}t}e^{-xw\bar{w}}, \tag{B.3}$$

which is just the well know Feynman trick, the integral becomes

$$\frac{1}{\Gamma\left(2+\frac{\alpha'}{4}t\right)}\int_{\mathbb{C}} d^2w\int_0^\infty dx e^{-xw\bar{w}+\left(2+\frac{\alpha'}{4}s\right)(w+\bar{w})}x^{1+\frac{\alpha'}{4}t}, \tag{B.4}$$

where the integral in w covers the entire complex plane, and it's gaussian. Now the integration order is change and the $\int d^2w$ is computed explicitly, recalling that $w=\sigma_1+i\sigma_2$ and $dw^2 = 2d\sigma_1 d\sigma_2$ one gets[1]

$$\begin{aligned}\int_{\mathbb{C}} d^2w e^{-xw\bar{w}+\left(2+\frac{\alpha'}{4}s\right)(w+\bar{w})} &= \int_{-\infty}^{\infty}\int_{-\infty}^{\infty} 2d\sigma_1 d\sigma_2 e^{-x\left(\sigma_1^2+\sigma_2^2\right)+\frac{\alpha'}{2}s\sigma_1},\\ &= 2e^{\frac{\alpha'^2}{16x}s^2}\int_{-\infty}^{\infty} d\sigma_1 e^{-\left(\sqrt{x}\sigma_1-\frac{\alpha'}{4\sqrt{x}}s\right)+\frac{\alpha'}{2}s\sigma_1}\int_{-\infty}^{\infty} d\sigma_2 e^{-x\sigma_2^2},\\ &= 2\pi\frac{1}{x}e^{\frac{\alpha'^2}{16x}s^2},\end{aligned}$$

putting back this into the amplitude

$$\mathcal{A}(s,t) = \frac{2\pi}{\Gamma\left(2+\frac{\alpha'}{4}t\right)}\int_0^\infty dx e^{\frac{\alpha'^2}{16x}s^2}x^{\frac{\alpha'}{4}t}. \tag{B.5}$$

The remaining integral already have the form of a gamma function but with the wrong sign in the exponential. Changing variables to $y=1/x$ and inserting the identity in the exponential argument $-\left(e^{i\pi/2}\right)^2 = 1$ the integral in the last expression becomes

$$\int_0^\infty dy y^{-2-\frac{\alpha'}{4}t}e^{-y\left(\frac{\alpha'}{4}se^{i\pi/2}\right)^2}. \tag{B.6}$$

Doing finally $y\to y\left(\frac{\alpha'}{4}se^{i\pi/2}\right)^2$ we get the desired gamma function integral form giving $\left(\frac{\alpha'}{4}se^{i\pi/2}\right)^{2+\frac{\alpha'}{2}t}\Gamma\left(1-\frac{\alpha'}{4}t\right)$ for this integral. The final result for the amplitude is then

$$\mathcal{A}(s,t) = 2\pi\frac{\Gamma\left(1-\frac{\alpha'}{4}t\right)}{\Gamma\left(2+\frac{\alpha'}{4}t\right)}\left(\frac{\alpha'}{4}se^{i\pi/2}\right)^{2+\frac{\alpha'}{2}t}. \tag{B.7}$$

[1] This is very well explained in several books, like for example in the first book of Polchinski.

B.3 OPE in flat space

Here the operator product expansion OPE of the two tachyon vertex operators is computed at basic level. In this section the normal order notation is reestablished for the sake of clarity. In flat space the OPE reduces to compute the normal order operator associated with the two operators involved and then Taylor expanding in the distance. This is because, as already mentioned, the worldsheet QFT is a free CFT and basically the computation is reduced to compute efficiently Wick contractions. Starting with the general formula (2.2.10) of Polchinski book [92]

$$:\mathcal{F}::\mathcal{G}:=\exp\left(-\frac{\alpha'}{2}\int dz_1^2dz_2^2\ln|z_{12}|^2\,\frac{\delta}{\delta X_F^\mu\left(z_1,\bar{z}_1\right)}\frac{\delta}{\delta X_{G\mu}\left(z_2,\bar{z}_2\right)}\right):\mathcal{FG}:, \tag{B.8}$$

then taking $z_1=w$, $z_2=0$, $\mathcal{F}=e^{ip_1\cdot X(w,\bar{w})}$ and $\mathcal{G}=e^{ip_2\cdot X(0)}$ and expanding the exponential in the previous formula in Taylor series

$$\begin{aligned}:e^{ip_1\cdot X(w,\bar{w})}::e^{ip_2\cdot X(0)}: \;&=\; \sum_{k=0}^{\infty}\frac{(-\alpha')^k}{k!}\left(\int dw^2dz_2^2\ln|w|\,\frac{\delta}{\delta X_F^\mu\left(w,\bar{w}\right)}\frac{\delta}{\delta X_{G\mu}\left(z_2,\bar{z}_2\right)}\right)^{(k)}\\ &\quad :e^{ip_1\cdot X(a,\bar{a})}e^{ip_2\cdot X\left(b,\bar{b}\right)}:|_{z_2=0}.\end{aligned} \tag{B.9}$$

The (k) notation in the exponent is to remark that this is a *functional* power expansion, this is, the value is obtained by applying it k times to the expression at the right. The subindices F and G is to denote that the functional derivatives act only on the variables that belongs to the operators $\mathcal{F}$ and $\mathcal{G}$ respectively. Noticing that

$$\begin{aligned}&\int dw^2dz_2^2\ln|w|\,\frac{\delta}{\delta X_F^\mu\left(w,\bar{w}\right)}\frac{\delta}{\delta X_{G\mu}\left(z_2,\bar{z}_2\right)}:e^{ip_1\cdot X(a,\bar{a})}e^{ip_2\cdot X\left(b,\bar{b}\right)}:|_{z_2=0}\\ &\qquad=:\int dw^2dz_2^2\ln|w|\,\frac{\delta e^{ip_1\cdot X(a,\bar{a})}}{\delta X^\mu\left(w,\bar{w}\right)}\frac{\delta e^{ip_2\cdot X\left(b,\bar{b}\right)}}{\delta X_\mu\left(z_2,\bar{z}_2\right)}:|_{z_2=0}\\ &=:\int dw^2dz_2^2\ln|w|\,p_1\cdot p_2e^{ip_1\cdot X(a,\bar{a})}e^{ip_2\cdot X\left(b,\bar{b}\right)}\delta^2\left(a,w\right)\delta^2\left(b,z_2\right):|_{z_2=0}\\ &\qquad=-\ln|w|\,p_1\cdot p_2:e^{ip_1\cdot X(w,\bar{w})}e^{ip_2\cdot X(0)}:,\end{aligned}$$

where $\delta^2\left(x,y\right)$ is the 2d Dirac delta function, then acting k times with the integral operator gives a factor of $\left(-\ln|w|\,p_1\cdot p_2\right)^k$, thus (B.9) reduces to

$$\begin{aligned}:e^{ip_1\cdot X(w,\bar{w})}::e^{ip_2\cdot X(0)}: \;&=\; \sum_{k=0}^{\infty}\frac{\left(\alpha'\ln|w|\,p_1\cdot p_2\right)^k}{k!}:e^{ip_1\cdot X(w,\bar{w})}e^{ip_2\cdot X(0)}:\\ &=\; \exp\left(\alpha'\ln|w|\,p_1\cdot p_2\right):e^{ip_1\cdot X(w,\bar{w})}e^{ip_2\cdot X(0)}:\\ &=\; |w|^{\alpha' p_1\cdot p_2}:e^{ip_1\cdot X(w,\bar{w})}e^{ip_2\cdot X(0)}:,\end{aligned}$$

which is the formula (2.2.13) of [92].

B.4 Expectation value on the sphere

Similar to a common QFT, one can define a generating functional $Z[J]$ in string theory such that one can compute all kind of correlation functions by just taking functional derivatives of it, or alternatively, choose wisely the source functions J.

At tree level the relevant Riemann surface for closed strings in flat space is a sphere, which is basically the complex plane plus a point at infinity. In this case is relatively simple to compute $Z[J]$ since the worldsheet theory is non interacting. Here we just the result appearing in Polchinski's book, formula (6.2.1)

$$Z[J] = \left\langle e^{i\int d\sigma J(\sigma)\cdot X(\sigma)} \right\rangle = Ce^{-\frac{1}{2}\int d\sigma d\sigma' J(\sigma)\cdot J(\sigma')G(\sigma,\sigma')}, \tag{B.10}$$

where $G(\sigma,\sigma') = \alpha' \ln|z_{12}|$ is the 2d Green's function of the Laplace operator. After doing the OPE with the first two operators in the 4 tachyon amplitude one is left with the expectation value of the following 3 operators

$$\left\langle e^{ik\cdot X(0)+p_1\cdot\left(w\partial+\bar{w}\bar{\partial}\right)X(0)} e^{ip_3\cdot X(1)} e^{ip_4\cdot X(\infty)} \right\rangle. \tag{B.11}$$

It is very easy to realize that the for of the sources that reproduce the above 3 point function is

$$J(\sigma) = \left(k + p_1\left(w\partial + \bar{w}\bar{\partial}\right)\right)\delta^2(\sigma-\sigma_0) + p_3\delta^2(\sigma-\sigma_1) + p_4\delta^2(\sigma-\sigma_\infty). \tag{B.12}$$

Notice that the derivatives ∂ and $\bar{\partial}$ acts on σ_0. Putting back this result in (B.10) one finds that

$$\left\langle e^{ik\cdot X(0)+p_1\cdot\left(w\partial+\bar{w}\bar{\partial}\right)X(0)} e^{ip_3\cdot X(1)} e^{ip_4\cdot X(\infty)} \right\rangle = e^{\left(2+\frac{\alpha' s}{4}\right)(w+\bar{w})}, \tag{B.13}$$

where $2+\frac{\alpha' s}{4} = \frac{1}{2}p_1\cdot p_3$ and the momentum delta function was omitted and the expression is normalized the same way as the amplitude. The only term that require a little attention is the first one but presents no difficulties. This proves that the integral Regge behavior can be obtained using the OPE.

C

Projection of tensor laplacian in Minkowski indices

It is illustrative to decompose the $d+1$ tensor laplacian into its boundary indices (non z ones)

$$D_a D^a \phi_{a_1 \ldots a_J}|_{a_i=\mu_i} \qquad\qquad a = (\mu, z) = 0, .., d. \tag{C.1}$$

For a general totally symmetric traceless rank J tensor one can proceed to write all the covariant derivatives and try to find the general pattern but we will do it in a different way as described below:

- Pass the tensor field $\phi_{a_1 \ldots a_J}$ to the tangent space $\phi_{A_1 \ldots A_J} = e^{a_1}_{A_1} \ldots e^{a_J}_{A_J} \phi_{a_1 \ldots a_J}$ using the frame formulation.
- Define a generating functional $|\Phi_J\rangle_B = \phi_{B A_1 \ldots A_J} \alpha^{A_1} \ldots \alpha^{A_J} |0\rangle$ where α^A, $\bar{\alpha}^A$ are creation and annihilation operators. This way we get rid of indices.
- Define a projection operator $\mathcal{P}_{B_1 \ldots B_J}$ that extract the tensor components $B_1 \ldots B_J$ from the generating functional. This way we can go back a forth from the space of Fock states to the space of symmetric tensors.
- Define a covariant derivative operator acting in the Fock state $|\Phi_J\rangle_B$ such that the projection of the state obtained by acting with this operator gives the covariant derivative of the encoded tensor field.
- The laplacian then is just twice the action of this operator. Extract the subset of interested components in the frame, which are in one to one correspondence with the target space ones.
- Translate back the result to the target space indices.

In this approach, one ends with a lot of definitions but with a minimum of computations to be explicitly done.

C.1 Computation

As stated before, the first step is to move to the tangent space

$$\phi_{A_1...A_J} = e^{a_1}_{A_1}...e^{a_J}_{A_J}\phi_{a_1...a_J}, \tag{C.2}$$

where $e^A_\mu = e^{A(z)}\delta^A_\mu$ the vielbein in our $AAdS$ space[1] which satisfy the frame postulate $D_A e^\mu_B = 0$. The relation between the laplacians in target/tangent space is just

$$D_a D^a \phi_{a_1...a_J} = e^{A_1}_{a_1}...e^{A_J}_{a_J} D_A D^A \phi_{A_1...A_J} = e^{JA(z)}\delta^{A_1}_{a_1}...\delta^{A_J}_{a_J} D_A D^A \phi_{A_1...A_J}, \tag{C.3}$$

where $D_A \equiv e^\mu_A D_\mu$. In our case e^A_a is diagonal, extracting the μ components of $D_a D^a \phi_{a_1...a_J}$ is equivalent to extract the $\hat{\mu}$ components of $D_A D^A \phi_{A_1...A_J}$ with $\hat{\mu} = \mu$.

To move forward it is convenient to use Metsaev formalism [93] to get rid of indices at this point. In fact, some modification is needed since we need to define properly the representation of the covariant derivative acting on the generating functional of a tensor with all but one contracted indices. Let's encode the indices $A_1...A_J$ of the totally symmetric tensor $\phi_{BA_1...A_J}$ in a Fock space vector generating functional $|\Phi_J\rangle_B = \phi_{BA_1...A_J}\alpha^{A_1}...\alpha^{A_J}|0\rangle$ where α^A, $\bar{\alpha}^A$ are creation and annihilation operators

$$\bar{\alpha}^A|0\rangle = 0, \qquad \left[\bar{\alpha}^A, \alpha^B\right] = \eta^{AB}, \qquad \left[\alpha^A, \alpha^B\right] = \left[\bar{\alpha}^A, \bar{\alpha}^B\right] = 0. \tag{C.4}$$

In this formalism, extracting the components $B_1...B_J$ of a some tensor represented by $|H\rangle$ is equal to project the Fock vector into the base of states created by $\alpha^{A_1}...\alpha^{A_J}|0\rangle$. The projector operator will be

$$\mathcal{P}_{B_1...B_J} \equiv \frac{1}{J!}\langle 0|\bar{\alpha}^{B_1}...\bar{\alpha}^{B_J}. \tag{C.5}$$

Lorentz covariant derivative acting on $|\Phi_J\rangle_B$ is found by requiring that its projection matches $D_C\phi_{BA_1...A_J}$

$$\begin{array}{ccc} \phi_{BA_1...A_J} & \xrightarrow{\alpha^{A_1}...\alpha^{A_J}} & |\Phi_J\rangle_B \\ D_C \big\downarrow & & \big\downarrow \hat{D}_C \\ D_C\phi_{BA_1...A_J} & \xleftarrow[\mathcal{P}_{A_1...A_J}]{} & \hat{D}_C|\Phi_J\rangle_B \end{array} . \tag{C.6}$$

It can be easily proved that

$$\hat{D}_C = \tilde{D}_C|\Phi_J\rangle_B + \omega_C{}^A{}_B|\Phi_J\rangle_A, \tag{C.7}$$

[1] Abusing of notation we have set A as a tangent space index and $A(z)$ is the warp factor of the metric.

$$\tilde{D}_C = \hat{\partial}_C + \omega_{CAB}\alpha^{[A}\bar{\alpha}^{B]}, \qquad \hat{\partial}_C \equiv e^{\mu}_C\partial_\mu, \qquad \omega^{AB}_C \equiv e^{\mu}_C\omega^{AB}_\mu, \tag{C.8}$$

where ω^{AB}_μ is the spin connection. Notice that $\tilde{D}_C$ is the operator in Metsaev paper and for a totally symmetric tensor, no B index, the result matches. Notice also that the extension for tensors $|\Phi_J\rangle_{B_1\ldots B_n}$ with an arbitrary number of extra indices is trivial: just to add new connection terms per index as in an ordinary covariant derivative. The whole point of all these definitions is that extracting the desired components is reduced to compute Wick contractions, which in principle should be easier to handle.

Before proceeding further let's first derive the formula for the scalar laplacian, since it will be useful later. Since it has no indices all Wick contractions give zero

$$D_\mu D^\mu\phi = D_A D^A\phi = \mathcal{P}\hat{D}_A\left(\hat{D}^A|\Phi_0\rangle\right) = \tag{C.9}$$

$$\langle 0|\left(\hat{\partial}_C + \omega_{CAB}\alpha^{[A}\bar{\alpha}^{B]}\right)\left(\hat{\partial}^C + \frac{1}{2}\omega^{CAB}\alpha^{[A}\bar{\alpha}^{B]}\right)\phi + \omega_C{}^C{}_D\left(\hat{\partial}^D + \frac{1}{2}\omega^D_{AB}\alpha^{[A}\bar{\alpha}^{B]}\right)\phi|0\rangle$$

$$\begin{aligned} &= \hat{\partial}_C\hat{\partial}^C\phi + \omega_C{}^C{}_D\hat{\partial}^D\phi = e^a_C\partial_a e^C_b\partial^b\phi + e^a_C e^D_b\omega_a{}^C{}_D\partial^b\phi \\ &= \partial^2\phi + e^a_C\left(\left(\partial_a e^C_b\right) + e^D_b\omega_a{}^C{}_D\right)\partial^b\phi \\ &= \partial^2\phi + e^a_C e^C_c\Gamma^c_{ab}\partial^b\phi = \partial^2\phi + \Gamma^a_{ab}\partial^b\phi, \end{aligned} \tag{C.10}$$

which is indeed the scalar laplacian. For a warped flat space $ds = e^{A(z)}\eta_{ab}dx^a dx^b$:

$$\tilde{D}^C = \hat{\partial}^C - \zeta(z)\left(\alpha^z\bar{\alpha}^C - \alpha^z\bar{\alpha}^C\right), \qquad \zeta(z) = \partial_z e^{-A(z)}. \tag{C.11}$$

We will be interested in the $B_1\ldots B_J = \hat{\mu}_1\ldots\hat{\mu}_J \neq z$ components of the $D_A D^A\phi_{A_1\ldots A_J}$ tensor, so we need to compute

$$\frac{1}{J!}\langle 0|\bar{\alpha}_{\hat{\mu}_1}\ldots\bar{\alpha}_{\hat{\mu}_J}\hat{D}_A\left(\hat{D}^A\phi_{A_1\ldots A_J}\alpha^{A_1}\ldots\alpha^{A_J}|0\rangle\right), \tag{C.12}$$

which after expanding and defining $|J^{A_i}\rangle \equiv \alpha^{A_1}\ldots\alpha^{A_J}|0\rangle$ gives

$$\begin{aligned} &\langle J^{B_i}|\hat{\partial}_C\hat{\partial}^C - \frac{1}{2}\left(\hat{\partial}_C\zeta(z) + 2\hat{\partial}_C\right)\alpha^{[z}\bar{\alpha}^{C]} + \frac{1}{4}\zeta(z)^2\,\alpha^{[z}\bar{\alpha}^{C]}\alpha^{[z}\bar{\alpha}^{C]} \\ &+ \omega_C{}^C{}_D\left(\hat{\partial}^D - \frac{1}{2}\zeta(z)\,\alpha^{[z}\bar{\alpha}^{D]}\right)|J^{A_i}\rangle\phi_{A_1\ldots A_J}. \end{aligned}$$

Let us quickly recognize that terms with no α's just give the scalar laplacian (C.10), so

$$\begin{aligned} &\nabla^2_0\phi_{\hat{\mu}_1\ldots\hat{\mu}_J} + \langle J^{B_i}|-2\left(\hat{\partial}_C\zeta(z) + 2\hat{\partial}_C\right)\alpha^{[z}\bar{\alpha}^{C]} + 4\zeta(z)^2\,\alpha^{[z}\bar{\alpha}^{C]}\alpha^{[z}\bar{\alpha}^{C]} \\ &- 2\omega_C{}^C{}_D\zeta(z)\,\alpha^{[z}\bar{\alpha}^{D]}|J^{A_i}\rangle\phi_{A_1\ldots A_J}. \end{aligned} \tag{C.13}$$

It remains to compute the Wick contractions

$$\frac{1}{J!}\phi_{A_1\ldots A_J}\langle J^{\hat{\mu}_i}|2\alpha^{[z}\bar{\alpha}^{C]}|J^{A_i}\rangle = \eta^{\hat{\mu}_1 C}\phi_{\hat{\mu}_2\ldots\hat{\mu}_J z} + (\hat{\mu}_i \to \hat{\mu}_{i+1}), \tag{C.14}$$

$$\frac{1}{J!}\phi_{A_1\ldots A_J}\langle J^{\hat{\mu}_i}|4\alpha^{[z}\bar{\alpha}^{C]}\alpha^{[z}\bar{\alpha}^{C]}|J^{A_i}\rangle = -J\phi_{\hat{\mu}_1\ldots\hat{\mu}_J} + J!\eta_{(\hat{\mu}_1\hat{\mu}_2}\phi_{\hat{\mu}_3\ldots\hat{\mu}_J)zz}.$$

Here +... means terms obtained by circular cycling permuting the $\hat{\mu}$ indices: $\hat{\mu}_i \to \hat{\mu}_{i+1}$ with $\hat{\mu}_{J+1} = \hat{\mu}_1$.

As one can guess the equation contain terms of the types $\phi_{\hat{\mu}\ldots\hat{\mu}}$, $\phi_{z\hat{\mu}\ldots\hat{\mu}}$ and $\phi_{zz\hat{\mu}\ldots\hat{\mu}}$. Projected into this indices, the tensor is no longer traceless neither transverse. We can now proceed to decompose $\phi_{\hat{\mu}\ldots\hat{\mu}}$ into irreducible representations of the boundary symmetries, $\phi_{\hat{\mu}_1\ldots\hat{\mu}_J} = \phi^{TT}_{\hat{\mu}_1\ldots\hat{\mu}_J} + \partial_{(\mu_1}\phi^1_{\hat{\mu}_2\ldots\hat{\mu}_J)} + \ldots$, in this process one can demand after evaluating the laplacian that the coefficients for each spin to be zero, giving the equation of motion for each one of them. Since $\phi^{TT}_{\hat{\mu}_1\ldots\hat{\mu}_J}$ can not mix with another field of the same spin, because there are not, then one conclude that the action of the laplacian in it is equal to the action on $\phi_{\hat{\mu}_1\ldots\hat{\mu}_J}$, thus, the *equation of motion* for this field is

$$\left(\nabla_0^2 - J\zeta\left(z\right)^2\right)\phi^{TT}_{\hat{\mu}_1\ldots\hat{\mu}_J} = \left(\nabla_0^2 - J\zeta\left(z\right)^2\right)e^{a_1}_{\hat{\mu}_1}\ldots e^{a_J}_{\hat{\mu}_J}\phi^{TT}_{a_1\ldots a_J} \tag{C.15}$$

This is the equation of motion in the tangent space, in target space will be

$$e^{\hat{\mu}_1}_{\mu_1}\ldots e^{\hat{\mu}_J}_{\mu_J}\left(\nabla_0^2 - J\zeta\left(z\right)^2\right)e^{a_1}_{\hat{\mu}_1}\ldots e^{a_J}_{\hat{\mu}_J}\phi^{TT}_{a_1\ldots a_J}, \tag{C.16}$$

which is just

$$\left(e^{JA(z)}\nabla_0^2 e^{-JA(z)} - JA'\left(z\right)^2 e^{-2A(z)}\right)\phi^{TT}_{\mu_1\ldots\mu_J}. \tag{C.17}$$

This is the same formula (2.20) written in [13] only for the +++ component considering a specific frame where the momentum components $+, -$ are zero. In that case there is no projection in the TT part, but one get the same formula if in (C.13) set $\hat{\mu}_i = +$ and demand that $\partial_+\phi_{+\ldots+z} = 0$ or considering $\phi_{z\hat{\mu}_2\ldots\hat{\mu}_J} = 0$.

D

Numerov's method

This is a numeric method to solve second order ordinary differential equations where the first derivative term is missing, the equation is in its "Schrodinger form". Briefly, given the equation

$$\left(\frac{d^2}{dx^2} + f(x)\right) y(x) = 0, \tag{D.1}$$

a solution can be build using the following recurrent relation:

$$y_{n+1} = \frac{\left(2 - \frac{5}{6h^2} f_n\right) y_n - \left(1 + \frac{h^2}{12} f_{n-1}\right) y_{n-1}}{1 + \frac{h^2}{12} f_{n+1}}, \tag{D.2}$$

where $f_n = f(x_n)$, $y_n = y(x_n)$ and $x_{n+1} - x_n = h$. In a one-dimensional Schrodinger problem, up to a constant, $f(x) = E - V(x)$ where E is the energy eigenvalue. The method can be extended also to the non homogeneous and non linear case.

In order to solve the 2 point boundary value problem (BVP) $y(-\infty) = y(\infty) = 0$[1], which represent bound states from the quantum perspective, a good idea is to determine first for which values of E the potential may have bound states. This can be easily guessed by plotting the potential function against x: bounds states may exist in those zones where there are wells and the range of E goes from the value of the potential at the bottom of the well up to the well's height. This considerably restrict the range of possible eigenvalues for bound states and also suggest the range of values for x, $\{x_{min}, x_{max}\}$ to be used in the numeric computation such that the eigenvalues found does not depend sensitively of this range.

A natural approach to solve the bound states problem would be to split the interval in $N = \frac{x_{max} - x_{min}}{h}$ pieces and, for a given E under the interval of possible values one

[1]The boundary of the space under consideration can vary, still the analysis is valid. For example while solving the radial part of the Schrodinger equation in the Hydrogen atom the boundary conditions are $y(0) = y(\infty) = 0$, as $x = r$ represents the radial coordinate.

have figured out for it, start from the left putting $y_0 = 0$ and $y_1 = 0.001$ for example and propagate this solution to the right using (D.2), and then check if at the right boundary $y_N = 0$, or close to it, if is not zero then change E a bit and check again. In most of the cases this does not work and the reason is the following: assuming the right boundary is inside the forbidden region ($E < V(x_{max})$), there are two possible solutions in its vicinity, one that grows to infinity and other that goes exponentially to zero, then starting from the left and propagating the solution to the right does not guarantee that the numerical computation will choose the decaying solution at the right. This is very subtle and instead and improved approach is frequently used: a solution is propagated from the left using $y_0 = 0$ and some value of y_1 and another solution is propagated from the right using $y_N = 0$ and y_{N-1} small, then they are required to match at a given point x_c, as well as its derivatives. In this way one can be sure that the correct solutions has been chosen at the boundaries, what is left is to change E until a good match between the left and right solutions is found at x_c. Calling $l(x)$ and $r(x)$ the solutions that starts at the left and right respectively, the connecting condition reads

$$diff(x_c) \equiv l(x_c) r'(x_c) - l'(x_c) r(x_c) = 0. \tag{D.3}$$

It turns out that good values for x_c are those where $f(x) = 0$, these are the classical returning points of the potential. The problem is reduced then to find those values of E such that $diff(x) = 0$.

A beautiful thing about using (D.3) as the eigenvalue condition is that the values of y_1 and y_{N-1} are irrelevant for the problem. Indeed, changing y_1 for another value will have the effect of scaling $l(x)$, as all its points are proportional to y_1 according to the way we obtain them (D.2). Now the value of E such that the connecting condition (D.3) is satisfied is insensitive to a scaling of $l(x)$, as the zeros of a scaled $diff(x_c)$ function are the same of an unscaled one, thus insensitive to the value of y_1. The same applies for the right solution.

While this is good for determining the eigenvalues it can lead to confusing results for the eigenfunctions. We can end satisfying the connecting condition for some $l(x)$ and $r(x)$ that actually do not match at $x = x_c$. But the solution of this is very easy: just have to rescale one of them such that $l(x_c) = r(x_c)$, this is equivalent to changing y_1 or y_{N-1}, thus giving the right values for the first derivatives of $y(x)$ at the boundaries. This method is cheaper than computing those values from the beginning using some kind of asymptotic expansions. The figure D.1 shows a specific case of the aforementioned situation and its solution.

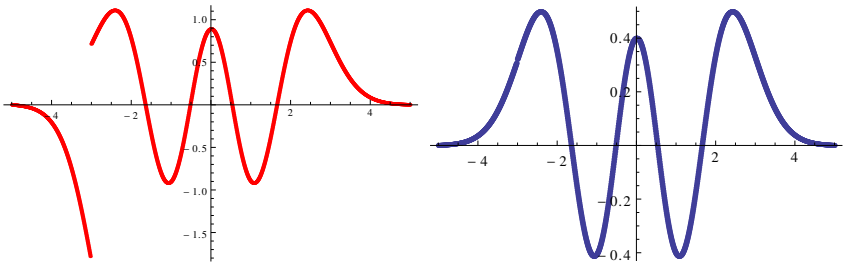

Figure D.1: Harmonic oscillator fifth level plot. At the left the configuration obtained when the connecting condition is satisfied. At the right the correct eigenfunction after scaling the left part to mach the right solution at $x = x_c$ and normalizing. For this example $V(x) = x^2$, $y_1 = -0.1$, $y_{N-1} = 0.04$, $h = 0.008$, $x_{min} = -5$, $x_{max} = 5$, the eigenvalue obtained is $E_5 = 9.00003$, the exact value is 9.

E

Numeric convergence

For the specific model we consider in chapter 3, configurations for the potential with a very large dip close to $z = 0$ appear for the 3rd and 4th trajectories, as can be seen in figure 3.8, requiring a careful analysis of the precision of the computation. As commented in the paper, we have used mainly a Chebyshev algorithm for solving the Schrödinger problem in which functions in the interval $[z_{min}, z_{max}]$ are discretized in N points. We have done first our minimization procedure starting with $N = 250$, and then gradually increased it to $N = 400$, 800 and 1000. At each one of these values of N, using as a starting point the best values obtained from the previous N, we run our minimization routine always obtaining a $\chi^2 \sim 1.7$. In figure E.1 it is shown the evolution of the best fit parameters with N, in the paper we reported values for the $N = 1000$ case.

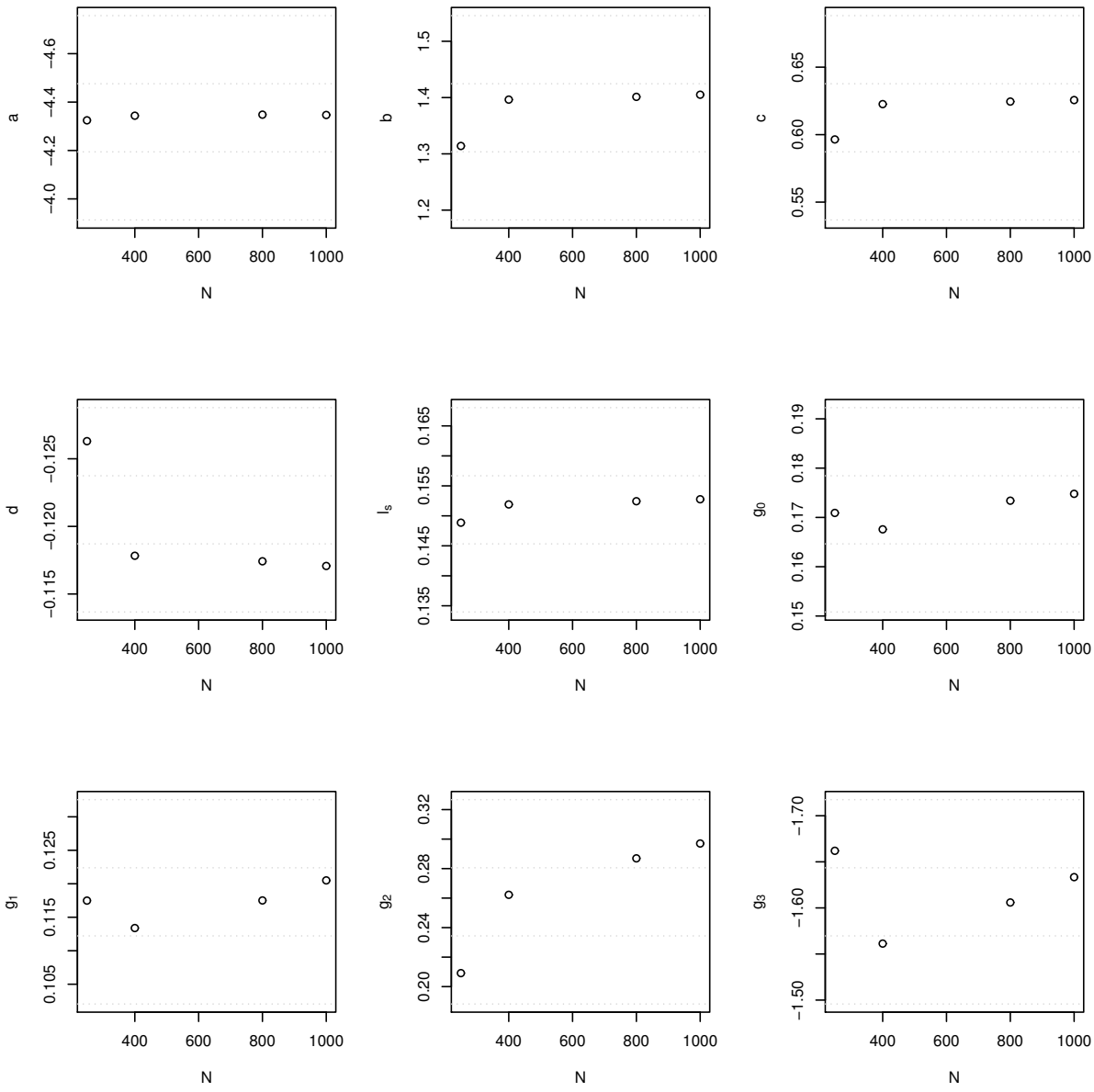

Figure E.1: Evolution of best fit parameters with the number of interpolation points N.

References

[1] F. Gelis, E. Iancu, J. Jalilian-Marian, and R. Venugopalan. The Color Glass Condensate. *Annual Review of Nuclear and Particle Science*, 60(1):463–489, November 2010. arXiv: 1002.0333.

[2] F. D. Aaron et al. Combined Measurement and QCD Analysis of the Inclusive e+- p Scattering Cross Sections at HERA. *JHEP*, 01:109, 2010.

[3] Harvey B. Meyer. Glueball Regge Trajectories. *arXiv:hep-lat/0508002*, August 2005. arXiv: hep-lat/0508002.

[4] Harvey B. Meyer and Michael J. Teper. Glueball Regge trajectories and the pomeron: a lattice study. *Physics Letters B*, 605(3–4):344–354, January 2005.

[5] A. Donnachie and P. V. Landshoff. Small x: two pomerons! *Physics Letters B*, 437(3-4):408–416, October 1998.

[6] The CMS Collaboration. Observation of a new boson at a mass of 125 GeV with the CMS experiment at the LHC. *Physics Letters B*, 716(1):30–61, September 2012. arXiv: 1207.7235.

[7] A. Donnachie and P. V. Landshoff. Total cross sections. *Physics Letters B*, 296(1-2):227–232, December 1992. arXiv: hep-ph/9209205.

[8] E. A. Kuraev, L. N. Lipatov, and Victor S. Fadin. The Pomeranchuk Singularity in Nonabelian Gauge Theories. *Sov.Phys.JETP*, 45:199–204, February 1977.

[9] Victor S. Fadin, E. A. Kuraev, and L. N. Lipatov. On the Pomeranchuk Singularity in Asymptotically Free Theories. *Phys.Lett.*, 60B:50–52, 1975.

[10] I. I. Balitsky and L. N. Lipatov. The Pomeranchuk Singularity in Quantum Chromodynamics. *Sov.J.Nucl.Phys.*, 28:822–829, 1978.

[11] H. Kowalski, L. N. Lipatov, D. A. Ross, and G. Watt. Using HERA Data to Determine the Infrared Behaviour of the BFKL Amplitude. *The European Physical Journal C*, 70(4):983–998, December 2010. arXiv: 1005.0355.

[12] Juan Maldacena. The Large-N Limit of Superconformal Field Theories and Supergravity. *International Journal of Theoretical Physics*, 38(4):1113–1133, April 1999.

[13] Richard C. Brower, Joseph Polchinski, Matthew J. Strassler, and Chung-I. Tan. The Pomeron and gauge/string duality. *Journal of High Energy Physics*, 2007(12):005, December 2007.

[14] Lorenzo Cornalba and Miguel S. Costa. Saturation in deep inelastic scattering from the AdS/CFT correspondence. *Physical Review D*, 78(9):096010, November 2008.

[15] E. Levin and I. Potashnikova. Inelastic processes in DIS and $\mathcal{N} = 4$ SYM. *Journal of High Energy Physics*, 2010(8):112, August 2010.

[16] Richard C. Brower, Marko Djurić, Ina Sarčević, and Chung-I. Tan. String-gauge dual description of deep inelastic scattering at small-x. *Journal of High Energy Physics*, 2010(11):1–26, November 2010.

[17] Miguel S. Costa and Marko Djurić. Deeply virtual Compton scattering from gauge/gravity duality. *Physical Review D*, 86(1):016009, July 2012.

[18] Miguel S. Costa, Marko Djurić, and Nick Evans. Vector meson production at low x from gauge/gravity duality. *Journal of High Energy Physics*, 2013(9):1–18, September 2013.

[19] Richard C. Brower, Marko Djuric, and Chung-I Tan. Diffractive Higgs Production by AdS Pomeron Fusion. *JHEP*, 09:097, 2012.

[20] Alfonso Ballon-Bayona, Robert Carcassés Quevedo, Miguel S. Costa, and Marko Djurić. Soft Pomeron in Holographic QCD. *arXiv:1508.00008 [hep-ph, physics:hep-th]*, July 2015. arXiv: 1508.00008.

[21] Alfonso Ballon-Bayona, Robert Carcasses Quevedo, and Miguel S. Costa. Unity of pomerons from gauge/string duality. *arXiv:1704.08280 [hep-ph, physics:hep-th]*, April 2017. arXiv: 1704.08280.

[22] Artur Amorim, Robert Carcassés Quevedo, and Miguel S. Costa. Non-minimal coupling contribution to DIS at low x in Holographic QCD. 2018.

[23] S. Donnachie, Hans Gunter Dosch, O. Nachtmann, and P. Landshoff. Pomeron physics and QCD. *Camb.Monogr.Part.Phys.Nucl.Phys.Cosmol.*, 19:1–347, 2002.

[24] J. Bros, H. Epstein, and V. Glaser. A proof of the crossing property for two-particle amplitudes in general quantum field theory. *Communications in Mathematical Physics*, 1(3):240–264, 1965.

[25] Jo Bros, H. Epstein, and V. Glaser. Some rigorous analyticity properties of the four-point function in momentum space. *Il Nuovo Cimento*, 31(6):1265–1302, 1964.

[26] H. Epstein, V. Glaser, and Daniel Iagolnitzer. Some analyticity properties arising from asymptotic completeness in quantum field theory. *Communications in Mathematical Physics*, 80(1):99–125, 1981.

[27] R. J. Eden. Threshold Behaviour in Quantum Field Theory. *Proceedings of the Royal Society of London. Series A, Mathematical and Physical Sciences*, 210(1102):388–404, January 1952.

[28] Richard John Eden, Peter Vincent Landshoff, David I. Olive, and John Charlton Polkinghorne. *The analytic S-matrix*. Cambridge University Press, 2002.

[29] V. N. Gribov. *The theory of complex angular momenta: Gribov lectures on theoretical physics*. UK: Cambridge University Press, Cambridge, 2003.

[30] Amanda Cooper-Sarkar Robin Devenish. *Deep inelastic scattering*. Oxford University Press, 2004.

[31] M. A. Braun. Structure function of the nucleus in the perturbative QCD with \$N_c\to\infty\$ (BFKL pomeron fan diagrams). *The European Physical Journal C - Particles and Fields*, 16(2):337–347, August 2000. arXiv: hep-ph/0001268.

[32] Ian Balitsky. Operator expansion for high-energy scattering. *Nuclear Physics B*, 463(1):99–157, March 1996. arXiv: hep-ph/9509348.

[33] Yuri V. Kovchegov. Small-x F_2 Structure Function of a Nucleus Including Multiple Pomeron Exchanges. *Physical Review D*, 60(3), June 1999. arXiv: hep-ph/9901281.

[34] Ian Balitsky and Giovanni A. Chirilli. Next-to-leading order evolution of color dipoles. *Phys.Rev.*, D77:014019, 2008.

[35] Nestor Armesto, Carlos A. Salgado, and Urs Achim Wiedemann. Relating high-energy lepton-hadron, proton-nucleus and nucleus-nucleus collisions through geometric scaling. *Physical Review Letters*, 94(2), January 2005. arXiv: hep-ph/0407018.

[36] Niklas Beisert, Changrim Ahn, Luis F. Alday, Zoltan Bajnok, James M. Drummond, Lisa Freyhult, Nikolay Gromov, Romuald A. Janik, Vladimir Kazakov, Thomas Klose, Gregory P. Korchemsky, Charlotte Kristjansen, Marc Magro, Tristan McLoughlin, Joseph A. Minahan, Rafael I. Nepomechie, Adam Rej, Radu Roiban, Sakura Schafer-Nameki, Christoph Sieg, Matthias Staudacher, Alessandro Torrielli, Arkady A. Tseytlin, Pedro Vieira, Dmytro Volin, and Konstantinos Zoubos. Review of AdS/CFT Integrability: An Overview. *Letters in Mathematical Physics*, 99(1-3):3–32, January 2012. arXiv: 1012.3982.

[37] I. R. Klebanov and A. M. Polyakov. AdS Dual of the Critical O(N) Vector Model. *Physics Letters B*, 550(3-4):213–219, December 2002. arXiv: hep-th/0210114.

[38] Simone Giombi and Xi Yin. Higher Spin Gauge Theory and Holography: The Three-Point Functions. *Journal of High Energy Physics*, 2010(9), September 2010. arXiv: 0912.3462.

[39] Tadakatsu Sakai and Shigeki Sugimoto. Low energy hadron physics in holographic QCD. *Progress of Theoretical Physics*, 113(4):843–882, April 2005. arXiv: hep-th/0412141.

[40] Tadakatsu Sakai and Shigeki Sugimoto. More on a holographic dual of QCD. *Progress of Theoretical Physics*, 114(5):1083–1118, November 2005. arXiv: hep-th/0507073.

[41] Anton Rebhan. The Witten-Sakai-Sugimoto model: A brief review and some recent results. *arXiv:1410.8858 [hep-ph, physics:hep-th, physics:nucl-th]*, October 2014. arXiv: 1410.8858.

[42] Andreas Karch, Emanuel Katz, Dam T. Son, and Mikhail A. Stephanov. Linear confinement and AdS/QCD. *Physical Review D*, 74(1):015005, July 2006.

[43] U. Gürsoy and E. Kiritsis. Exploring improved holographic theories for QCD: part I. *Journal of High Energy Physics*, 2008(02):032, February 2008.

[44] U. Gürsoy, E. Kiritsis, and F. Nitti. Exploring improved holographic theories for QCD: part II. *Journal of High Energy Physics*, 2008(02):019, February 2008.

[45] C. FRONSDAL. Elementary Particles in a Curved Space. *Reviews of Modern Physics*, 37(1):221–224, January 1965.

[46] V. E. Didenko and E. D. Skvortsov. Elements of Vasiliev theory. *arXiv:1401.2975 [hep-th]*, January 2014. arXiv: 1401.2975.

[47] Sungho Hong, Sukjin Yoon, and Matthew J. Strassler. On the Couplings of Vector Mesons in AdS/QCD. *Journal of High Energy Physics*, 2006(04):003–003, April 2006. arXiv: hep-th/0409118.

[48] Henrique Boschi-Filho, Nelson R. F. Braga, and Hector L. Carrion. Glueball Regge trajectories from gauge/string duality and the Pomeron. *Physical Review D*, 73(4), February 2006. arXiv: hep-th/0507063.

[49] George A. Jaroszkiewicz and P. V. Landshoff. Model for diffraction excitation. *Phys. Rev.*, D10:170–174, 1974.

[50] Frederic Brünner and Anton Rebhan. Glueball Decay in the Witten-Sakai-Sugimoto Model and Finite Quark Masses. *PoS*, CD15:124, 2015.

[51] K. A. Olive et al. Review of Particle Physics. *Chin. Phys.*, C38:090001, 2014.

[52] Jacob Sonnenschein and Dorin Weissman. Rotating strings confronting PDG mesons. *Journal of High Energy Physics*, 2014(8), August 2014. arXiv: 1402.5603.

[53] A. Donnachie and P. V. Landshoff. Elastic Scattering at the LHC. *arXiv:1112.2485 [hep-ex, physics:hep-pho*, December 2011. arXiv: 1112.2485.

[54] A Donnachie and P. V Landshoff. New data and the hard pomeron. *Physics Letters B*, 518(1-2):63–71, October 2001.

[55] A. Donnachie and P. V. Landshoff. Perturbative QCD and Regge theory: closing the circle. *Physics Letters B*, 533(3-4):277–284, May 2002.

[56] A. Donnachie and P. V. Landshoff. pp and total cross sections and elastic scattering. *Physics Letters B*, 727(4-5):500–505, December 2013.

[57] Miguel S. Costa, Vasco Goncalves, and João Penedones. Conformal Regge theory. *Journal of High Energy Physics*, 2012(12):1–50, December 2012.

[58] Lorenzo Cornalba. Eikonal methods in AdS/CFT: Regge theory and multi-reggeon exchange. 2007.

[59] Simon Caron-Huot, Zohar Komargodski, Amit Sever, and Alexander Zhiboedov. Strings from Massive Higher Spins: The Asymptotic Uniqueness of the Veneziano Amplitude. 2016.

[60] Umut Gürsoy, Elias Kiritsis, Liuba Mazzanti, Georgios Michalogiorgakis, and Francesco Nitti. Improved Holographic QCD. *arXiv:1006.5461 [hep-lat, physics:hep-ph, physics:hep-th]*, 828:79–146, 2011. arXiv: 1006.5461.

[61] Xián O. Camanho, José D. Edelstein, Juan Maldacena, and Alexander Zhiboedov. Causality constraints on corrections to the graviton three-point coupling. *Journal of High Energy Physics*, 2016(2):20, February 2016.

[62] Y. Hatta, E. Iancu, and A. H. Mueller. Deep inelastic scattering at strong coupling from gauge/string duality: the saturation line. *Journal of High Energy Physics*, 2008(01):026, 2008.

[63] B. Pire, C. Roiesnel, L. Szymanowski, and S. Wallon. On AdS/QCD correspondence and the partonic picture of deep inelastic scattering. *Physics Letters B*, 670(1):84–90, December 2008.

[64] Javier L. Albacete, Yuri V. Kovchegov, and Anastasios Taliotis. DIS on a large nucleus in AdS/CFT. *Journal of High Energy Physics*, 2008(07):074, 2008.

[65] Yoshitaka Hatta. Relating e + e - annihilation to high energy scattering at weak and strong coupling. *Journal of High Energy Physics*, 2008(11):057, 2008.

[66] E. Levin, J. Miller, B. Z. Kopeliovich, and Ivan Schmidt. Glauber-Gribov approach for DIS on nuclei in N = 4 SYM. *Journal of High Energy Physics*, 2009(02):048, 2009.

[67] Richard C. Brower, Marko Djuric, and Chung-I. Tan. Saturation and Confinement: Analyticity, Unitarity and AdS/CFT Correspondence. *arXiv:0812.1299 [hep-ph]*, December 2008. arXiv: 0812.1299.

[68] Richard Brower, Marko Djuric, and Chung-I. Tan. Elastic and Diffractive Scattering after AdS/CFT. *arXiv:0911.3463 [hep-ph]*, November 2009. arXiv: 0911.3463.

[69] Jian-Hua Gao and Bo-Wen Xiao. Polarized deep inelastic and elastic scattering from gauge/string duality. *Physical Review D*, 80(1):015025, July 2009.

[70] Yoshitaka Hatta, Takahiro Ueda, and Bo-Wen Xiao. Polarized DIS in $\mathcal{N} = 4$ SYM: where is spin at strong coupling? *Journal of High Energy Physics*, 2009(08):007, 2009.

[71] Yuri V. Kovchegov, Zhun Lu, and Amir H. Rezaeian. Comparing AdS/CFT calculations to HERA F_2 data. *Physical Review D*, 80(7):074023, October 2009.

[72] E. Avsar, E. Iancu, L. McLerran, and D. N. Triantafyllopoulos. Shockwaves and deep inelastic scattering within the gauge/gravity duality. *Journal of High Energy Physics*, 2009(11):105, 2009.

[73] Lorenzo Cornalba, Miguel S. Costa, and João Penedones. Deep inelastic scattering in conformal QCD. *Journal of High Energy Physics*, 2010(3):1–65, March 2010.

[74] Fabio Dominguez. Particle production in DIS off a shockwave in AdS. *Journal of High Energy Physics*, 2010(9):7, September 2010.

[75] Lorenzo Cornalba, Miguel S. Costa, and João Penedones. AdS Black Disk Model for Small-x Deep Inelastic Scattering. *Physical Review Letters*, 105(7):072003, August 2010.

[76] M. A. Betemps, V. P. Gonçalves, and J. T. de Santana Amaral. Diffractive deep inelastic scattering in an AdS/CFT inspired model: A phenomenological study. *Physical Review D*, 81(9):094012, May 2010.

[77] Jian-Hua Gao and Zong-Gang Mou. Polarized deep inelastic scattering off the neutron from gauge/string duality. *Physical Review D*, 81(9):096006, May 2010.

[78] Yuri V. Kovchegov. R-current dis on a shock wave: Beyond the eikonal approximation. *Physical Review D*, 82(5):054011, September 2010.

[79] Sophia K. Domokos, Jeffrey A. Harvey, and Nelia Mann. Setting the scale of the pp and $p\overline{p}$ total cross sections using AdS/QCD. *Physical Review D*, 82(10):106007, November 2010.

[80] Neil Anderson, Sophia K. Domokos, Jeffrey A. Harvey, and Nelia Mann. Central production of η and η' via double Pomeron exchange in the Sakai-Sugimoto model. *Physical Review D*, 90(8):086010, October 2014.

[81] Richard Nally, Timothy G. Raben, and Chung-I Tan. Inclusive Production Through AdS/CFT. 2017.

[82] Xiangdong Ji. Deeply Virtual Compton Scattering. *Physical Review D*, 55(11):7114–7125, June 1997. arXiv: hep-ph/9609381.

[83] A. V. Radyushkin. Nonforward parton distributions. *Phys.Rev.*, D56:5524–5557, 1997.

[84] Ismail Zahed and Alexander Stoffers. Diffractive and deeply virtual Compton scattering in holographic QCD. 2012.

[85] Edward Witten. Baryons And Branes In Anti de Sitter Space. *Journal of High Energy Physics*, 1998(07):006–006, July 1998. arXiv: hep-th/9805112.

[86] Joseph Polchinski and Matthew J. Strassler. The String Dual of a Confining Four-Dimensional Gauge Theory. *arXiv:hep-th/0003136*, March 2000.

[87] Charlotte Sleight and Massimo Taronna. Spinning Witten Diagrams. *arXiv:1702.08619 [gr-qc, physics:hep-th]*, February 2017. arXiv: 1702.08619.

[88] F. D. Aaron, M. Aldaya Martin, C. Alexa, K. Alimujiang, V. Andreev, B. Antunovic, S. Backovic, A. Baghdasaryan, E. Barrelet, W. Bartel, K. Begzsuren, A. Belousov, J. C. Bizot, V. Boudry, I. Bozovic-Jelisavcic, J. Bracinik, G. Brandt, M. Brinkmann, V. Brisson, D. Bruncko, A. Bunyatyan, G. Buschhorn, L. Bystritskaya, A. J. Campbell, K. B. Cantun Avila, K. Cerny, V. Cerny, V. Chekelian, A. Cholewa, J. G. Contreras, J. A. Coughlan, G. Cozzika, J. Cvach, J. B. Dainton, K. Daum, M. Deak, Y. de Boer, B. Delcourt, M. Del Degan, J. Delvax, E. A. De Wolf, C. Diaconu, V. Dodonov, A. Dossanov, A. Dubak, G. Eckerlin, V. Efremenko, S. Egli, A. Eliseev, E. Elsen, A. Falkiewicz, L. Favart, A. Fedotov, R. Felst, J. Feltesse, J. Ferencei, D.-J. Fischer, M. Fleischer, A. Fomenko, E. Gabathuler, J. Gayler, Samvel Ghazaryan, A. Glazov, I. Glushkov, L. Goerlich, N. Gogitidze, M. Gouzevitch, C. Grab, T. Greenshaw, B. R. Grell, G. Grindhammer, S. Habib, D. Haidt, C. Helebrant, R. C. W. Henderson, E. Hennekemper, H. Henschel, M. Herbst, G. Herrera, M. Hildebrandt, K. H. Hiller, D. Hoffmann, R. Horisberger, T. Hreus, M. Jacquet, M. E. Janssen, X. Janssen, L. Jonsson, Andreas Werner Jung, H. Jung, M. Kapichine, J. Katzy, I. R. Kenyon, C. Kiesling, M. Klein, C. Kleinwort, T. Kluge, A. Knutsson, R. Kogler, P. Kostka, M. Kraemer, K. Krastev, J. Kretzschmar, A. Kropivnitskaya, K. Kruger, K. Kutak, M. P. J. Landon, W. Lange, G. Lastovicka-Medin, P. Laycock, A. Lebedev, G. Leibenguth, V. Lendermann, S. Levonian, G. Li, K. Lipka, A. Liptaj, B. List, J. List, N. Loktionova, R. Lopez-Fernandez, V. Lubimov, A. Makankine, E. Malinovski, P. Marage, Ll Marti, H.-U. Martyn, S. J. Maxfield, A. Mehta,

A. B. Meyer, H. Meyer, H. Meyer, J. Meyer, V. Michels, S. Mikocki, I. Milcewicz-Mika, F. Moreau, A. Morozov, J. V. Morris, Matthias Ulrich Mozer, M. Mudrinic, K. Muller, P. Murin, Th Naumann, P. R. Newman, C. Niebuhr, A. Nikiforov, D. Nikitin, G. Nowak, K. Nowak, M. Nozicka, B. Olivier, J. E. Olsson, S. Osman, D. Ozerov, V. Palichik, I. Panagoulias, M. Pandurovic, Th Papadopoulou, C. Pascaud, G. D. Patel, O. Pejchal, E. Perez, A. Petrukhin, I. Picuric, S. Piec, D. Pitzl, R. Placakyte, B. Pokorny, R. Polifka, B. Povh, V. Radescu, A. J. Rahmat, N. Raicevic, A. Raspiareza, T. Ravdandorj, P. Reimer, E. Rizvi, P. Robmann, B. Roland, R. Roosen, A. Rostovtsev, M. Rotaru, J. E. Ruiz Tabasco, Z. Rurikova, S. Rusakov, D. Salek, D. P. C. Sankey, M. Sauter, E. Sauvan, S. Schmitt, L. Schoeffel, A. Schoning, H.-C. Schultz-Coulon, F. Sefkow, R. N. Shaw-West, L. N. Shtarkov, S. Shushkevich, T. Sloan, Ivan Smiljanic, Y. Soloviev, P. Sopicki, D. South, V. Spaskov, Arnd E. Specka, Z. Staykova, M. Steder, B. Stella, G. Stoicea, U. Straumann, D. Sunar, T. Sykora, V. Tchoulakov, G. Thompson, P. D. Thompson, T. Toll, F. Tomasz, T. H. Tran, D. Traynor, T. N. Trinh, P. Truol, I. Tsakov, B. Tseepeldorj, J. Turnau, K. Urban, A. Valkarova, C. Vallee, P. Van Mechelen, A. Vargas Trevino, Y. Vazdik, S. Vinokurova, V. Volchinski, M. von den Driesch, D. Wegener, Ch Wissing, E. Wunsch, J. Zacek, J. Zalesak, Z. Zhang, A. Zhokin, T. Zimmermann, H. Zohrabyan, F. Zomer, and R. Zus. Deeply Virtual Compton Scattering and its Beam Charge Asymmetry in e+- Collisions at HERA. *Phys.Lett.*, B681:391–399, 2009.

[89] S. Chekanov, M. Derrick, S. Magill, B. Musgrave, D. Nicholass, J. Repond, R. Yoshida, M. C. K. Mattingly, P. Antonioli, G. Bari, L. Bellagamba, D. Boscherini, A. Bruni, G. Bruni, G. Cara Romeo, F. Cindolo, M. Corradi, G. Iacobucci, A. Margotti, T. Massam, R. Nania, A. Polini, S. Antonelli, M. Basile, M. Bindi, L. Cifarelli, A. Contin, F. Palmonari, S. De Pasquale, G. Sartorelli, A. Zichichi, D. Bartsch, I. Brock, H. Hartmann, E. Hilger, H. P. Jakob, M. Jungst, A. E. Nuncio-Quiroz, E. Paul, U. Samson, V. Schonberg, R. Shehzadi, M. Wlasenko, N. H. Brook, G. P. Heath, J. D. Morris, M. Kaur, P. Kaur, I. Singh, M. Capua, S. Fazio, A. Mastroberardino, M. Schioppa, G. Susinno, E. Tassi, J. Y. Kim, Z. A. Ibrahim, F. Mohamad Idris, B. Kamaluddin, W. A. T. Wan Abdullah, Y. Ning, Z. Ren, F. Sciulli, J. Chwastowski, A. Eskreys, J. Figiel, A. Galas, K. Olkiewicz, B. Pawlik, P. Stopa, L. Zawiejski, L. Adamczyk, T. Bold, I. Grabowska-Bold, D. Kisielewska, J. Lukasik, M. Przybycien, L. Suszycki, A. Kotanski, W. Slominski, O. Behnke, U. Behrens, C. Blohm, A. Bonato, K. Borras, D. Bot, R. Ciesielski, N. Coppola, S. Fang, J. Fourletova, A. Geiser, P. Gottlicher, J. Grebenyuk, I. Gregor, T. Haas, W. Hain, A. Huttmann,

F. Januschek, B. Kahle, I. I. Katkov, U. Klein, U. Kotz, H. Kowalski, M. Lisovyi, E. Lobodzinska, B. Lohr, R. Mankel, I. A. Melzer-Pellmann, S. Miglioranzi, A. Montanari, T. Namsoo, D. Notz, A. Parenti, L. Rinaldi, P. Roloff, I. Rubinsky, U. Schneekloth, A. Spiridonov, D. Szuba, J. Szuba, T. Theedt, J. Ukleja, G. Wolf, K. Wrona, A. G. Yagues Molina, C. Youngman, W. Zeuner, V. Drugakov, W. Lohmann, S. Schlenstedt, G. Barbagli, E. Gallo, P. G. Pelfer, A. Bamberger, D. Dobur, F. Karstens, N. N. Vlasov, P. J. Bussey, A. T. Doyle, W. Dunne, M. Forrest, M. Rosin, D. H. Saxon, I. O. Skillicorn, I. Gialas, K. Papageorgiu, U. Holm, R. Klanner, E. Lohrmann, H. Perrey, P. Schleper, T. Schorner-Sadenius, J. Sztuk, H. Stadie, M. Turcato, C. Foudas, C. Fry, K. R. Long, A. D. Tapper, T. Matsumoto, K. Nagano, K. Tokushuku, S. Yamada, Y. Yamazaki, A. N. Barakbaev, E. G. Boos, N. S. Pokrovskiy, B. O. Zhautykov, V. Aushev, O. Bachynska, M. Borodin, I. Kadenko, A. Kozulia, V. Libov, D. Lontkovskyi, I. Makarenko, Iu Sorokin, A. Verbytskyi, O. Volynets, D. Son, J. de Favereau, K. Piotrzkowski, F. Barreiro, C. Glasman, M. Jimenez, L. Labarga, J. del Peso, E. Ron, M. Soares, J. Terron, C. Uribe-Estrada, M. Zambrana, F. Corriveau, C. Liu, J. Schwartz, R. Walsh, C. Zhou, T. Tsurugai, A. Antonov, B. A. Dolgoshein, D. Gladkov, V. Sosnovtsev, A. Stifutkin, S. Suchkov, R. K. Dementiev, P. F. Ermolov, L. K. Gladilin, Yu A. Golubkov, L. A. Khein, I. A. Korzhavina, V. A. Kuzmin, B. B. Levchenko, O. Yu Lukina, A. S. Proskuryakov, L. M. Shcheglova, D. S. Zotkin, I. Abt, A. Caldwell, D. Kollar, B. Reisert, W. B. Schmidke, G. Grigorescu, A. Keramidas, E. Koffeman, P. Kooijman, A. Pellegrino, H. Tiecke, Monica Luisa Vazquez Acosta, L. Wiggers, N. Brummer, B. Bylsma, L. S. Durkin, A. Lee, T. Y. Ling, Philip Daniel Allfrey, M. A. Bell, A. M. Cooper-Sarkar, R. C. E. Devenish, J. Ferrando, B. Foster, C. Gwenlan, K. Horton, K. Oliver, A. Robertson, R. Walczak, A. Bertolin, F. Dal Corso, S. Dusini, A. Longhin, L. Stanco, P. Bellan, R. Brugnera, R. Carlin, A. Garfagnini, S. Limentani, B. Y. Oh, A. Raval, J. J. Whitmore, Y. Iga, G. D'Agostini, G. Marini, A. Nigro, J. E. Cole, J. C. Hart, C. Heusch, H. Sadrozinski, A. Seiden, R. Wichmann, D. C. Williams, H. Abramowicz, R. Ingbir, S. Kananov, A. Levy, A. Stern, M. Kuze, J. Maeda, R. Hori, S. Kagawa, N. Okazaki, S. Shimizu, T. Tawara, R. Hamatsu, H. Kaji, S. Kitamura, O. Ota, Y. D. Ri, R. Cirio, M. Costa, M. I. Ferrero, V. Monaco, C. Peroni, R. Sacchi, V. Sola, A. Solano, N. Cartiglia, S. Maselli, A. Staiano, M. Arneodo, M. Ruspa, S. Fourletov, J. F. Martin, T. P. Stewart, S. K. Boutle, J. M. Butterworth, T. W. Jones, J. H. Loizides, M. Wing, B. Brzozowska, J. Ciborowski, G. Grzelak, P. Kulinski, P. Luzniak, J. Malka, R. J. Nowak, J. M. Pawlak, W. Perlanski, T. Tymieniecka, A. F. Zarnecki, M. Adamus, P. Plucinski,

A. Ukleja, Y. Eisenberg, D. Hochman, U. Karshon, E. Brownson, D. D. Reeder, A. A. Savin, W. H. Smith, H. Wolfe, S. Bhadra, C. D. Catterall, Y. Cui, G. Hartner, S. Menary, U. Noor, J. Standage, and J. Whyte. A Measurement of the Q**2, W and t dependences of deeply virtual Compton scattering at HERA. *JHEP*, 0905:108, 2009.

[90] Felipe G. Ben, Magno V. T. Machado, and Werner K. Sauter. Geometrical scaling description for the exclusive production of vector mesons and deeply virtual Compton scattering. *arXiv:1803.08442 [hep-ph]*, March 2018. arXiv: 1803.08442.

[91] Deog Ki Hong, Takeo Inami, and Ho-Ung Yee. Baryons in AdS/QCD. *Physics Letters B*, 646(4):165–171, March 2007. arXiv: hep-ph/0609270.

[92] J. Polchinski. *String theory. Vol. 1: An introduction to the bosonic string.* Cambridge Monographs on Mathematical Physics. Cambridge University Press, 2007.

[93] R. R. Metsaev. Light-cone form of field dynamics in anti-de Sitter space-time and AdS/CFT correspondence. *Nuclear Physics B*, 563(1-2):295–348, December 1999.